Dissertation

submitted to the

Combined Faculties for the Natural Sciences and for Mathematics

of the Ruperto–Carola University of Heidelberg, Germany

for the degree of

Doctor of Natural Sciences

presented by

Dipl. phys. Claudia Martina Wagenknecht

born in Hilden, Rhld. (Germany)

Oral examination: November 18^{th} 2009

Experimental Manipulation of Photonic Entanglement

* * *

Applications in Quantum Communication, Quantum Teleportation and Quantum Computation

Referees: Prof. Dr. Jian-Wei Pan
Prof. Dr. Mete Atatüre

Zusammenfassung

Experimantelle Manipulation von photonischer Verschränkung

Die Quanteninformationsverarbeitung (QIV) und ihre Anwendungen im Bereich der Quantenkommunikation und Quantenrechnung war in den letzten zwanzig Jahren eines der am stärksten wachsenden Gebitet der Physik. In der Zukunft wird die QIV beeindruckende Verbesserungen unter anderem auf den Gebieten der Kommunikationssicherheit, der Rechengeschwindigkeit und der Fähigkeit zur Simulation von quantenmechanischen Prozessen erlauben. Diese Dissertation beschreibt vier Experimente zur Physik der Verschränkung mehrerer Photonen und ihre Anwendung auf dem Gebiet der QIV: Die Implementierung einer deterministischen Quelle für polarisationsverschränkte Photonenpaare. Die Entwicklung eines Interferometers zur Erzeugung von Viel-Teilchen-Verschränkung mit bis zu sechs Photonen. Die erzeugte Sechs-Teilchen-Verschränkung wurden dann zur ersten experimentellen Quanten Teleportation eines zusammengesetzten Zwei-Teilchen Zustandes, zur ersten "Ubertragung von Verschränkung über mehrere Abschnitte und zur ersten Implementierung eines teleportationsbasierten 'bedingten-NICHT-Gatters' für eine fehlerto- lerante Quantenrechnung verwendet. Die in dieser Dissertation entwickelten experimentellen Techniken sind fundamental sowohl fuer Anwendungen in der QIV als auch für zukünftige grundlegende Experimente der Quantenmechanik.

Abstract

Experimental Manipulation of Photonic Entanglement

Quantum information processing (QIP) with its applications in quantum communication and quantum computation has been one of the most rapidly emerging field of physics over the last twenty years. QIP is promising to allow tremendous improvements in communication security, computational speed and the ability to simulate quantum mechanical processes. This thesis describes four experiments on the physics of multi-photon entanglement and its application in QIP: We have implemented an event-ready source of polarization entangled photon pairs. We have developed an interferometer to generate multipartite entanglement between up to six photons. By exploiting the generated six-photon entanglement, we report the first experimental quantum teleportation of a two-qubit composite system, the first realization of multistage entanglement swapping and the first implementation of a teleportation-based controlled-NOT gate for fault-tolerant quantum computation. The experimental techniques developed in the course of this thesis are of great significance as well for applications in QIP as for future fundamental experiments on quantum mechanics.

Contents

Abstract i

Contents iii

List of figures v

1 Introduction 1

2 Photonic Entanglement 7
- 2.1 Quantum Bits . . . 7
- 2.2 Quantum Entanglement . . . 9
  - 2.2.1 Manipulating and Controlling Photonic Qubits . . . 9
  - 2.2.2 Quantum Interference . . . 12
  - 2.2.3 Bipartite Entanglement and Bell-States . . . 14
- 2.3 Generation of Entanglement . . . 20
  - 2.3.1 Spontaneous Parametric Down Conversion (SPDC) . . . 20
  - 2.3.2 A Stable High-Intensity Entangled Photon Source . . . 24
- 2.4 Multipartite Entanglement . . . 26
  - 2.4.1 Construction of multi-photon entanglement . . . 27
  - 2.4.2 Classes of Multipartite Entanglement . . . 28
- 2.5 Detection and Verification of Entanglement . . . 31
  - 2.5.1 Bell State Analyzer . . . 31
  - 2.5.2 Verification Criteria . . . 34

3 A Heralded Source for Polarisation Entangled Photon Pairs 39
- 3.1 Introduction . . . 39
- 3.2 Conditional Preparation of Entangled Photon Pairs . . . 40
- 3.3 Experimental Setup . . . 44
- 3.4 Experimental Results . . . 46
- 3.5 Discussion . . . 49

4 Quantum Teleportation of a Two-Qubit Composite System 51
- 4.1 Introduction . . . 51
- 4.2 Theory of Quantum Teleportation . . . 51

4.3 Teleportation of a Two-Qubit System . . . 55
4.4 Experimental Setup . . . 57
4.5 Experimental Results . . . 59
4.6 Discussion . . . 62

5 Multistage Entanglement Swapping 65
5.1 Introduction . . . 65
5.2 Multistage Entanglement Swapping . . . 66
5.3 Experimental Setup . . . 68
5.4 Experimental Results . . . 68
5.5 Discussion . . . 72

6 Teleportation-Based Controlled-NOT Gate for Fault-Tolerant Quantum Computation 73
6.1 Introduction . . . 73
6.2 The Teleportation-Based C-NOT gate . . . 74
6.3 Experimental Setup . . . 80
6.4 Experimental Results . . . 81
6.5 Discussion . . . 84

7 Conclusions and Outlook 87

Appendix 91

Acknowledgement 93

Bibliography 95

List of Figures

2.1 Bloch sphere . . . 8
2.2 BS . . . 10
2.3 PBS . . . 11
2.4 Experimental Hong-Ou-Mandel-dip . . . 13
2.5 Hadamard gate . . . 18
2.6 Controlled-NOT (C-NOT) gate . . . 18
2.7 Quantum circuit for generation and detection of Bell states . . . 19
2.8 Principle of type-II parametric down-conversion . . . 21
2.9 Method to increase the power of the ultraviolet light . . . 25
2.10 Performance of the LBO crystal . . . 25
2.11 Six-photon polarization entanglement source . . . 27
2.12 Bell state analyzers . . . 32
2.13 Entanglement witness . . . 35
2.14 Witnesses for three partite entanglement . . . 36

3.1 Principle of the heralded entanglement source . . . 41
3.2 Experimental setup of the heralded entanglement source . . . 45
3.3 State preparation efficiencies . . . 47
3.4 Fidelity of the entangled state . . . 48

4.1 The principle of quantum teleportation . . . 52
4.2 The principle of two-qubit teleportation . . . 55
4.3 Schematic diagram of the experimental setup of two-qubit teleportation . . . 58
4.4 Experimental results for the teleportation of two separable states . . . 60
4.5 Experimental results for the teleportation of an entangled state . . . 61

5.1 Principle of multistage entanglement swapping . . . 67
5.2 Schematic diagram of the experimental setup of multi-stage entanglement swapping . . . 69
5.3 Experimental results for the entanglement witness of the swapped state . . . 70
5.4 Quantum state tomography before entanglement swapping . . . 71

6.1 Principle of fault-tolerant C-NOT gate 75
6.2 Schematic diagram of the experimental setup of a fault-tolerant C-NOT gate 77
6.3 Experimental results for truth table of the C-NOT gate. The first qubit is the target and the second is the control qubit. The average fidelity for the truth table is 0.72 ± 0.05. 81
6.4 Experimental results for the fidelity measurement of the entangled state in the computational basis 83
6.5 Experimental results for the fidelity measurement of the entangled state in the diagonal basis 83
6.6 Experimental results for the fidelity measurement of the entangled state in the circular basis 83

Chapter 1

Introduction

In 1905, basing his work on PlanckŠs quantum hypothesis, Albert Einstein showed that an electromagnetic wave such as light could be described by a particle, individual quanta called 'photon' carrying a discrete energy dependent on its frequency. This led to a theory called waveŰ́particle duality, in which particles and waves were neither one nor the other, but had certain properties of both. From Einstein's simple postulation was born a flurry of debating, theorizing and testing, and thus, the entire field of quantum physics. Quantum theory was born and, during the twentieth century, proved to be a successful theory.

Quantum theory and quantum mechanics do not account for single measurement outcomes in a deterministic way. According to an accepted interpretation of quantum mechanics known as the Copenhagen interpretation, a measurement causes an instantaneous collapse of the wave function describing the quantum system into an eigenstate of the observable that was measured. This principle of superposition is the fundamental basis of quantum mechanics (QM) and a rather counterintuitive concept to human kind: According to classical physics a system is in one state at a time. In contrary to this, a quantum mechanical system can be in a superposition of arbitrary many states with certain probabilities at the same time. QM predicts probabilities in situations where classical physics predicts certainties. Its correctness was later on proven by several interferometric experiments, e.g. by Young's Double-Slit experiment and others [1, 2, 3, 4].

What are the consequences of this superposition principle?

In 1935 Einstein, Podolsky and Rosen [5] performed the following Gedankenexperiment for the combined system of two or more subsystems: they considered two distant particles that have interacted in the past and are in a superposition of states of the combined system. Depending on the choice of measurement of one physical parameter (e.g. momentum or position) of particle A, particle B will collapse into a different state. This behaviour, that Einstein called "spooky action at a distance", acts instantaneous and is completely independent of the distance between the two particles. According to its authors the EPR experiment yields a paradox. Either

1. The result of a measurement performed on particle A of the quantum system

has a non-local effect on the physical reality of the other distant particle B, in the sense that quantum mechanics can predict outcomes of some measurements carried out at B;

or...

2. Quantum mechanics is incomplete in the sense that some element of physical reality corresponding to B cannot be accounted for by quantum mechanics (that is, some extra variable is needed to account for it.)

They claim that given a specific experiment, in which the outcome of a measurement could be known before the measurement takes place, there must exist something in the real world, an "element of reality", which determines the measurement outcome. They postulate that these elements of reality are local, in the sense that they belong to a certain point in spacetime. This element may only be influenced by events which are located in the backward light cone of this point in spacetime. Even though these claims sound reasonable and convincing, they are founded on assumptions about nature which constitute what is now known as local realism.

How to deal with the problem that QM predicts correlations, which violate the principle of local realism?

The solution came in 1964, when Bell proposed an experimental test of the local hidden variable model (LHVM), which was invented complete QM to circumvent the EPR paradox [6]. LHVM assumes that (i) measurement results are determined by properties the particles already carry before, and independent of, the measurement (reality), (ii) results obtained in one location are independent of actions performed in a space like separated place (locality), and (iii) that the measurement apparatus is not influenced by the hidden variables, which determine the local results (free will). He found an inequality, which holds for any LHVM , but is allowed to be violated by QM, since the expectation values for any LHVM and for QM differ for specific sets of measurements. This "Bell inequality" was first violated experimentally by Aspect et al. in 1982 [7, 8, 9] and afterwards has been tested in subsequent experiments, which have overwhelmingly supported QM [10, 11]. However, there still exist experimental problems, known as "loopholes", that affect the validity of these experimental findings and, in principle, allow other interpretations than the QM one.

Quantum entanglement, this strange phenomenon of QM first described by EPR, is a possible property of a quantum mechanical state of a system of two or more objects, in which the quantum states of the constituting objects are linked together so that one object can no longer be adequately described without full mention of its counterpart - even though the individual objects may be spatially separated. This interconnection leads to non-classical correlations between observable physical properties of remote systems, often referred to as nonlocal correlations. Entanglement is one of the properties of quantum mechanics that caused Einstein and others to dislike the theory. However, after Bell had recognized that entanglement leads to experimentally testable deviations of QM from classical physics, entanglement was recognized as a resource for testing quantum mechanics and with the advent of

quantum information theory attracted the attention of many scientists.

Over the past twenty years quantum information processing (QIP) has become an emerging field of modern physics exploiting entanglement as a new quantum resource for tasks that cannot be performed by means of classical resources [12]. Entanglement can be manipulated, broadcasted, controlled and distributed [13] and its intrinsic properties allowed significant progress in many QIP protocols.

QIP can mainly be divided into the two areas of quantum communication and quantum computation [14, 15]:

- Quantum communication describes the transfer of quantum states over large distances, which can lead to drastic improvements in security – quantum cryptography [16, 17] – and channel capacity – quantum dense coding [18]. It further covers the distribution of bi- or multi-partite entanglement between different parties, separated by large distances [19, 20]. Remarkable experimental and theoretical effort has been employed to the implementation of different areas of QIP. Quantum cryptography, in particular quantum key distribution [16, 17] is an example for quantum communication, which is already at the verge to commercial use, while as well research on quantum repeaters [21, 22], essential building blocks for the realization of entanglement distribution over large distances, made fast progress.

- Quantum computation is dedicated to the implementation of algorithms that exploit the superposition character of quantum entanglement to dramatically speed up computational tasks such as a reduction of time needed to search an unsorted database of N elements. Probably the most famous quantum algorithm is Shor's algorithm to factorize large numbers [23]. Its introduction in 1994 has triggered tremendous efforts in the new field of QIP, both on the theoretical and experimental side. Although, realizations of quantum computers to implement quantum algorithms are still at the very first stages and a great deal of fundamental research still lays ahead.

There are several candidates of quite different physical systems that can in principle be used to implement QIP, all holding their experimental advantages and disadvantages. Promising candidates are, but not limited to, ion traps [24], nuclear magnetic resonance [25], quantum dots [26, 27], super-conducting devices (Josephson junction) [28] and photons [29].

We try to implement QIP with photons and linear optics for various reasons such as very strong robustness against de-coherence, extremely fast and accurate implementations of universal single qubit operations and the vast availability of already existing electro-optic devices. We exploit spontaneous parametric down-conversion (SPDC)[30], which is still the best source for entangled photon pairs, together with basic linear optics elements to generate multi-photon entanglement. With these

building blocks at hand, we on the one hand conduct experimental tests of the fundamental nature of quantum mechanics and on the other hand try to design and develop new techniques and methods necessary for future applications in QIP. Performing these multi-photon experiments we already experienced the limits of efficiency introduced by the probabilistic nature of the SPDC process. This motivated us to implement a novel scheme of a heralded photon source, which still makes use of the advantages provided by SPDC and at the same time allows to significantly improve the feasibility and application of the developed techniques for their future use in QIP.

In this thesis we report the experimental implementation of a heralded source for entangled photon pairs, the first quantum teleportation of a two-qubit composite system, the first experimental realization of multi-stage entanglement swapping and the first implementation of a teleportation-based quantum gate for fault-tolerant quantum computation. The main contents of the thesis are organized as follow:

Chapter 1 gives a brief introduction to the field of quantum entanglement and QIP and s short overview over the contents of this thesis.

Chapter 2 presents the theoretical background of some fundamental concepts of QIP and the necessary experimental prerequisites, which provide the basis for all the experiments performed in the course of this thesis. In the first section we introduce quantum bits. In the second section we discuss their manipulation and control, explain the fundamental concept of quantum interference and how to produce bipartite entanglement. In the third section we present the source for entangled photon pairs used throughout all experiments in this thesis. In section four we discuss the construction of multipartite entanglement, including some of its classes and their properties. In section five we introduce ways to detect, classify and verify it.

In Chapter 3 we report the experimental demonstration of a heralded source for polarization entangled photons. Entanglement sources based on the probabilistic generation process of SPDC allow demonstrations of a number of quantum protocols, but do not permit on-demand applications, deterministic quantum computing and significantly limit the efficiency of multi-photon experiments. Therefore the controlled generation of entangled states is a long-standing goal in quantum information processing. Here we present a source for entangled photon pairs generated in event-ready manner by conditioned detection of auxiliary photons: a scheme, which profits from the stable and robust properties of SPDC and requires only modest experimental means. We introduce the experimental setup and evaluate and compare the performance of the implemented source.

In Chapter 4 we demonstrate the first quantum teleportation of a two-qubit composite system. Quantum teleportation, a way to transfer the state of a quantum system from one location to another, is central to quantum communication and plays an important role in a number of quantum computation protocols Quantum teleportation of a single photonic state has first been demonstrated in 1997. We

depict the design and development of a six-photon interferometer that has been used in most of the experiments described within this thesis.

In Chapter 5 we report the first experimental realization of multistage entanglement swapping. Entanglement swapping is of fundamental interest since it can be used to entangle particles that have never physically interacted in the past. Its realization over multiple stages, however, is an essential prerequisite for the implementation of quantum repeaters. The experimental results clearly show the entanglement of the final outgoing photon pair.

In Chapter 6 we finally present the first experimental realization of a teleportation-based controlled-NOT gate that can, in principle, be used for fault-tolerant quantum computation. The coupling of quantum states to their environment imposes a major challenge to the implementation of realistic quantum computers. Quantum error correcting codes and fault-tolerant quantum gates are thus of significant importance to QIP.

In Chapter 7 we conclude this thesis by summarizing its main results and provide an outlook to future work.

Chapter 2

Photonic Entanglement

Quantum entanglement describes correlations between quantum systems that are much stronger than any classical correlation could be. It is an essential feature of quantum mechanics [31] and therefore a fundamental tool in quantum information processing (QIP): experimental realizations of entangled photon pairs were used to demonstrate the quantum nature of polarization correlations, to confirm quantum predictions and falsify semi-classical models, such as test Bell's theorem and exclude local realistic descriptions of the observed quantum phenomena [6, 7, 8, 9]. It followed the discovery of QIP, partly triggered by the introduction of quantum cryptography[16, 17]. Quantum entanglement is a fundamental resource for QIP as a computational source [29], as a quantum channel in quantum communication (e.g. for quantum state teleportation [32, 33] or quantum dense coding [18, 34]).

In this chapter some basic concepts and procedures of quantum entanglement and QIP are introduced, which are essential to the experiments performed within the framework of this thesis. We start with the introduction to quantum bits and the possibilities of their control and manipulation by the means of linear optics and the creation of entangled photons. Here we first discuss the meaning of entanglement, first in bipartite systems giving the definition of the Bell-state basis. We introduce the source, that we used in our experiments to generate entangled photon pairs. We then proceed to multipartite entanglement and outline different classes of states. We show how they can be detected by briefly discussing the experimental realization of key elements, e.g. the Bell-state analyzer, that were used in all experimental setups. Finally we discuss the detection, including its technical limitations, and introduce some measures for existence and quality of quantum entanglement.

2.1 Quantum Bits

In classical information processing the smallest unit carrying information is a bit, a binary digit taking the value 0 or 1. In analogy, a quantum bit is the state vector of a two-level system with the basis states $|0\rangle$ and $|1\rangle$. In contrast to a classical bit a

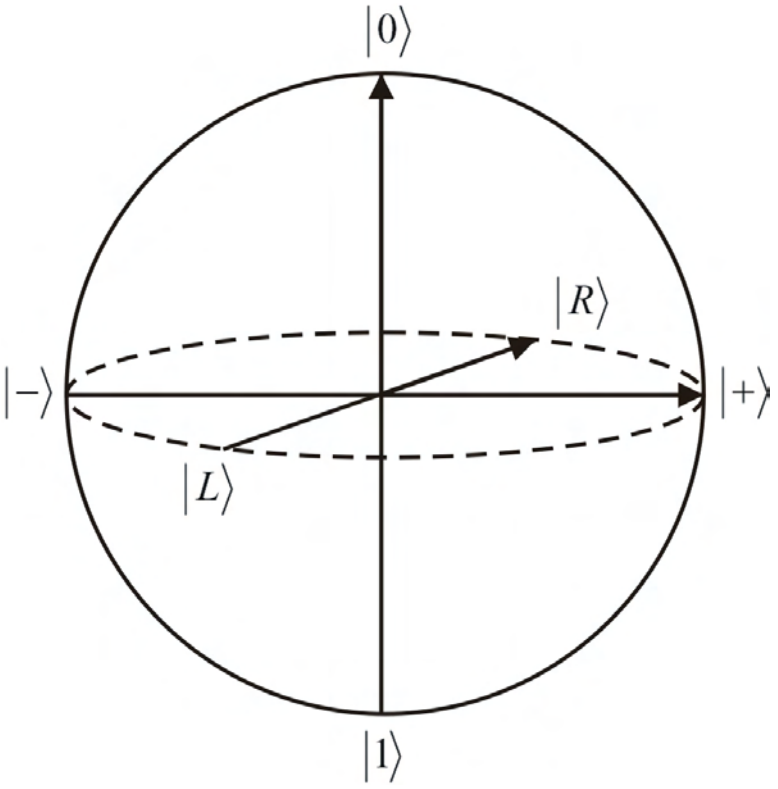

Figure 2.1: *Bloch sphere. A vector from the origin to the surface of the sphere represents the state of the qubit.* $|0\rangle/|1\rangle$ *are the eigenstates in the computational basis,* $|\pm\rangle = \frac{1}{\sqrt{2}}(|0\rangle \pm |1\rangle)$ *in the diagonal basis, and* $|R\rangle/|L\rangle = \frac{1}{\sqrt{2}}(|0\rangle \pm i|1\rangle)$ *in the circular basis*

quantum bit, commonly know as qubit, can take values that are in a superposition of the two basis states:

$$|\Psi\rangle = \alpha\,|0\rangle + \beta\,|1\rangle \tag{2.1}$$

The pre-factors α and β can be any complex numbers satisfying $|\alpha|^2 + |\beta|^2 = 1$.

A graphic interpretation of a qubit is the Bloch sphere, which is shown in Fig. (2.1). The state of the qubit is represented by a vector from the origin to the surface of the unit sphere. The complex nature of the relative phase between α and β accounts for the three axes given by $|0\rangle/|1\rangle$, $|+\rangle/|-\rangle$ and $|R\rangle/|L\rangle$. Here,

$$\begin{aligned} |H\rangle = |0\rangle \quad &, \quad |V\rangle = |0\rangle, \\ |+\rangle = \frac{1}{\sqrt{2}}(|0\rangle + |1\rangle) \quad &, \quad |-\rangle = \frac{1}{\sqrt{2}}(|0\rangle - |1\rangle), \\ |R\rangle = \frac{1}{\sqrt{2}}(|0\rangle + i|1\rangle) \quad &, \quad |L\rangle = \frac{1}{\sqrt{2}}(|0\rangle - i|1\rangle) \end{aligned} \tag{2.2}$$

are the three in QIP commonly used orthonormal bases. In analogy to the polarization state of light they are often called H/V basis, diagonal ($|+\rangle/|-\rangle$) and

circular ($|R\rangle/|L\rangle$) basis, respectively. Note that, for a qubit in a pure state, the state vector always has unit length. However, for a qubit in a mixed state, the length is smaller than unity. For example, the state vector for a completely random qubit is represented by a point at the origin.

2.2 Quantum Entanglement

2.2.1 Manipulating and Controlling Photonic Qubits

Simple Optical Elements

In our experiments we try to implement QIP with photons and linear optics for various reasons such as very strong robustness against de-coherence, extremely fast and accurate implementations of universal single qubit operations, the vast availability of already existing electro-optic devices and the implementation under modest experimental requirements. As already mentioned, aside from photons of course there are also other promising candidates for the implementation of QIP, such as ion traps [24], nuclear magnetic resonance [25], quantum dots [26, 27] and super-conducting devices (Josephson junction) [28], which all provide their experimental advantages and also disadvantages, e.g liquid helium cooling or large volume setups.

The possibility of applying coherent control of a photonic qubit to perform QIP tasks is based on the fact that the information can be encoded in the polarization degree of freedom of the individual photon and that this photon can be manipulated with a high precision of about 99% by simple optical elements. Aside from wave retardation plates (their working principle can be found in standard textbooks as [35]), two main optical elements for photonic manipulation are polarizing and non-polarizing beam splitters.

The BS is polarization independent and is characterized by the following transformation on the incoming modes a and b

$$\begin{aligned} a &\rightarrow \frac{1}{\sqrt{2}}c + \frac{i}{\sqrt{2}}d \\ b &\rightarrow \frac{i}{\sqrt{2}}c + \frac{1}{\sqrt{2}}d \end{aligned} \tag{2.3}$$

For the standard 50:50 BS the particle will be found with equal probability (50%) in output mode c or d, independently from the incoming mode. The factor i in Eq. 2.3 is a consequence of unitary and describes the physical effect of a phase jump upon reflection at the semi-transparent mirror [36].

Now suppose that two photons, 1 and 2, enter the BS: photon 1 in the state $|\Psi\rangle_1 = \alpha|H\rangle + \beta|V\rangle$ ($|\alpha|^2 + |\beta|^2 = 1$) enters in input mode a, and photon 2 in the state $|\Psi\rangle_2 = \gamma|H\rangle + \delta|V\rangle$ ($|\gamma|^2 + |\delta|^2 = 1$) enters in input mode b. For this general case, four different possibilities arise: both particles are (1)reflected or (2)

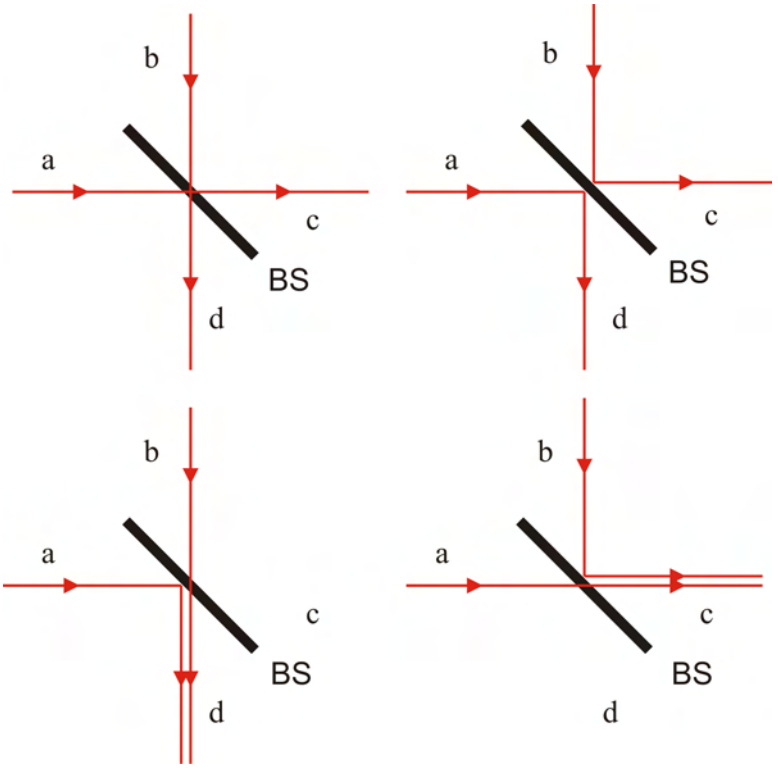

Figure 2.2: *Function of the BS. The BS coherently transforms two spatial input modes a and b into two output modes c and d. The four possibilities how two incoming photons can leave the BS are displayed.*

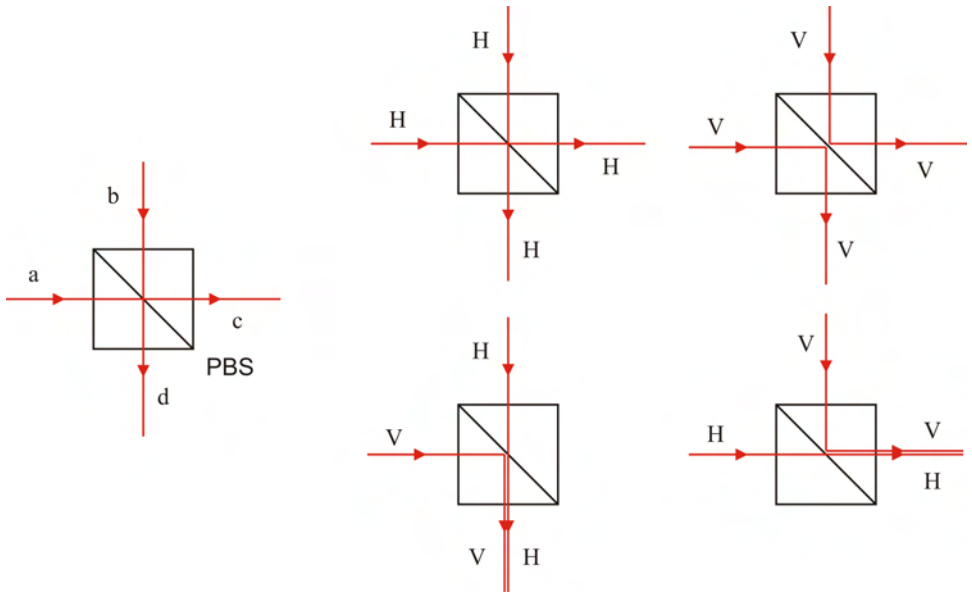

Figure 2.3: *Function of the PBS. The PBS transmits horizontal, and reflects vertical polarization. If the two photons have identical polarization they will always exit at different ports, such that there will be exactly one photon in each output mode. If the two photons have opposite polarization they will exit at the same port, such that there will be two photons in one of the ports and therefore none in the other.*

transmitted, (3) the first particle is reflected and the second one is transmitted, and (4) the first one is transmitted and the second one is reflected. If the two photons have the same frequency and arrive at the BS simultaneously, we have to consider coherent superpositions of the amplitudes for these different possibilities.

For photons 1 and 2 passing through the BS their spatial modes will undergo a corresponding unitary transformation. The two-photon state thus evolves into

$$|\Psi\rangle_{12} = \tfrac{1}{\sqrt{2}} \quad \begin{aligned}&[(\alpha|H\rangle_1 + \beta|V\rangle_1)(i|c\rangle_1 + |d\rangle_1)\otimes \\ &(\gamma|H\rangle_2 + \delta|V\rangle_2)(|c\rangle_1 + i|d\rangle_1)]\end{aligned} \tag{2.4}$$

Because the total two-photon state, including spatial and spin part, needs to obey bosonic statistics, we also need to include its exchange wave function to symmetrize the state to the exchange of the labels 1 and 2. Such the final outgoing state is

$$|\Psi\rangle = |\Psi\rangle_{12} + |\Psi\rangle_{21} \tag{2.5}$$

After this transformation photons 1 and 2 are not distinguishable anymore. In the following we will see that we have produced a two-photon state which already allows us to project it onto a maximally polarization entangled state.

The polarizing beam splitter (PBS) has two spatial input modes a and b and two output modes c and d (Fig. 2.3). If a photonic qubit in the general state $|\Psi\rangle =$

$\alpha|H\rangle + \beta|V\rangle$is directed onto a PBS it will be found in the transmitted (reflected) beam with probability $|\alpha|^2$ ($|\beta|^2$)

$$\begin{array}{l}(\alpha|H\rangle + \beta|V\rangle)\,|a\rangle \rightarrow \alpha|H\rangle|c\rangle + i\beta|V\rangle|d\rangle \\ (\alpha|H\rangle + \beta|V\rangle)\,|b\rangle \rightarrow i\beta|V\rangle|c\rangle + \alpha|H\rangle|d\rangle\end{array} \tag{2.6}$$

where $|a\rangle$ ($|b\rangle$) describes the spatial quantum state of the photon in input beam $a(b)$. The PBS perfectly transmits (reflects) horizontally (vertically) polarized light. Here again, the factor i in front of the reflected term is a consequence of unity and corresponds to a phase jump upon reflection.

Thus the input state of the two photons will undergo the following transformation

$$\begin{array}{rl}|\Psi\rangle_{12} = \frac{1}{\sqrt{2}} & [(\alpha+\beta)|H\rangle_1|c\rangle_1|H\rangle_2|d\rangle_2 + i(\gamma+\delta)|H\rangle_1|c\rangle_1|V\rangle_2|c\rangle_2 \\ & +i(\gamma-\delta)|V\rangle_1|d\rangle_1|H\rangle_2|d\rangle_2 + (\alpha-\beta)|V\rangle_1|d\rangle_1|V\rangle_2|c\rangle_2]\end{array} \tag{2.7}$$

If the two photons incident into the beam splitter have identical polarization they will always exit in different directions, whereas if they carry orthogonal polarization they will both exit into the same output mode and none in the other. This way the PBS acts as a polarization comparer.

By placing two half wave plates (HWP) before the entrance facets of the PBS, we can retard the polarization of the input photons to the diagonal basis. Assuming the two incident photons are now both in the state $\frac{1}{\sqrt{2}}(|H\rangle + |V\rangle)$ the PBS acts the same way as the 50:50 BS. Thus also the PBS is suitable for creating entanglement.

With these simple optical elements, which exploit the concept of interference, large optical networks can be constructed to map an arbitrary input state onto an output state. In the following chapter we will discuss these quantum interference phenomena in more detail before we will proceed to discuss, what actually is entanglement.

2.2.2 Quantum Interference

The Hong-Ou-Mandel Interference

Quantum interference phenomena occur due to the indistinguishability of photons. Since photons obey the bosonic statistics, all interference effects which result from their indistinguishability can be obtained by the symmetrization of the amplitudes of the final state. Because the photons are not labelled their exchange will not lead to a change of the sign of their amplitude. It is convenient to describe the HOM interference in terms of the formalism of bosonic creation and annihilation operators, as its algebra already takes into account this symmetrization.

We start with the most elementary optical interference effect: the Hong-Ou-Mandel (HOM) interference at a beam splitter. This photon-photon interaction, which is also exploited in the standard projective BSM measurement, is required

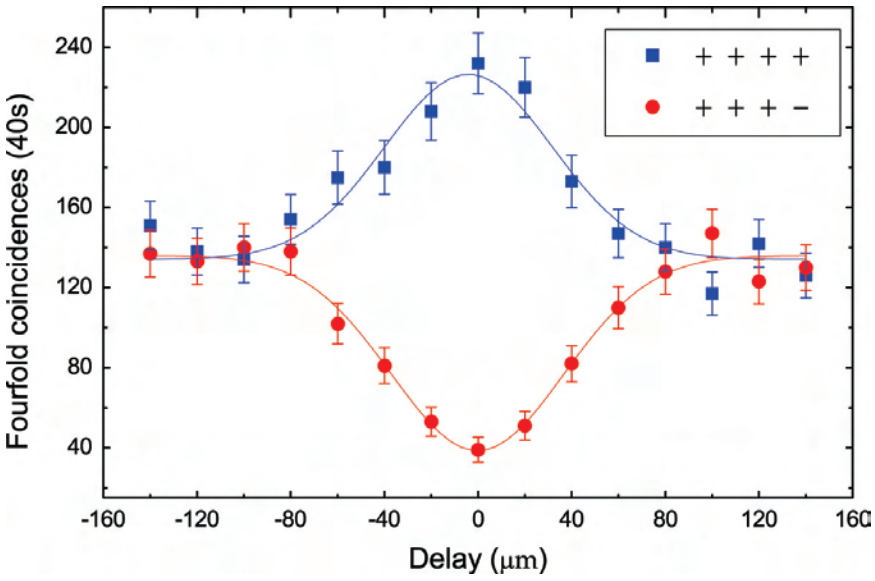

Figure 2.4: *Two-photon interference of "Hong-Ou-Mandel-dip " kind. Two photons, each from a pair in the Bell state $|\Phi^+\rangle$ are interfered on a PBS and detected in the diagonal basis. The remaining two photons are used as triggers to reduce noise contributions. The data points are fitted with Gaussian curves to guide the eye. Outside the coherence length there is no interference because of the temporal distinguishability. Maximum interference occurs at zero delay between the two photons at the interference PBS.*

for the realization of two photon quantum logic gates [29, 37]. As we have seen previously, upon reflection off a symmetric 50:50 beam splitter (we now call the input modes a_1 and a_2 and the output modes b_1 and b_2) a photon picks a phase shift i. Thus, if we have two spectrally identical photons arriving simultaneously at the opposite input ports $1, 2$ of the beam splitter, the initial state $\hat{a}_1^\dagger \hat{a}_2^\dagger |\Omega\rangle$ is transformed into

$$\frac{1}{\sqrt{2}}(\hat{a}_1^\dagger + i\hat{a}_2^\dagger)\frac{1}{\sqrt{2}}(\hat{a}_2^\dagger + i\hat{a}_1^\dagger)|\Omega\rangle = i\frac{1}{2}(\hat{a}_1^{\dagger 2} + \hat{a}_2^{\dagger 2})|\Omega\rangle.$$

Since $i^2 = -1$, which results in the cancellation of the two terms describing the cases, in which the photons exit through different exit ports. This cancellation occurs due to the assumed perfect indistinguishability of the two photons $\hat{a}_1\hat{a}_2 = \hat{a}_2\hat{a}_1$. The final state reads $i\frac{1}{2}[(\hat{a}_1^\dagger)^2 + (\hat{a}_2^\dagger)^2]|\Omega\rangle$, namely, the two photons will exit the BS at the same output port. The so-called photon's bunching effect due to the bosonic character of photons will thus not allow any coincidences between the output ports.

If the photons are not indistinguishable we shall describe them by annihilation operators $\hat{a}$ and $\hat{b}$), so that the initial state is given by $\hat{a}_1^\dagger \hat{b}_2^\dagger |\Omega\rangle$. Since $a \neq b$ there is no cancellation of the terms, also the terms $\frac{1}{2}(\hat{a}_1^\dagger \hat{b}_2^\dagger - \hat{a}_2^\dagger \hat{b}_1^\dagger)|\Omega\rangle$, in which each photon exits through a different exit port contribute. Therefore the Hong-Ou-Mandel effect, which depends entirely on the indistinguishability of photons, will not appear.

The bunching effect of two photons described above constitutes the basis of the Hong-Ou-Mandel dip in coincidences recorded between two single-photon detectors in modes b_1 and b_2 as function of the flight time difference of the incident photons; no coincidence can be observed for zero flight time difference for the usual symmetric spatial state of the two photons. The two incident photons can also be in an antisymmetric spatial state (which occurs if the two-photon polarization state is also antisymmetric). In this case, the two amplitudes interfere constructively. This results in the two photons always exiting in separate beams for zero flight time difference, namely, a coincidence peak instead of dip appears. This effect is thus called photon anti-bunching.

As discussed in the previous chapter it is also possible to create quantum interference at a PBS. In this case we will also find a similar kind of HOM dip. The dip shown in Fig. 2.4 is recorded at one of our interference PBS. In the experiment a translation stage with a resolution of 0.5 nm allows us to adjust the flight time difference between the interferometric arms.

2.2.3 Bipartite Entanglement and Bell-States

We have seen in the chapter 2.2.1 that we can use the HOM interference at a BS or PBS to make two single photons indistinguishable. In the following we will define what a so called maximally entangled state is and discuss its fascinating features, as bipartite system already allow to observe many of these fascinating features of quantum entanglement and observe some fundamental predictions of QM. Moreover we will see, that many operations in QIP can be reduced to two particle operations.

We start with the most simple case, the entanglement of two single particles, called bipartite entanglement. As we have seen in the previous two sections, by interfering two spectrally identical photons at a BS we can make them indistinguishable and delete any information about the input port of the photon (Welcher-Weg-Information). The full expansion of the final outgoing state behind the BS given by Eq. 2.5 is

$$\begin{aligned}|\Psi\rangle = \tfrac{1}{2\sqrt{2}}[&(\alpha\gamma+\beta\delta)(|H\rangle_1|H\rangle_2+|V\rangle_1|V\rangle)_2 \times i(|c\rangle_1|c\rangle_2+|d\rangle_1|d\rangle_2)\\ &+(\alpha\gamma-\beta\delta)(|H\rangle_1|H\rangle_2-|V\rangle_1|V\rangle_2)\times i(|c\rangle_1|c\rangle_2+|d\rangle_1|d\rangle_2)\\ &+(\alpha\delta+\beta\gamma)(|H\rangle_1|V\rangle_2+|V\rangle_1|H\rangle_2)\times i(|c\rangle_1|c\rangle_2+|d\rangle_1|d\rangle_2)\\ &+(\alpha\delta+\beta\gamma)(|H\rangle_1|V\rangle_2-|V\rangle_1|H\rangle_2)\times(|d\rangle_1|c\rangle_2-|c\rangle_1|d\rangle_2)].\end{aligned} \tag{2.8}$$

The combined state of two qubits forms a four-dimensional Hilbert space. It can be easily seen, that by applying an appropriate measurement protocol the resulting two-photon state can be projected onto any of the four maximally entangled Bell-states

$$\begin{aligned}|\Phi^{\pm}\rangle_{12} &= \frac{1}{\sqrt{2}}(|H\rangle_1|H\rangle_2 \pm |V\rangle_1|V\rangle_2)\\ |\Psi^{\pm}\rangle_{12} &= \frac{1}{\sqrt{2}}(|H\rangle_1|V\rangle_2 \pm |V\rangle_1|H\rangle_2)\end{aligned} \tag{2.9}$$

The Bell states can not be expressed as a product of two single-particle wave functions. Particles in a Bell state are thus non-separable, they are entangled!

To emphasize the importance of this characteristic we will perform a little Gedanken-experiment. Let us assume that two friends, in QIP commonly known as Alice and Bob, choose to share a pair of qubits that are in the entangled Bell state $|\Phi^+\rangle$ (e.g. polarization-entangled photons or spin-entangled electrons). Now Alice chooses to measure her qubit in the computational basis yielding either a $|H\rangle$ or $|V\rangle$ with equal probability. However, since her qubit was originally entangled with Bob's qubit, the combined state collapses to one of the two separable terms of $|\Phi^+\rangle$ ($|H\rangle|H\rangle$ or $|V\rangle|V\rangle$). Therefore, Bob's measurement will now with certainty yield the same result that Alice has obtained. In other words, Alice's measurement has changed the combined state and thereby the state of Bob's qubit.

Either one of Alice and Bob can transform the combined system to another Bell state without any help or even knowledge of the other, just by applying a local (only at her/his side) unitary (LU) Pauli operation

$$\begin{aligned}\hat{I} &= \begin{pmatrix}1 & 0\\ 0 & 1\end{pmatrix}, \quad \hat{\sigma}_x = \begin{pmatrix}0 & 1\\ 1 & 0\end{pmatrix},\\ \hat{\sigma}_y &= \begin{pmatrix}1 & 0\\ 0 & -1\end{pmatrix}, \quad \hat{\sigma}_z = \begin{pmatrix}0 & -1\\ 1 & 0\end{pmatrix}\end{aligned} \tag{2.10}$$

If, for example, Alice wants to change the state from $|\Phi^+\rangle$ to $|\Phi^-\rangle$, all she needs to do, is to apply a unitary $\hat{\sigma}_z$ Pauli operation to her qubit. Likewise, she can transform the state into the other two Bell states by applying a $\hat{\sigma}_x$ or $\hat{\sigma}_y$ operation, respectively. The Bell states are thus equivalent under LU.

One may now claim that the same results could have been obtained by simply using a machine that randomly distributes a pair of equal classical bits to Alice and Bob. Then Alice's result is again completely random and is always in a perfect correlation to Bob's result. However, if Alice and Bob are also allowed to measure their qubit in the diagonal basis, things become different. Some measurement results can no longer be explained by classical physics. To understand this, consider the following scenario: Alice and Bob again share a pair of qubits in the state $|\Phi^+\rangle$. They now choose to measure their qubit in the computational or diagonal basis independently of each other. There are thus four possible combinations:

	Alice's choice of basis	Bob's choice of basis	measurement results are
1	$\|0\rangle/\|1\rangle$	$\|0\rangle/\|1\rangle$	correlated
2	$\|0\rangle/\|1\rangle$	$\|+\rangle/\|-\rangle$	not correlated
3	$\|+\rangle/\|-\rangle$	$\|0\rangle/\|1\rangle$	not correlated
4	$\|+\rangle/\|-\rangle$	$\|+\rangle/\|-\rangle$	correlated

(2.11)

The first row describes the case already discussed above. In the second case Alice's measurement again projects the combined state onto $|0\rangle|0\rangle$ or $|1\rangle|1\rangle$. However, since Bob now decides to measure in the diagonal basis, he obtains $|+\rangle$ or $|-\rangle$ with equal probability. Alice's and his results are thus not correlated. The argument for the third case works analogous. The measurement results in the last case on the other hand are perfectly correlated. These results become obvious by rewriting $|\Phi^+\rangle$ in the diagonal basis:

$$|\Phi^+\rangle = \frac{1}{\sqrt{2}}(|+\rangle|+\rangle + |-\rangle|-\rangle) \tag{2.12}$$

Since Alice and Bob both measure in the diagonal basis, this case is identical to the first case up to a simple transformation of basis. However, under no circumstances are we able to construct a classical machine that yields the combined measurement results for the four cases of Table (2.11).

The projection of the combined state by Alice's measurement acts instantaneous and is completely independent of the distance between Alice and Bob and such was considered as a "spooky action at a distance" violating locality. Or, as Einstein, Podolsky and Rosen (EPR) [5] argued, that a physical property of a system cannot be considered real if its value is undefined until measurement, and therefore entanglement contradicts realism.

However, in our above example the value of Alice's qubit is undefined until she decides to measure it. Alice's measurement forces the combined state to collapse and thereby changes the state of Bob's qubit independently of Bob's location. Due to this controversy EPR reasoned that quantum mechanics (QM) must be incomplete.

This contradiction is called the EPR paradox. To solve this problem, local hidden variable theories (LHV) were suggested. The idea is that all properties of a physical system are well defined at all times by a set of variables that is not or not yet accessible to us. Hence, no outcome of a measurement is random, but already predetermined by these variables. In 1964, Bell proposed an experimental test [6] for LHV theories that were considered to complement QM and thus to circumvent its counterintuitive characteristics. He noticed that the expectation values for any LHV and QM differ for specific sets of measurements. More precisely, he formulated an inequality, which holds for any LHV, but is allowed to be violated by QM. This "Bell inequality" was first violated experimentally by Aspect et al. in 1982 [7, 8, 9].

However, there are two technical limitations that impose severe drawbacks on most experimental setups and in principal leave the back door open for some other interpretation than the quantum mechanical one.

1. *The detector efficiency loophole.* In many setups based on photons, photodetectors detect photons only in a fraction of the experiments, while those experiments in which there are no photons detected (no "clicks") go unnoticed. We assume, naturally, that the unnoticed experiments have the same statistical properties as the noticed ones. However, a so far unknown mechanism could cheat us in this respect. It could happen, that all the experiments together would not violate a Bell inequality, however, the subset, for which our detectors click, violate it [38].

2. *The locality loophole.* Ideally, before each correlation measurement the circuits connected to the detectors should decide locally which operator to measure. This has to be done such that the detectors cannot communicate their choice if we assume that the speed of this communication cannot be larger than the speed of light. In practice this means that the event of deciding the measurement direction for one of the detectors must be space-like separated from event of reading out the measurement on the other detector.

When we experimentally test Bell Inequality, these two loopholes make it in principle still possible that the experimental results can be explained with a LHV model. Closing these loopholes still is a technically challenging task.

Note that despite the violation of realism and locality, quantum entanglement can not be used to contradict special relativity. Since it still requires a classical communication channel Bob to learn anything about Alice's measurement, superluminal information transfer is not possible.

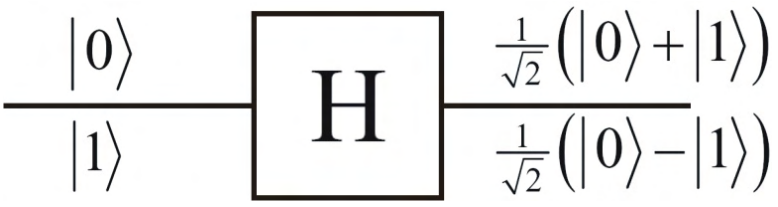

Figure 2.5: *Hadamard gate. The unitary single-qubit gate transforms states from the computational basis to the diagonal basis.*

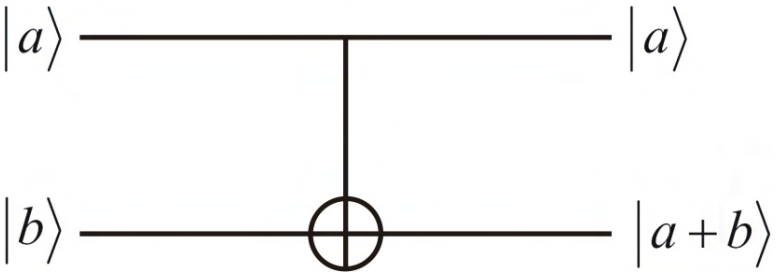

Figure 2.6: *Controlled-NOT (C-NOT) gate. The unitary two-qubit gate flips the second qubit (target) under the condition that the first qubit (control) is a* $|1\rangle$.

Preparation of Bell-States

Any change introduced to a quantum state when passing through an optical circuit can be described using the language of quantum computation. Analogous to the way a classical computer is build from an electrical circuit containing electric wires and logic gates, a quantum computer is build from a quantum circuit containing wires and quantum gates to transfer and manipulate the quantum state. To introduce this concept, in this section we will describe the quantum circuit, which is able to create and measure a Bell state.

In many QIP protocols particle pairs in one of the four Bell states are used as an entanglement resource. Also projective measurements of particles onto the Bell basis are performed to entangle other particles, which can be spatially separated and do not share a common past. The properties of the individual qubits of an maximally entangled pair are completely undefined. Since it is not straight forward to prepare (or to identify) them, a quantum circuit consisting of Hadamard and controlled-NOT gates is needed for this task. The action of a Hadamard gate (Fig. 2.5) is equivalent to the following unitary transformation

$$\begin{aligned} |0\rangle &\rightarrow \frac{1}{\sqrt{2}}(|0\rangle + |1\rangle) \\ |1\rangle &\rightarrow \frac{1}{\sqrt{2}}(|0\rangle - |1\rangle) \end{aligned} \tag{2.13}$$

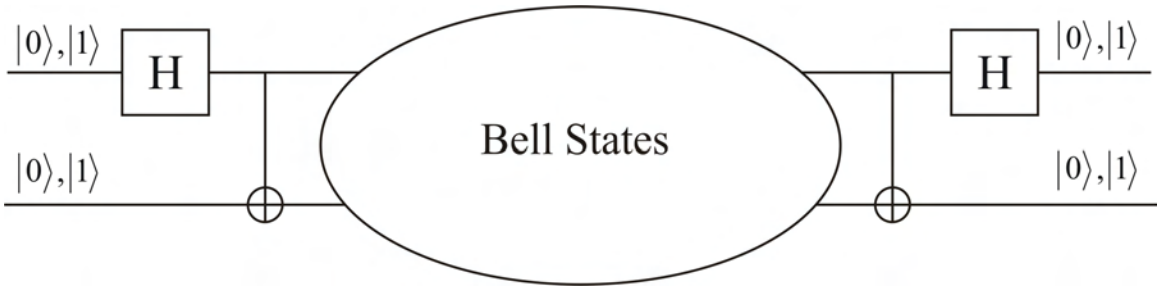

Figure 2.7: *Quantum circuit for generation and detection of Bell states. The inputs and outputs are two qubits in the computational basis, respectively.*

The controlled-NOT (C-NOT) gate (Fig. 2.6) flips the second of two qubits, if and only if the first is $|1\rangle$, namely

$$\begin{aligned} |0\rangle|0\rangle &\rightarrow |0\rangle|0\rangle \\ |0\rangle|1\rangle &\rightarrow |0\rangle|1\rangle \\ |1\rangle|0\rangle &\rightarrow |1\rangle|1\rangle \\ |1\rangle|1\rangle &\rightarrow |1\rangle|0\rangle. \end{aligned} \tag{2.14}$$

Now consider the network shown in Fig. (2.7). Under the action of the gates on the left-hand side of the network, the input two-qubit states will undergo a series of unitary transformations. For example, after passing through the two gates the input state $|0\rangle|0\rangle$, will be transformed into:

$$\begin{aligned} |0\rangle|0\rangle \quad &\overset{Hadamard}{- - - \longrightarrow} \quad \tfrac{1}{\sqrt{2}}\left(|0\rangle|0\rangle + |1\rangle|0\rangle\right) \\ &\overset{C-NOT}{- - - \longrightarrow} \quad \tfrac{1}{\sqrt{2}}\left(|0\rangle|0\rangle| + |1\rangle|1\rangle\right) \quad = \quad |\Phi^+\rangle \end{aligned} \tag{2.15}$$

We have thus been able to create one of the four Bell states. Correspondingly, the network can prepare the two qubits in one of the remaining three Bell states:

$$\begin{aligned} |1\rangle|0\rangle &\longrightarrow \frac{1}{\sqrt{2}}\left(|0\rangle|0\rangle| - |1\rangle|1\rangle\right) = \left|\Phi^-\right\rangle \\ |0\rangle|1\rangle &\longrightarrow \frac{1}{\sqrt{2}}\left(|0\rangle|1\rangle| + |1\rangle|0\rangle\right) = \left|\Psi^+\right\rangle \\ |1\rangle|1\rangle &\longrightarrow \frac{1}{\sqrt{2}}\left(|0\rangle|1\rangle| - |1\rangle|0\rangle\right) = \left|\Psi^-\right\rangle \end{aligned} \tag{2.16}$$

The right hand side of the network shown in Fig. 2.7 then corresponds to the measurement of the Bell state by disentangling the state. This way the Bell measurement is reduced to two single particle measurements.

Before we proceed to the creation of multi-partite entanglement we will first introduce a source for bipartite entanglement, that we used in all experiments throughout this thesis. Bipartite entanglement can be generated by an decay process of a single photon inside a non-linear crystal. The output of this decay process will be a pair of photons in a maximally entangled Bell state. After detailed discussion of the conversion process and the technical requirements, that are needed to build such a source, we will afterwards continue with the discussion how one can use these maximally entangled pairs to construct multipartite entanglement.

2.3 Generation of Entanglement

In the previous chapters we have seen that entanglement can be generated from single photons by applying an appropriate optical circuit. But there exists also a source, which produces photons in a maximally entangled state, provided we obey some technical conditions, e.g. filtering spatial and frequency modes.

2.3.1 Spontaneous Parametric Down Conversion (SPDC)

In this section, we will describe the process of spontaneous parametric down-conversion, the source for entangled photon pairs that was used for all experiments performed in the course of this thesis. SPDC is still the best source for producing entangled photon pairs with sufficient intensity and in good purity. In the experiment, the desired polarization-entangled state is produced directly out of a single nonlinear crystal [BBO (β-barium-borate)], which is a non-centrosymmetric crystal with nonlinear electric susceptibility. In such a medium, an incoming photon can decay inside the crystal with relatively small probability of $p \approx 0.001$ into two photons in a way that energy and momentum are conserved. In the following we will describe a simple technique to produce polarization-entangled photon pairs using the process of non-collinear type-II parametric down-conversion [30].

The generated photons are emitted into two cones with opposite polarizations (Fig. 2.8) while their emission directions [30, 39] always add up to the momentum of the pump photon. Thus, the emission direction of each individual photon is completely uncertain within the cone, but once one photon is registered, and thus its emission direction is defined, the other photon is found just exactly opposite with respect to the pump beam on the other cone. Thus, at the intersections $\hat{a}$ and $\hat{b}$ the polarization of neither photon is defined, but what is defined is the fact that the two photons have to have different polarizations.

Of course, during the SPDC process also more than one entangled photon pair can be generated. The Hamiltonian governing the down-conversion process in the weak conversion regime describes two independent processes: the generation and the annihilation of a photon pair in the output modes $\hat{a}_x; \hat{b}_y$ or $\hat{a}_y; \hat{b}_x$, where indices x and y denote the polarization. The two processes add coherently with opposite

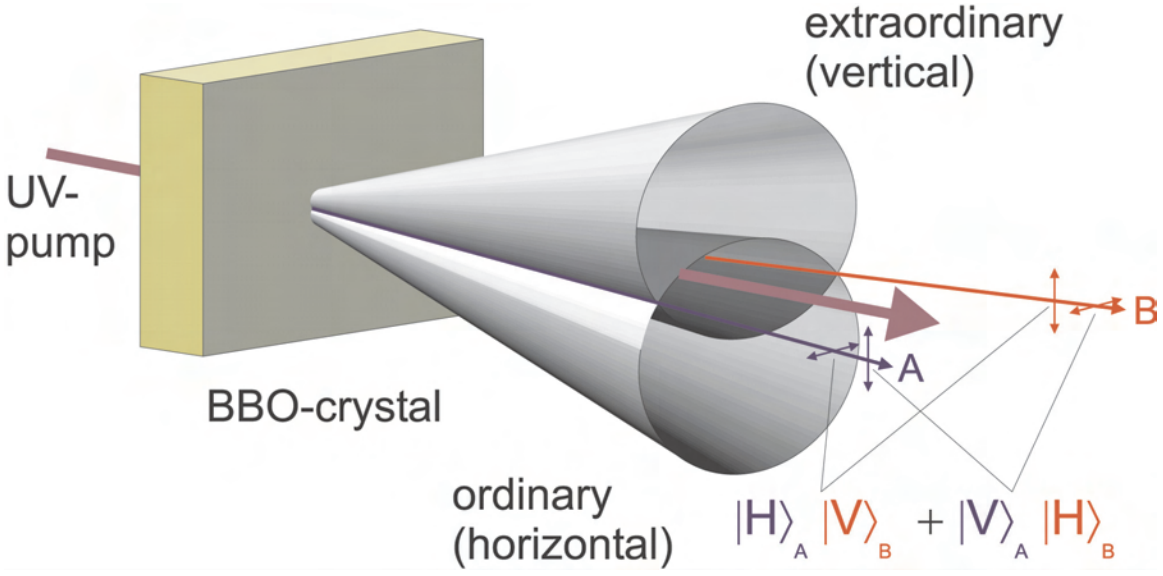

Figure 2.8: *Principle of type-II parametric down-conversion from a β-barium-borate crystal (BBO). Inside the nonlinear crystal the incoming pump photon decays spontaneously (with a probability of $p \approx 0.001$) into two photons. The two down-converted photons are emitted into cones with orthogonal polarization. Each photon is e. The photon of the top cone is vertically polarized while its exactly opposite partner in the bottom cone is horizontally polarized. At the intersection of the cones their polarizations are undefined; all that is known is that they have to be different, which results in polarization entanglement between the two photons in intersections A and B.*

probability amplitudes. Assuming the effective dimensionless interaction time of the UV pulse in the photonic crystal is r, we can decompose the output state into terms that contain a fixed number of down-converted photons [40, 41]

$$|\Psi\rangle = \exp[r(\hat{a}_x^\dagger \hat{b}_y^\dagger - \hat{a}_x \hat{b}_y) - r(\hat{a}_y^\dagger \hat{b}_x^\dagger - \hat{a}_y \hat{b}_x)]|vac\rangle \tag{2.17}$$

$$= \sum_{n=0}^{\inf} \lambda_n |\Psi_n\rangle \tag{2.18}$$

with

$$\lambda_n = \sqrt{n+1}(\tanh^n r / \cosh^2 r). \tag{2.19}$$

being the probability amplitude of generating n photon pairs. From Eq. 2.18 one can see that the complete emission of the down conversion process is a superposition of all n-pair emissions.

The value for the dimensionless interaction parameter r is not easy to obtain theoretically, since it contains many parameters that depend on the structure of the crystal and its non-linear properties. That's why we derived the value for λ_1 from our experimental one pair rate per second according to

$$\lambda_{n,exp} = \left(\frac{\#\text{ coinc/s}}{\#\text{ pulses/s}}\right)^n \times \left(\frac{1}{(\text{detection efficiency})^2}\right)^n$$

For $n = 1$ just multiplying the number of two photon coincidences per pulse with the 1/detection efficiency for the pair (we only detect a fraction of the generated photons) will leave us with the creation probability for one pair. The number of pulses per second is determined by the repetition rate of the laser. From λ_1 we then calculated r. The probabilities for higher order emission can also be calculated by Eq. 2.3.1 assuming that, as a first order approximation, for the creation probability of n pairs holds $p_n = p_1^n$.

From the theoretical formular given in Eq. 2.19 (using the experimentally derived value for r), as well as from Eq. 2.3.1 using only the experimental values, we will obtain the following probabilities λ_n for the emission of $n = 1, 2, 3, 4$ pairs per UV pulse:

λ_n	theoretical estimation	experiment value
λ_1	0.0467	0.0468
λ_2	0.00172	0.00219
λ_3	0.00000565	0.0000102
λ_4	0.000001738	0.00000479

The result shows that our experimental values are in the same order as the theoretically calculated values using an experimentally derived value for r.

Starting from Eq. 2.18 the normalized n-pair wave function then takes the following form

$$|\Psi_n\rangle = \frac{1}{\sqrt{n+1}} \sum_{m=0}^{n} (-1)^m |n-m, m; m, n-m\rangle \tag{2.20}$$

$$= \frac{1}{n!\sqrt{n+1}} (\hat{a}_x^\dagger \hat{b}_y^\dagger - \hat{a}_y^\dagger \hat{b}_x^\dagger)^n |vac\rangle. \tag{2.21}$$

The occupation numbers n, m in the first line correspond to the to the ordering of the modes as $|\hat{a}_x, \hat{a}_y; \hat{b}_x, \hat{b}_y\rangle$. So the total quantum mechanical state of the SPDC emission is a superposition of all n^{th} order pairs in the emission modes.

For simplicity, let's step back to the case $n = 1$: Measurement on each of the individual photons is totally random and gives with equal probability vertical or horizontal polarization. But once one photon, for example photon A, is measured, the polarization of the other photon B must be orthogonal! Choosing an appropriate basis, e.g. $|H\rangle$ and $|V\rangle$, the state at the two intersections A and B is thus a superposition of $|H\rangle|V\rangle$ and $|V\rangle|H\rangle$

$$\frac{1}{\sqrt{2}} (|H\rangle_A |V\rangle_B + e^{i\alpha} |V\rangle_A |H\rangle_B) \tag{2.22}$$

where the relative phase α arises from the crystal birefringence and an overall phase shift is omitted.

Using an additional birefringent phase shifter the value of α can be adjusted, e.g. to the values 0 or π. A net phase shift of π may be obtained by a 90° rotation of a quarter wave plate in one of the paths. Similarly, a half wave plate in one path can be used to change horizontal polarization to vertical and vice versa. One can thus very easily produce any of the four Bell states of Eq's. (2.9).

The birefringent nature of the down-conversion crystal complicates the actual entangled state produced, since the ordinary (o) and extraordinary (e) photons have different velocities inside the crystal, and propagate along different directions even though they become collinear outside the crystal. The resulting longitudinal and spatial walk-offs between the two terms in the state of Eq. (2.22) are maximal for pairs created near the entrance face, which consequently acquire a relative time delay $\delta T = L(1/u_o - 1/u_e)$ (L is the crystal length, and u_o and u_e are the ordinary and extraordinary group velocities, respectively) and a relative lateral displacement $d = L \tan \rho$ (ρ is the angle between the ordinary and extraordinary beams inside the crystal). If the longitudinal walk-off $\delta T \geq \tau_c$, the coherence time of the down-conversion light, then the terms in Eq. (2.22) become, in principle, distinguishable by the order in which the detectors would fire, and no interference will be observable.

Similarly, if d is larger than the coherence width, the terms can become partially labelled by their spatial location.

Because the photons are produced coherently along the entire length of the crystal, one can completely compensate for the spatial and longitudinal walk-off [42]. After compensation, interference occurs pairwise between processes where the photon pair is created at distances $\pm x$ from the middle of the crystal. The ideal compensation is to use two crystals, one in each path, which are identical to the down-conversion crystal, but only half as thick. If the polarization of the light is first rotated by 90° (e.g. with a half wave plate) and then send through the compensation crystals, which are oriented along the same direction as the down conversion crystal itself, the retardation between the o and e components is exchanged and complete spatial and temporal indistinguishability is restored. In the following experiments we always slightly tilted the orientation of one of the compensation crystals to tune the relative phase $\alpha = \pi$.

The BBO crystal in our experiments is 2.0mm thick and was cut at $\theta_{pm} = 43.5°$ (the angle between the crystal optical axis and the direction of the pump beam). To optimize the coupling efficiency, the cones have to intersect with orthogonal tangents, which was the case, if the cone-overlap directions and the direction of the pump beam include a 3°. The transverse walk-off d (0.2mm) was negligible compared to the coherent pump beam width (2mm). However, it was necessary to compensate for longitudinal walk-off of $\delta T = 260$fs, while the coherence length τ_c, determined by the interference filters centered at 780nm and a bandwidth of 3.2nm (FWHM), was at about of the same order. Therefore we used an additional BBO crystal of 1.0mm thickness ($\theta_{pm} = 43.5°$) in each path, preceded by a half wave plate to exchange the roles of the horizontal and vertical polarizations.

2.3.2 A Stable High-Intensity Entangled Photon Source

Photons are robust against de-coherence and high precision unitary transformations on photons can be carried out with linear optical devices, while various efforts have been made to greatly improve the brightness and stability of the entangled photon sources. Therefore in the presented experiments we chose to use polarization-entangled photon pairs generated by parametric down-conversion [30].

A natural way to obtain a brighter entangled photon source is to increase the power of the ultraviolet (UV) light necessary for parametric down-conversion. To achieve this, we needed a more powerful ultra-fast infrared (IR) laser system for the up-conversion process: we have used an all-solid-state CW laser Verdi-V18 to pump a modified mode-locked Ti:sapphire laser system Mira900-HP (Mira) as is shown in Fig. (2.9). Unfortunately, a brighter pump laser into the Mira cavity will make the output IR pulse unstable. A new output coupler with higher transmission efficiency is used in the cavity to stabilize the output laser. Moreover, we constantly flush the Mira's Ti:sapphire crystal with nitrogen of highest purity in order to keep it clean,

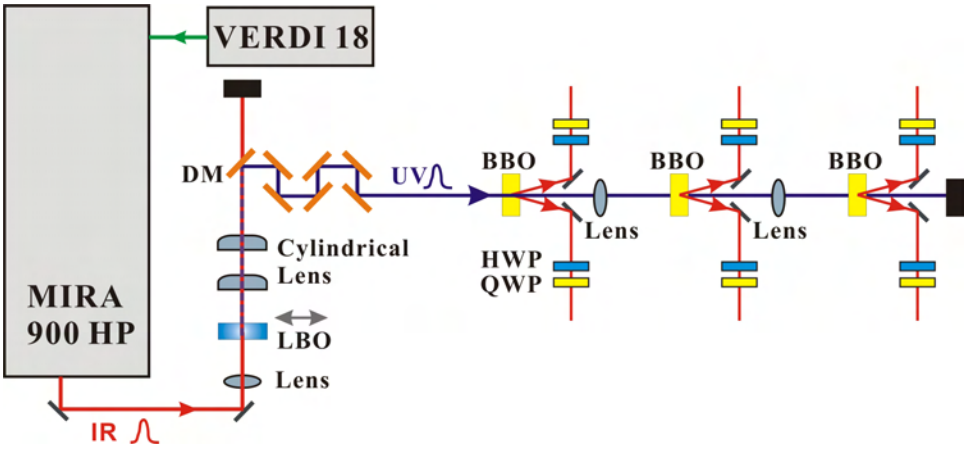

Figure 2.9: *Method to increase the power of the ultraviolet (UV) light. A modified mode-locked Ti:sapphire laser (MIRA), pumped with an all-solid-state CW laser Verdi-V18 (operating at 14W), is used to produce high-intensity ultra-fast infrared (IR) light pulses. The IR light pulse passes through the LBO crystal to generate via up-conversion the UV pulse necessary for parametric down-conversion. Behind the LBO, two cylindrical lenses with orthogonal axes, (one horizontal and one vertical) are used to shape and focus the ultraviolet beam and five dichroic mirrors (DM) are used to separate the UV from the IR light.*

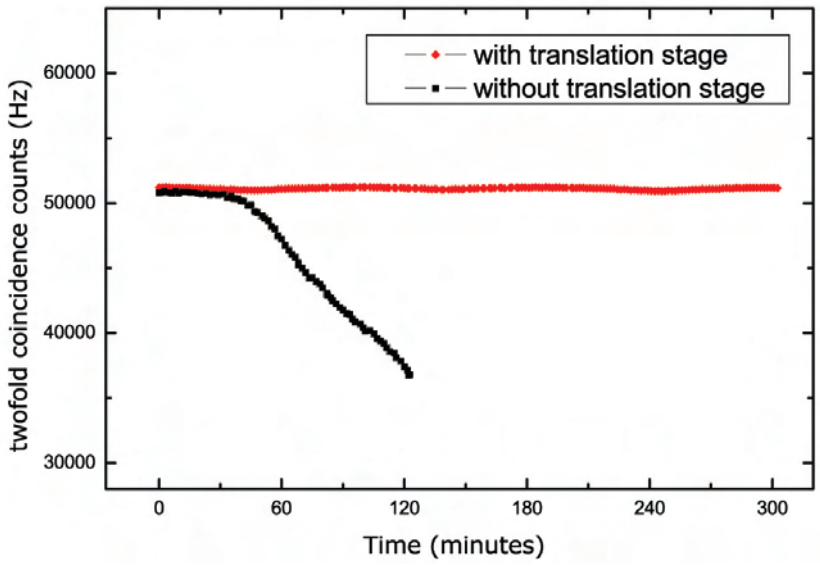

Figure 2.10: *Performance of the LBO crystal. Measured two-fold coincidences with and without moving the translation stage of the LBO up-conversion crystal over time.*

have constantly low humidity and provide highest temperature stability in addition to the improved water cooling cycle. After these innovations, we achieved an ultra fast IR pulse with an output power of about 2.9W with the Verdi-V18 operated at 14W, which is almost twice as high as before.

The high power IR pulse was properly focussed on a LiB_3O_5 (LBO) crystal to achieve the best up-conversion efficiency. To avoid damage to the LBO, caused by the focussed laser beam, the LBO is mounted on a motorized translation stage and will be moved by a distance of 10 μm to another point once the reference - single count rate of chosen detector - is below a certain threshold. To demonstrate the advantage of this technique, we measure the two-fold coincidence count rates over time, first without and then with moving the translation stage of the LBO. As can be observed in Fig. (2.10), our feedback control system greatly improves the stability of the down-conversion rates. Since back-reflection of the LBO into the Mira system can destroy the mode-lock condition, perfect control of the LBO motion is crucial.

Due to the brighter IR pulse we needed better filtering to separate the UV from the IR light. Therefore we installed two additional dichroic mirrors (to have a total of seven) in comparison to former experiments, to decrease the IR noise introduced into our experimental cycle.

To have a better collection efficiency of entangled photon pairs, we significantly shortened the distance between the BBOs and the fiber couplers to make our setup more compact. The best collection efficiency was achieved at a distance of 55 cm. Besides the improvement in collection efficiency, a compact setup also helps to significantly improve the stability, especially for the interferometer based experiments.

In the experiments, which use more than one BBO we optimized the collection efficiency for all three entangled photon pairs by choosing a 10 cm focus lens between the BBOs to refocus the ultraviolet pulse, such that it has the same beam parameters in all BBO pumping processes. As we discovered stability problems with the 20 cm radius concave mirror behind the second BBO, we later on exchanged this one by an additional 10 cm lens and at third BBO to create the third pair. With these modifications, we achieved a stable high-intensity entangled photon source.

2.4 Multipartite Entanglement

The interest to create and observe entanglement of more than two particles originates from the possibility to observe dramatic conflicts between on the one hand side EPR's ideas and local realism and quantum mechanics on the other side [43]. Tests of quantum mechanics that are conceptually different from standard bipartite Bell tests become possible with multipartite entanglement. For example all-versus-nothing tests with tripartite systems do not violate any inequalities but yield expectation values that are genuinely different for quantum and classical physics [44, 45]. Besides the interest in fundamental physics, multipartite entanglement attracts a lot of research as it is the most important resource for many quantum computation algo-

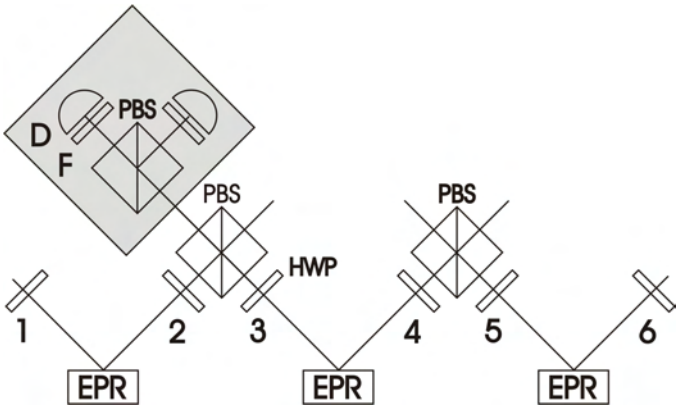

Figure 2.11: *Six-photon polarization entanglement source. Two diagonally polarized photons, one at* $= 45°$ *and one at* $-45°$*, originating from an entangled pair each are interfered on a PBS. Due to the fact that a PBS always transmits horizontally polarized and reflects vertically polarized light, a signal in all six output modes detects the occurrence of a six-photon GHZ-state. F denotes the narrow band width filters, D the detectors.*

rithms and protocols such as Grover's search algorithm for unsorted databases [46], Shor's algorithm for factoring large numbers [23] and the Deutsch-Jozsa algorithm [47].

2.4.1 Construction of multi-photon entanglement

While for the implementation of the heralded entanglement source we used a higher order emission of the SPDC process from one photonic crystal, for the other multi-photon experiments performed throughout this thesis we constructed the multi-photon entanglement by interfering photons from different SPDC pairs according to the scheme presented in Fig. 2.12

As discussed in chapters 2.2.1, 2.2.2 and 2.2.3 the interference of two photons on a BS or a PBS will delete any information about the origin of the single photon and result in an entangled two-photon state. In our experiments we used an extension of the scheme to create four-photon polarization entanglement, which was originally proposed by Zeilinger et al. and first implemented by Pan and Zeilinger [48, 49]

To explain the working principle we start with the emission of only two EPR sources: for simplicity consider the two sources emitting one pair each in the same entangled state $\frac{1}{\sqrt{2}}(|H\rangle|H\rangle + |V\rangle|V\rangle)$. Interfering two photons, one photon from each pair, at a PBS will result in the state

$$\begin{aligned} &\tfrac{1}{2}(|H_1\rangle|H_2\rangle|H_3\rangle|H_4\rangle + |V_1\rangle|V_2\rangle|V_3\rangle|V_4\rangle \\ &+|H_1\rangle|H_2\rangle|V_3\rangle|V_4\rangle + |V_1\rangle|V_2\rangle|H_3\rangle|H_4\rangle). \end{aligned} \tag{2.23}$$

Only for the superposition $|H_1\rangle|H_2\rangle|H_3\rangle|H_4\rangle + |V_1\rangle|V_2\rangle|V_3\rangle|V_4\rangle$ we will observe a fourfold coincidence in the appropriate detectors (either only all detectors detecting H or only all detectors detecting V fire) each of the four arms. For the moment it is sufficient to know that this state resembles a four-photon Greenberger-Horne-Zeilinger (GHZ) state [44]. In the following chapter we will define, what a GHZ state is and discuss its properties. Experimentally we cannot distinguish the GHZ state from the really prepared full state due to the finite detector efficiency. Even if we would be able to only generate full GHZ states we could only detect a fraction of them. Thus we conclude that a conditional GHZ state is sufficient to experimentally demonstrate all features of a full four-particle GHZ state.

Now we can easily extend this scheme to six photons: adding another EPR source emitting a third photon pair in the state $\frac{1}{\sqrt{2}}(|H\rangle|H\rangle+|V\rangle|V\rangle)$ and following the same procedure will also allow us to prepare

$$\begin{aligned}
&\tfrac{1}{2}(|H_1\rangle|H_2\rangle|H_3\rangle|H_4\rangle + |V_1\rangle|V_2\rangle|V_3\rangle|V_4\rangle \\
&+|H_1\rangle|H_2\rangle|V_3\rangle|V_4\rangle + |V_1\rangle|V_2\rangle|H_3\rangle|H_4\rangle) \quad \bigotimes \quad \tfrac{1}{\sqrt{2}}(|H\rangle|H\rangle + |V\rangle|V\rangle)
\end{aligned}$$

$$\begin{aligned}
= \tfrac{1}{2\sqrt{2}}&(|H_1\rangle|H_2\rangle|H_3\rangle|H_4\rangle|H_5\rangle|H_6\rangle + |V_1\rangle|V_2\rangle|V_3\rangle|V_4\rangle|V_5\rangle|V_6\rangle \\
&+|V_1\rangle|V_2\rangle|V_3\rangle|V_4\rangle|H_5\rangle|H_6\rangle + |H_1\rangle|H_2\rangle|V_3\rangle|V_4\rangle|H_5\rangle|H_6\rangle \\
&+|V_1\rangle|V_2\rangle|H_3\rangle|H_4\rangle|H_5\rangle|H_6\rangle + |H_1\rangle|H_2\rangle|H_3\rangle|H_4\rangle|V_5\rangle|V_6\rangle \\
&+|H_1\rangle|H_2\rangle|V_3\rangle|V_4\rangle|V_5\rangle|V_6\rangle + |V_1\rangle|V_2\rangle|H_3\rangle|H_4\rangle|V_5\rangle|V_6\rangle) \qquad (2.24)
\end{aligned}$$

Here only for the superposition $|H_1\rangle|H_2\rangle|H_3\rangle|H_4\rangle|H_5\rangle|H_6\rangle+|V_1\rangle|V_2\rangle|V_3\rangle|V_4\rangle|V_5\rangle|V_6\rangle$, which resembles a six-photon Greenberger-Horne-Zeilinger (GHZ) state, we will observe a sixfold coincidence in all the appropriate detectors (either only all detectors detecting H or only all detectors detecting V fire) each of the six arms.

To ensure that when detecting the photons at least some of them cannot be identified anymore, neither on the basis of their path nor their creation time, we moreover have to ensure that their coherence time will be artificially prolonged by using the appropriate narrow band with filters to be larger than the pulse length, during which they were created. This we achieve by using the appropriate narrow band with filters (F) before the detectors.

2.4.2 Classes of Multipartite Entanglement

Multipartite entanglement is genuinely different from entanglement in quantum systems consisting of two parts: In contrast to bipartite systems, multipartite systems may contain different types of entanglement. The complexity of a physical system grows exponentially with the number of its dimensions or degrees of freedom. To illustrate this difference, let us consider a quantum system that is composed of several qubits. Each of the qubits is thought to be held by a separated party, respectively.

It may come as quite a surprise that depending on the type of entanglement between the qubits, a single party may or may not be able to destroy the entanglement of the entire system with a single measurement. The different kinds of entanglement may differ for various characteristics such as robustness against de-coherence, connectivity or violation of classical physics.In the following we will shortly discuss different kinds of multipartite entanglement and their properties.

The smallest number of dimensions for a physical system to feature more than one class of entanglement is three [50]. The degree of entanglement of a multipartite system can range between highly entangled and fully separable. However, many multipartite entangled states feature almost exactly the same characteristics and as a matter of fact can be categorized to posses the same class of entanglement.

Assuming a pure three-qubit state we will find different notions of entanglement and separability. In the case of the fully separable state

$$|\Psi^{fs}\rangle_{1|2|3} = |\alpha\rangle_1 \otimes |\beta\rangle_2 \otimes |\gamma\rangle_3 \tag{2.25}$$

the three particles show no entanglement at all. In the bi-separable case two particles are grouped together, e.g.

$$|\Psi^{bs}\rangle_{1|23} = |\alpha\rangle_1 \otimes |\delta\rangle_{23} \tag{2.26}$$

where δ denotes a two particle state, that might be entangled. Finally, if the state is neither separable nor bi-separable, we call it a genuine tripartite entangled state, such as e.g. the GHZ or the W state.

Green-Horne-Zeilinger (GHZ) States

The class of GHZ- states are represented by

$$|\Psi^{\pm}\rangle = \frac{1}{\sqrt{2}}(|H\rangle_1|H\rangle_2|H\rangle_3 + |V\rangle_1|V\rangle_2|V\rangle_3) \tag{2.27}$$

States of the GHZ-class can demonstrate strong violations of local realism [44, 43, 51] and for many Bell inequalities it can be shown, that they are the unique state leading to maximal violation [52]. Moreover they allow applications such as quantum secret sharing [53], open destination teleportation [54] and quantum computation [55]. Unfortunately, GHZ states are more sensitive to de-coherence or the loss of a qubit. If one particle of the system prepared in a GHZ- state is traced out, the remaining two particles will be left completely unentangled. This means that, if one of the parties sharing the system prepared in a GHZ state decides not to cooperate with the other two, or if for some reason the information about one of the qubits is lost, then the remaining two parties cannot use their entanglement resources to perform communication tasks.

W States

The class of W states [50] is represented by

$$|W\rangle = \frac{1}{\sqrt{3}}(|H\rangle_1|V\rangle_2|V\rangle_3 + |V\rangle_1|H\rangle_2|V\rangle_3) + |V\rangle_1|V\rangle_2|H\rangle_3). \tag{2.28}$$

The W-class states feature fundamentally different behaviors. On the one hand, states of the W-class can only demonstrate less strong violations of locality , on the other hand, the W-class is much more robust against de-coherence and the loss of a qubit. If in a three-qubit system prepared in a W state one of the qubits is traced out then the remaining two qubits remain entangled . Indeed, from a single copy of the reduced density matrix for any two qubits belonging to a state form the W-class, one can always obtain a state which is arbitrarily close to a Bell state by means of a filtering measurement [56]. This means that, if one of the parties sharing the system prepared in a W state decides not to cooperate with the other two, or if for some reason the information about one of the qubits is lost, then the remaining two parties still can use their entanglement resources to perform communication tasks.

Any genuinely tripartite entangled state can be converted by the means of local operations and classical communication (LOCC) into one of two standard forms, namely either a GHZ state [44] or else a W state. If a state $|\Psi\rangle$ can be converted into the state $|GHZ\rangle$ of Eq. (2.27) under LOCC and another state $|\Phi\rangle$ can be converted into the state $|W\rangle$ of Eq. (2.28), then it is not possible to transform, even with only a very small probability of success, $|\Psi\rangle$ into $|\Phi\rangle$ nor the other way round. There are thus two classes of entanglement for genuinely tripartite entangled states.

Graph States

For higher dimensional multipartite entanglement the number of entanglement classes equivalent under LOCC already become numerous and difficult to characterize. However, there exist certain patterns, which reoccur in all multi-partite systems. There exists a graphical representation of these patterns, which is closely related to the entanglement properties of these so called graph states [57].

Graph-states can be associated with graphs of vertices and edges. Each vertex represents a qubit prepared in the state

$$|+\rangle = \frac{1}{\sqrt{2}}(|0\rangle + |1\rangle) \tag{2.29}$$

and each edge represents a *controlled-phase* (C-phase) gate having been applied between the two connected qubits. A C-phase gate flips the sign of the state if and

only if both qubits are $|1\rangle$, namely:

$$\begin{array}{rcl} |0\rangle|0\rangle & \rightarrow & |0\rangle|0\rangle \\ |0\rangle|1\rangle & \rightarrow & |0\rangle|1\rangle \\ |1\rangle|0\rangle & \rightarrow & |1\rangle|0\rangle \\ |1\rangle|1\rangle & \rightarrow & -|1\rangle|1\rangle \end{array} \tag{2.30}$$

and thus entangles two qubits initially prepared in the state $|+\rangle$ of Eq. (2.29).

For a given number of dimensions there exists a finite (large) number of possibilities for different graph states.

We will not discuss graph states and their properties in detail, but immediately proceed to one special subclass, the cluster state, which can serve as an essential resource for many QIP tasks. As it is also universal resource for quantum computational tasks, we have constructed and used such a cluster state in our experiment presented in Chapter 6.

Cluster states

While the two-qubit cluster state and the three-qubit cluster state are LOCC-equivalent to a maximally entangled Bell state and a three-qubit GHZ state, respectively, the four-qubit cluster state features a new type of entanglement [58].

A cluster state can produced experimentally using the spatially and polarization entangled output of SPDC and linear optical elemnts presented in Chapter 2.2.1. Then the cluster state emerges from entangling two neighboring qubits prepared in state 2.29 by the phase controlled operation in given in 2.30. The choice of the qubits and the specific entangling operation determines the structure of the cluster. The structure of the cluster predefines which basic quantum circuit it can implement. Measurement on a qubit in the computational basis H/V have the effect of disentangling (removing) the qubit from the cluster and will thus change its structure and the imprinted circuit.

2.5 Detection and Verification of Entanglement

2.5.1 Bell State Analyzer

The projective measurement of two photons on one of the four Bell state, a so called Bell State Measurement (BSM), is a fundamental procedure in QIP. It is an essential component in many protocols, e.g. as quantum teleportation. To detect a Bell state one employs the fixed optical circuit shown in Fig. 2.12(a): a Bell state analyzer. Here we will describe its implementation with linear optics as we have used it in the experiments described in the following chapters.

The Bell state analyzer is based on the two-photon interference effect at a non-polarizing beam splitter (BS) or a polarizing beam splitter (PBS). The first Bell

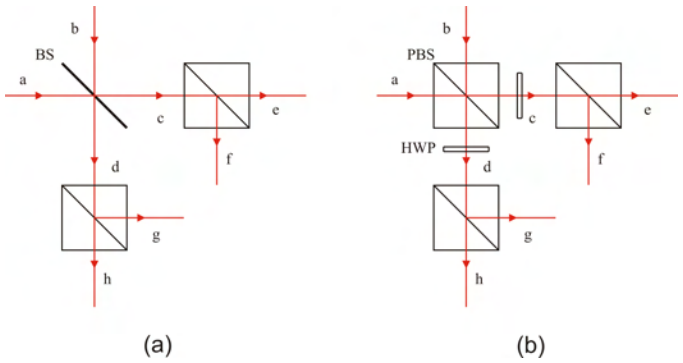

Figure 2.12: *Bell state analyzer (a) using a BS. Two photons in input modes a and b are interfered on the BS. The two output modes c and d are analyzed with the help of a PBS. A coincidence detection of photons in modes e+g or f+h corresponds to a $|\Psi^-\rangle$ detection, whereas a signal in e+f or g+h coincidence corresponds to a $|\Psi^+\rangle$ detection. (b) Two photons in input modes a and b are interfered on the first PBS. The two output modes c and d are analyzed with a half-wave plate (HWP) and a second PBS, respectively. A coincidence detection of photons in modes e+h or f+g corresponds to a $|\Phi^-\rangle$ detection, whereas a e+g or f+h coincidence corresponds to a $|\Phi^+\rangle$ detection.*

state analyzer proposed by Weinfurter et al. only utilizes a BS and a polarization analyzers in each output mode. As we have mentioned in chapter 2.2.1, by interfering two photons in the general state $|\Psi\rangle_1 = \alpha|H\rangle + \beta|V\rangle$ and $|\Psi\rangle_2 = \gamma|H\rangle + \delta|V\rangle$ at a BS we are able to create a two-photon state, which can already be projected onto a maximally entangled state. From Eq. 2.8 it is easy to verify that the two outgoing photons only exit at different ports, if and only if their polarization state is in the state $\frac{1}{\sqrt{2}}(|H\rangle|V\rangle - |V\rangle|H\rangle) \equiv |\Psi^-\rangle$. Inserting additional PBS in the outgoing modes c and d enable us to split the vertically polarized photons from the horizontally. An outcoming photon, e.g. in mode c, with horizontal polarization will give rise to a signal in detector e, a horizontally polarized photon will yield a signal in f. Looking at Fig. 2.12 it is obvious that for the case $\frac{1}{\sqrt{2}}(|H\rangle|V\rangle - |V\rangle|H\rangle) \equiv |\Psi^-\rangle$ we should detect one photon each either in detectors e and g or f and h. The additional PBS moreover alow us to identify the state $\frac{1}{\sqrt{2}}(|H\rangle|V\rangle + |V\rangle|H\rangle) \equiv |\Psi^+\rangle$: even though the two photons will exit into the same outgoing mode c (or d) they carry orthogonal polarization and therefore they can be separated to to be detected in e and f (or g and h). With this setup using a BS we can thus identify two out of the four Bell states, namely $|\Psi^+\rangle$ and $|\Psi^-\rangle$.

In our experiments we mainly used the slightly modified setup [59], where the BS is replaced by a PBS and two half wave plates are inserted in the output modes The entire setup is shown in Fig. 2.12(b). As shown in Eq. (2.6), for photons 1 and 2 passing through the PBS their spatial modes will undergo a corresponding unitary transformation. The two-photon state thus evolves into

$$|\Psi\rangle_{12} = \tfrac{1}{\sqrt{2}} \quad \begin{array}{l}[(\alpha+\beta)|H\rangle_1|c\rangle_1|H\rangle_2|d\rangle_2 + i(\gamma+\delta)|H\rangle_1|c\rangle_1|V\rangle_2|c\rangle_2 \\ +i(\gamma-\delta)|V\rangle_1|d\rangle_1|H\rangle_2|d\rangle_2 + (\alpha-\beta)|V\rangle_1|d\rangle_1|V\rangle_2|c\rangle_2]\end{array} \tag{2.31}$$

The HWP in output modes c and d are set with their fast axis to an angle of 22.5° to the horizontal axis. By this, the HWPs essentially implement Hadamard gates and the state of Eq. (2.31) evolves to

$$\begin{array}{rl}|\Psi_f\rangle_{12} = \tfrac{1}{2\sqrt{2}}\{ & (\alpha+\beta)[|H\rangle_1|H\rangle_2 + |H\rangle_1|V\rangle_2 + |V\rangle_1|H\rangle_2 + |V\rangle_1|V\rangle_2]|c\rangle_1|d\rangle_2 \\ & +i(\gamma+\delta)[|H\rangle_1|H\rangle_2 - |H\rangle_1|V\rangle_2 + |V\rangle_1|H\rangle_2 - |V\rangle_1|V\rangle_2]|c\rangle_1|c\rangle_2 \\ & +i(\gamma-\delta)[|H\rangle_1|H\rangle_2 + |H\rangle_1|V\rangle_2 - |V\rangle_1|H\rangle_2 - |V\rangle_1|V\rangle_2]|d\rangle_1|d\rangle_2 \\ & -(\alpha-\beta)[|H\rangle_1|H\rangle_2 - |H\rangle_1|V\rangle_2 - |V\rangle_1|H\rangle_2 + |V\rangle_1|V\rangle_2]|d\rangle_1|c\rangle_2\}\end{array} \tag{2.32}$$

After that the the output modes c and d are directed onto the PBSs of the polarization analyzers. Just like in Eq. (2.31) the photons in modes c and d will undergo corresponding unitary transformations:

$$\begin{array}{rll}|\Psi_f\rangle_{12} = \tfrac{1}{2\sqrt{2}}\{ & (\alpha+\beta) & [|H\rangle_1|e\rangle_1|H\rangle_2|h\rangle_2 + i|H\rangle_1|e\rangle_1|V\rangle_2|g\rangle_2 \\ & & +i|V\rangle_1|f\rangle_1|H\rangle_2|h\rangle_2 - |V\rangle_1|f\rangle_1|V\rangle_2|g\rangle_2] \\ & +i(\gamma+\delta) & [|H\rangle_1|e\rangle_1|H\rangle_2|e\rangle_2 - i|H\rangle_1|e\rangle_1|V\rangle_2|f\rangle_2 \\ & & +i|V\rangle_1|f\rangle_1|H\rangle_2|e\rangle_2 + |V\rangle_1|f\rangle_1|V\rangle_2|f\rangle_2] \\ & +i(\gamma-\delta) & [|H\rangle_1|h\rangle_1|H\rangle_2|h\rangle_2 + i|H\rangle_1|h\rangle_1|V\rangle_2|g\rangle_2 \\ & & -i|V\rangle_1|g\rangle_1|H\rangle_2|h\rangle_2 + |V\rangle_1|g\rangle_1|V\rangle_2|g\rangle_2] \\ & -(\alpha-\beta) & [|H\rangle_1|h\rangle_1|H\rangle_2|e\rangle_2 - i|H\rangle_1|h\rangle_1|V\rangle_2|f\rangle_2 \\ & & -i|V\rangle_1|g\rangle_1|H\rangle_2|e\rangle_2 - |V\rangle_1|g\rangle_1|V\rangle_2|f\rangle_2]\}\end{array} \tag{2.33}$$

Close inspection of Eq. (2.33) shows that we can identify two out of the four Bell states, namely $|\Psi^+\rangle_{12}$ and $|\Psi^-\rangle_{12}$.The probability to find a photon each in output modes e and h is exactly $|\beta|^2/2$. The same probability arises for a coincidence detection of photons in modes f and g. The overall probability for these two cases is thus $|\beta|^2$,which is exactly the probability for photons 1 and 2 to be in the Bell state $|\Phi^-\rangle_{12}$. Thus for $\beta = 1$ ($\beta = 0$) we know with certainty that the photons will (never) jointly emerge either from modes e and h or modes f and g. Since our system only consists of two particles, we are forced to conclude that a coincidence detection of photons in modes e+h or f+g projects photons 1 and 2 onto the state $|\Phi^-\rangle_{12}$. Correspondingly, we are able to identify the state $|\Phi^+\rangle_{12}$ by registering a coincidence in modes e and g or f and h (probability = $|\alpha|^2$). Note, that we are not able to distinguish between the states $|\Psi^+\rangle_{12}$ and $|\Psi^-\rangle_{12}$ since no coincidence configuration can be genuinely associated with either one of them. With the help of our Bell state analyzer we are thus able to identify two out of the four Bell states via two-fold coincidence analysis and post selection.

Since the SPDC happens with some small probability most of the time the pump photons pass through the crystal without down-conversion. Therefore it is essential to detect the right number of photons in the right modes to ensure the experiment was performed successfully. In experiments with more than two photons, the photons are usually generated by higher order emissions of SPDC or by interaction of entangled photon pairs via beam splitters. Then, it happens that the N photons are not equally distributed over the N spatial modes, i.e., with some probability one mode may contain more than one photon and some modes may contain none. This means that only those events, when all N detectors register a photon are counted.

This counting is called post-selection and implies, that the generated state will be destroyed by this measurement. Therefore we cannot really claim, that we have 'prepared' a certain state in our experiment.

2.5.2 Verification Criteria

In the above sections, we have discussed several aspects of quantum entanglement and QIP. Up to now we have silently assumed that we are able to generate perfectly pure states with certainty. In the experiment, however, this is not the case. We are only able to generate mixed states that resemble the desired pure states up to a certain degree. Therefore we have to include a term representing the noise introduced to our pure state $|\psi\rangle\langle\psi|$, so that as a simple approximation one may consider a mixed state ϱ of the form

$$\varrho(p) = p|\psi\rangle\langle\psi| + (1-p)\frac{\mathbb{1}}{4}, \tag{2.34}$$

where $\mathbb{1}/4$ is the maximally mixed state of two qubits, $\hat{\varrho}$ is the density matrix of the generated mixed state and $|\Psi\rangle$ is the state vector of the desired pure state. It is thus necessary to obtain knowledge of the quality of the generated states. Complete knowledge of the density matrix gives in principle all information about the state of a system.

Fidelity

Quantum fidelity is a measure for the purity of the created state $\varrho(p)$ and is defined as

$$F = Tr[\hat{\rho}|\Psi\rangle\langle\Psi|] \tag{2.35}$$

The fidelity can take values between 1, the generated state is perfectly equal to the desired state, and 0, the generated state contains no parts of the desired state.

For all procedures in QIP there exists a certain threshold that marks the minimum fidelity for which a task can still be accomplished.

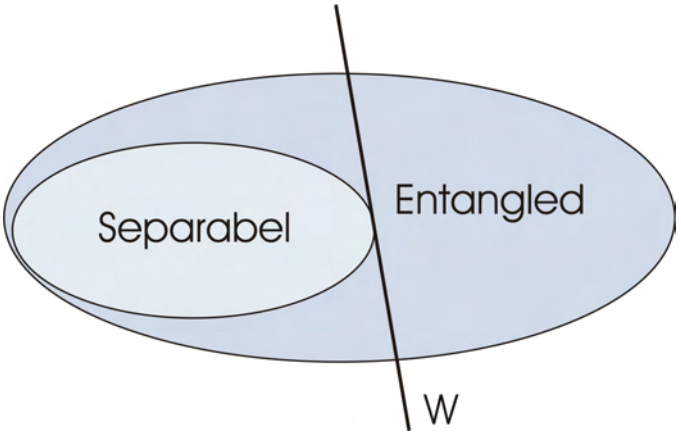

Figure 2.13: *Schematic picture of the set of all states and the set of separable states as nested set. The black line represent the hyperplane, where* $Tr(\hat{\mathcal{W}}\varrho) = 0$.

Entanglement Witnesses

For many experiments, though, it is sufficient to proof the presence of genuine multipartite entanglement. Entanglement witnesses are a recently developed criterion to detect the presence of entanglement in terms of directly measurable observables with only a minimum number of measurements involved. For a detailed overview over the field of entanglement detection see the review paper by Guehne and Toth [60].

Here will try to introduce the basic idea of the working principal of entanglement witnesses.

An observable $\hat{\mathcal{W}}$ is called an entanglement witness (short: witness), if

$$\begin{aligned} Tr(\hat{\mathcal{W}}\varrho_s) &\geq 0 \qquad \text{for all separable states } \varrho_s, \\ Tr(\hat{\mathcal{W}}\varrho_e) &< 0 \qquad \text{for entangled states } \varrho_e. \end{aligned} \tag{2.36}$$

If $Tr(\hat{\mathcal{W}}\varrho) < 0$ one knows for sure that the state ϱ is entangled.

Entanglement witnesses have a clear geometrical meaning: the set of states where $Tr(\hat{\mathcal{W}}\varrho) = 0$ holds is a hyperplane in the set of all states, cutting this set into two parts. In the part with $Tr(\hat{\mathcal{W}}\varrho) > 0$ lies the set of all separable states, the other part [with $Tr(\hat{\mathcal{W}}\varrho) < 0$] is the set of states detected by $\hat{\mathcal{W}}$. This idea is sketched in Fig. 2.13. From this geometrical interpretation it follows that to detect a particular entangled state one has to construct the appropriate witness $\hat{\mathcal{W}}$.

Taking into account that in the experiment we never fully succeed to create pure states, the witness to detect our state can be constructed from the consideration, that states close to an entangled state must also be entangled. Therefore, one may try for a given entangled pure state $|\psi\rangle$ to write down a projector-based witness like $\hat{\mathcal{W}} = \alpha\,\mathbb{1} - |\psi\rangle\langle\psi|$. This witness can be interpreted as follows: The quantity $Tr(\varrho)|\psi\rangle\langle\psi| = \hat{1}|\psi\rangle\varrho\langle\psi|$ is the fidelity of the state $|\psi\rangle$ in the mixed state ϱ, and if

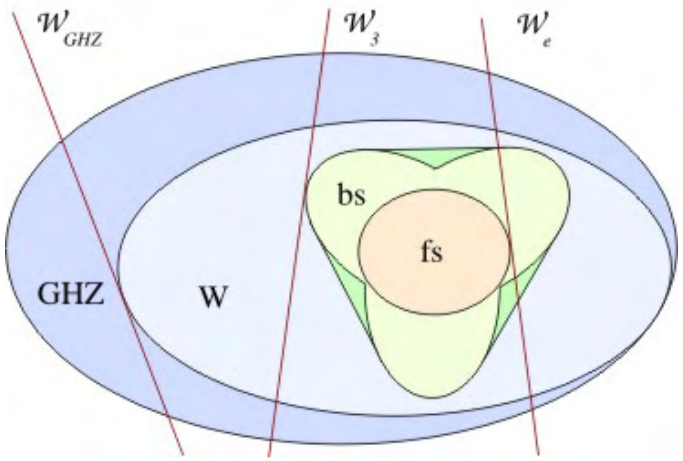

Figure 2.14: *Schematic picture of the set of mixed three-qubit states with three witnesses: The witness*
mathcal$\hat{W}_{GHZ}$ detects GHZ-type states, the witness $\hat{\mathcal{W}}_3$ tells apart three-qubit entanglement from bi-separable (bs) states, and the witness $\hat{\mathcal{W}}_e$ rules out full separability (fs).(Picture is taken from [[60]])

this fidelity exceeds a critical value α, then the expectation value of the witness is negative and the state ϱ must be entangled.

Clearly, witnesses can also be used to distinguish the different classes of multipartite entanglement. Contrary to the bipartite case, one has several types of witnesses, for the different types of multipartite entanglement. A quantum witness of genuine n-partite entanglement is an observable which has a positive expectation value on states with $(n-1)$-partite entanglement and a negative expectation value on some n-partite entangled states. The latter states and their entanglement, respectively, are said to be detected by $\hat{\mathcal{W}}$. As depicted in Fig. 2.14 witnesses for genuine tripartite entanglement, denoted by $\hat{\mathcal{W}}_3$, have a positive expectation value on all bi-separable (bs) states, thus a negative expectation value indicates the presence of true tripartite entanglement. Witnesses for bi-separable entanglement $\hat{\mathcal{W}}_e$ have a positive expectation value on all fully separable (fs) states, thus a negative expectation value is still a signature of entanglement, which might be only bi-separable entanglement.

In our 'Multistage swapping' experiment described in Chapter 5 we apply a witness measurement to determine the entanglement of our bi-partite output state. Since a witness is, up to a constant, a projector onto one of the Bell states and such a nonlocal observable it cannot easily be implemented into an experiment. But, as mentioned previously, the polarization state of a qubit is completely described by its density matrix ϱ and our experimentally accessible observables are the Pauli spin matrices $\hat{\sigma}_x, \hat{\sigma}_y, \hat{\sigma}_z$ and the identity operator $\mathbb{1}$. We can express the expectation

value of these observables in terms of the density operator as

$$\begin{aligned} \langle \hat{\sigma}_z \rangle &= Tr[\varrho \hat{\sigma}_z] = \varrho_{H,H} - \varrho_{V,V} \\ \langle \hat{\sigma}_x \rangle &= Tr[\varrho \hat{\sigma}_x] = \varrho_{H,V} + \varrho_{V,H} \\ \langle \hat{\sigma}_y \rangle &= Tr[\varrho \hat{\sigma}_y] = i(\varrho_{H,V} - \varrho_{V,H}), \end{aligned} \tag{2.37}$$

where $\varrho_{i,j}$ are the elements of the density matrix ϱ representing the density operator in the H/V basis. Provided that we are able to subsequently produce many identical copies of our state, it can be easily seen that, this way it is possible to determine all elements by measuring just local observables. By increasing statistics this can be done as accurate as desired.

This technique can easily be extended to two and more photons: also for multipartite states local observables like $\langle \sigma_z \otimes \sigma_z \rangle$ or projectors like $\langle |0\rangle\langle 0| \otimes |0\rangle\langle 0| \rangle$ can easily be measured in any experiment. For the experimental implementation it is just necessary to decompose the witness into operators that can be measured locally [61]. Thus, we need a decomposition into projectors onto product vectors of the form

$$\hat{\mathcal{W}} = \sum_{i=1}^{k} c_i |e_i\rangle\langle e_i| \otimes |f_i\rangle\langle f_i|, \tag{2.38}$$

which can be measured locally: Alice and Bob measure the expectation values of the $|e_i\rangle\langle e_i| \otimes |f_i\rangle\langle f_i|$ and add their results with the weights c_i. One can construct such a decomposition in many ways, but it is reasonable to do it in a way that corresponds to the smallest possible experimental effort for Alice and Bob.

How to construct an appropriate witness is explained in detail in the review by Gühne and Tóth [60].

We have seen that with the help of a local decomposition entanglement witnesses can be used for the experimental detection of entanglement. For two qubits, this required only three local measurements, which is less than quantum state tomography that would require $3^2 = 9$ measurements, namely the measurement of all correlations $\langle \sigma_i \otimes \sigma_j \rangle$.

Quantum State Tomography

In some cases though it is not possible to apply a witness operator, e.g. if the kind of entanglement is unknown, so that an appropriate witness cannot be constructed, or to explicitly exclude the possibility that the analyzed state reveals any entanglement whatsoever.

By considering the expectation values of all different combinations of Pauli operator products for all n photons of the analyzed state, we can reconstruct every entry of the density matrix $\varrho_{i,j} = \langle i|\hat{\varrho}|j\rangle$ from the measured expectation values of all Pauli

matrix combinations $\langle \hat{\sigma}_i^1 \hat{\sigma}_i^2 \hat{\sigma}_i^3 ... \hat{\sigma}_i^n \rangle$. Here, i identifies one of the Pauli matrices or the identity $[x, y, z, I]$ and n is the number of qubits in the system. However, the number of measurements needed for quantum state tomography grows exponentially with n, which can result in a very long measurement time and is thus unpractical for various experimental applications.

Chapter 3

A Heralded Source for Polarisation Entangled Photon Pairs

3.1 Introduction

Quantum entangled states are one of the key resources in quantum information processing and communication. Besides the feature to reveal fundamental aspects of quantum mechanics, they are also crucial for a variety of quantum information tasks [62, 15]. In particular, photonic entangled states are robust against decoherence, easy to manipulate, show little loss rates, both in fiber and free space, and thus are exceptionally well suitable for long distance quantum communication and quantum computing. The controlled generation of entangled states is a long-standing goal in quantum information processing, since it is indispensable for quantum computing and a number of quantum protocols [62, 15].

The generation of polarization entangled photon pairs by spontaneous parametric down conversion (SPDC) [30] is widely used, however, its emission is probabilistic and can only be utilized with post selection and destructive photon detection. Entanglement sources based on the probabilistic generation process of SPDC allow demonstrations of a number of quantum protocols, but do not permit on-demand applications, deterministic quantum computing and significantly limit the efficiency of multi-photon experiments. Consequently, an event-ready source for entangled photonic states is of great importance, both from fundamental and practical point of view.

In the following we present a source for entangled photon pairs generated in event-ready manner by conditioned detection of auxiliary photons: a scheme, which profits from the stable and robust properties of SPDC and requires only modest experimental means. Alternative solutions such as the controlled biexciton emission of a single quantum dot [63, 64, 65] or the creation of heralded entanglement from atomic ensembles [66] face severe experimental disadvantages, such as liquid-helium temperature environment and large-volume setups. Moreover, there has been consid-

erable progress in generating photonic entanglement in a non-probabilistic manner, like the Knill-Laflamme-Milburn scheme [29] or the scheme proposed by Browne and Rudolph [67]. However, both schemes require on-demand single photon sources and the still unavailable photon-number-resolving detectors. Novel ideas based on conditional detection of auxiliary photons or multi-photon interference were recently proposed to overcome the probabilistic character of SPDC [68, 69, 70, 71, 72, 73, 74, 75]. Following this line, we demonstrate the experimental realization of an – in principle deterministic – entanglement source proposed by Śliwa and Banaszek [70]. The scheme is based on the conditional detection of four auxiliary photons heralding the presence of one polarization entangled pair, which then can be used in event ready manner. The fully deterministic implementation cannot be realized due current technical limitations, but employing beam splitters with different transmission ratios allows to significantly increase the state preparation efficiency of the source up to 52 %. Together with a fidelity better than 87 % this is a significant improvement compared with previous experiments for on-demand sources [75]. The source also presents a substantial advancement over the general methods by using linear optics [29], which require simultaneous emission of four pairs [68].

The demonstrated source might be of promising use in essential photon based quantum information tasks. It is feasible to support on-demand applications, such as the controlled storage of photonic entanglement in quantum memory [76] to realize the quantum repeater scheme [21]. Moreover, it is suitable to serve on-chip waveguide quantum circuit applications, which are potential candidates for profound new technologies in quantum optics [77].

3.2 Conditional Preparation of Entangled Photon Pairs

The idea of the experiment is employ a type-II SPDC source [30] as presented in Chapter 2.3.1 using its three pair emission component as the desired input state into the optical circuit, since three photon pairs are the minimum number required to generate one event ready pair of polarization entangled photons by detection of four auxiliary triggers [69]. Through the linear optics circuit shown in Fig. 3.1, in an ideal case the three-pair state can provide a maximally entangled photon pair in the output modes, if and only if the rest of the photons give a fourfold coincidence between the four trigger modes.

In Chapter 2.3.1 we have already introduced the higher order emission of the SPDC source and stated that the randomness of the type-II SPDC process for photonic entanglement is manifested through the indeterministic creation of states with n indistinguishable photon pairs. Remind, that any n^{th} order of SPDC emission can

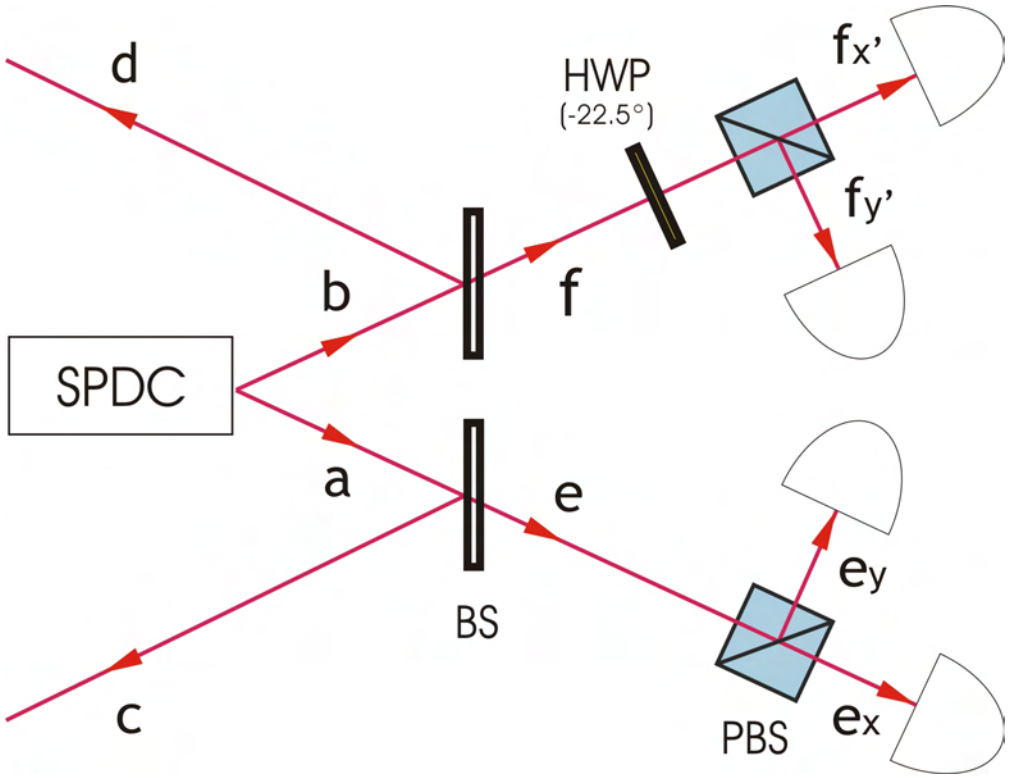

Figure 3.1: *Schematic representation of the setup for the heralded generation of entangled photon pairs. Partial reflecting beam splitters split mode a (b) into a transmitted mode e (f) and the output mode c (d). The auxiliary trigger photons are detected in* (f'_x, f'_y) *in the diagonal basis and in* e_x, e_y *in the computational (H/V) basis.*

then be expressed in the following form [40]

$$|\Psi_n\rangle = \frac{1}{n!\sqrt{n+1}}(\hat{a}_x^\dagger \hat{b}_y^\dagger - \hat{a}_y^\dagger \hat{b}_x^\dagger)^n |vac\rangle. \tag{3.1}$$

Creation operator $\hat{a}^\dagger$ ($\hat{b}^\dagger$) denotes that the photon will be emitted into the corresponding mode, index $x(y)$ denotes the horizontal (vertical) polarization of the photon. Indeed, the state generated from the source is a coherent superposition of all n-pair photon states. Nevertheless, lower-order contributions to the trigger, namely from second order emission , don't need to be considered, since they will vanish due to the destructive two-photon bunching effect [78, 41] induced by the optical circuit.

According to the first line in Eq. (2.21) the initial state given in Eq. (3.1) can also be expressed as

$$|\Psi_3\rangle = \tfrac{1}{\sqrt{2}}(|3,0;0,3\rangle - |2,1;1,2\rangle + |1,2;2,1\rangle - |0,3;3,0\rangle), \tag{3.2}$$

where the occupation numbers correspond to the ordering of the modes as $|\hat{a}_x, \hat{a}_y; \hat{b}_x, \hat{b}_y\rangle$.

The complete optical linear circuit placed after the nonlinear crystal can be expressed by the following transformation of the operators of the down conversion modes:

$$\begin{aligned}
\hat{a}_x &= \sqrt{T_a}\hat{c}_x + \sqrt{R_a}\hat{e}_x \\
\hat{a}_y &= \sqrt{T_a}\hat{c}_y + \sqrt{R_a}\hat{e}_y \\
\hat{b}_x &= \sqrt{T_b}\hat{d}_x + \sqrt{R_b}\tfrac{1}{\sqrt{2}}(\hat{f}_{x'} - \hat{f}_{y'}) \\
\hat{b}_y &= \sqrt{T_b}\hat{d}_y + \sqrt{R_b}\tfrac{1}{\sqrt{2}}(\hat{f}_{x'} + \hat{f}_{y'})
\end{aligned} \tag{3.3}$$

As depicted in Fig. 3.1 the photons in modes $(\hat{a}_x, \hat{a}_y)$ and $(\hat{b}_x, \hat{b}_y)$ are directed onto a non-polarizing partial reflecting beam splitters (BS) with the amplitude transmission coefficients $T_{a/b}$, so that a fraction of the amplitude $R_{a/b} = 1 - T_{a/b}$ is reflected to the trigger modes $(\hat{e}_x, \hat{e}_y)$ and $(\hat{f}_x, \hat{f}_y)$, respectively, while the transmitted fraction will go to output modes $(\hat{c}_x, \hat{c}_y)$ and $(\hat{d}_x, \hat{d}_y)$. In $(\hat{f}_x, \hat{f}_y)$ the trigger mode is transformed by a half wave plate to $\hat{f}_x = (\hat{f}_{x'} - \hat{f}_{y'})/\sqrt{2}$, $\hat{f}_y = (\hat{f}_{x'} + \hat{f}_{y'})/\sqrt{2}$. Only the second and third term of $|\Psi_3\rangle$, which contain at least one photon of each polarization in mode $\hat{a}$ and $\hat{b}$, can contribute to a desired trigger signal, since for a two fold trigger in mode $\hat{e}_x$ and $\hat{e}_y$ the photons taken from mode $(\hat{a}_x, \hat{a}_y)$ have to have different polarization. Thus the remaining photons are in the state $-|1,0;1,2\rangle + |0,1;2,1\rangle$. Whereas to obtain a trigger in $\hat{f}_{x'}$ and $\hat{f}_{y'}$ the photons need to originate from the same polarization mode, either $\hat{b}_x$ or $\hat{b}_y$, and therefore their joint state in mode $(\hat{f}_x, \hat{f}_y)$ before the half wave plate was the coherent superposition $|2,0\rangle - |0,2\rangle/\sqrt{2}$. The remaining photons exiting at the output modes $(\hat{c}_x, \hat{c}_y)$ and $(\hat{d}_x, \hat{d}_y)$ will consequently be in the state $|1,0;1,0\rangle + |0,1;0,1\rangle$.

After the transformation by the optical circuit the desired output state is of the following form

$$\begin{aligned} |\Psi_3\rangle &= \tfrac{1}{\sqrt{2}} T_a T_b \sqrt{R_a}\sqrt{R_b}\tfrac{1}{\sqrt{2}}(\hat{c}_x^\dagger \hat{d}_x^\dagger + \hat{c}_y^\dagger \hat{d}_y^\dagger) \\ &\quad \times(\hat{e}_x^\dagger \hat{e}_y^\dagger \hat{f}_{x'}^\dagger \hat{f}_{y'}^\dagger)|vac\rangle + ... \end{aligned} \tag{3.4}$$

and under detection of the four auxiliary triggers in modes $(\hat{e}_x, \hat{e}_y; \hat{f}_{x'}, \hat{f}_{y'})$ the two photons in the output modes $(\hat{c}_x, \hat{c}_y)$ and $(\hat{d}_x, \hat{d}_y)$ collapse to the maximally entangled Bell state

$$|\Phi^+\rangle = \tfrac{1}{\sqrt{2}}(\hat{c}_x^\dagger \hat{d}_x^\dagger + \hat{c}_y^\dagger \hat{d}_y^\dagger))|vac\rangle. \tag{3.5}$$

We note, that this Ansatz silently assumes, that the photons emitted by the down conversion process are detected behind filters with a bandwidth smaller than that of the pump light, and that the time window in which they are recorded as coincidences is narrower than the inverse bandwidth of the radiation [79, 80].

Now one might say, that according to this calculation any time we observe a trigger we will for sure obtain an entangled photon pair in the output. However, this is not the case due two technical limitations of the standard single photon detectors most frequently used in photonic experiments, which significantly affect the performance of many experimental setup: With single photon resolving detectors and 100% detection efficiency we could ensure that only perfectly created three-pair component contributes to the measured final state. However, with the widely used standard single photon counting modules (SPCM) one cannot discriminate single photons and only provide a limited detection efficiency resulting from limited collection and detector efficiencies. The limited detection efficiency is therefore considered in the theoretical calculation by replacing the creation operator for each trigger mode, e.g. $\hat{e}_x$ by a combination $\sqrt{\eta}\hat{e}_x + \sqrt{1-\eta}\hat{\tilde{e}}_x$, where the last term represents the undetected fraction of photons. The inability to discriminate single photons leads to the significant problem of the proposed scheme: under counting photons. It means that the trigger detectors give a trigger even though more than two photons from either mode $(\hat{a}_x, \hat{a}_y)$ or $(\hat{b}_x, \hat{b}_y)$ or both have been transmitted to the trigger channels.

As already indicated by "..." in Eq. (3.4) the complete output state includes additional terms

$$|\Psi_3\rangle = \alpha|\theta\rangle_{\mathbf{t}}|\Phi^+\rangle_{\mathbf{s}} + \beta|\vartheta\rangle_{\mathbf{ts}} + \gamma|\varphi\rangle_{t\mathbf{s}}. \tag{3.6}$$

The first term of Eq. (3.6) denotes the desired output state as given in Eq. (3.5), where $|\theta\rangle$ describes the perfect four photon trigger state, whose appearance will herald a photon pair in state $|\Phi^+\rangle$ in the output with a probability of 100 %. The second term $\beta|\vartheta\rangle_{\mathbf{ts}}$ represents all additional states, which yield a trigger in $(\hat{e}_x, \hat{e}_y)$ and $(\hat{f}_{x'}\hat{f}_{y'})$ generated by more than four photons, but the state in the output $(\hat{c}_x, \hat{c}_y)$ and $(\hat{d}_x, \hat{d}_y)$ contains only a single photon or vacuum. These states are orthogonal

to the desired output state. For completeness, the last term $\gamma|\varphi\rangle_{ts}$ represents states, which do not contribute to the trigger, but contain more than two photons in the output modes. These states do not affect our experimental results since without trigger signal their contribution is not recorded. All normalization factors are summarized in α, β and γ. For the results of the theoretical calculation see Table I.

According to Eq. (3.6) anytime we obtain a trigger, we can expect the state $|\Phi^+\rangle$ in the output with a certain probability. Then we can define the probability of getting state $|\Phi^+\rangle$ as the state preparation efficiency of our source. Obviously, additional terms yielding triggers will thus result in a reduction of the preparation efficiency. Their emergence can be limited by decreasing the transmission coefficients $T_{a/b} = T$ of the BS. In this regime, the probability of transmitting more than the minimum number of photons to the trigger becomes lower and such the danger of under counting photons in the trigger detectors decreases. Fig. 3.3 demonstrates that for low enough transmission coefficients the state preparation efficiency will approach unity and under this condition the source could be called deterministic. However, enhancing the state preparation efficiency in this way will lower the over all preparation rate. In order to show that the efficiency of successful state preparation depends on the transmission coefficients T of the partial reflecting beam splitters as

$$\text{eff}_{theory} = \frac{R^2}{(1 - \frac{\eta_{trig}}{2}T)^2}, \tag{3.7}$$

we have chosen BS with three different reflection/transmission ratios: 50/50, 60/40 and 70/30 in the experiment (Fig. 3.2). Eq. (3.7) is directly derived from the definition of the state preparation efficiency. The effect of limited detection efficiency has been considered. The dependence of the preparation efficiency on the variation of the transmission coefficient is shown in Fig. 3.3.

3.3 Experimental Setup

A schematic diagram of the experimental setup for the heralded entanglement source is illustrated in Fig. 3.2. In contrary to the previous experiments the pulsed high-intensity ultraviolet (UV) laser passes through only one β-Barium-Borate (BBO) crystal generating three polarization entangled photon pairs via third order type-II SPDC process. The third order emission takes place with a probability of $p \equiv 0.0001$. At an average power of 880 mW UV-light we observe $\sim 80 \times 10^3$ photon pairs per second at a visibility of $V = 91 \pm 3\%$.

The aim of the experiment is to show that the emergence of additional triggers can be limited by decreasing the transmission coefficients T_a and T_b. In this regime the probability of transmitting more than the minimum number of photons to the trigger becomes lower and such the danger of under counting photons in the trigger detectors decreases. In order to show that the efficiency of successful state preparation depends on the amplitude transmission coefficients T_a and T_b of the partial reflecting beam

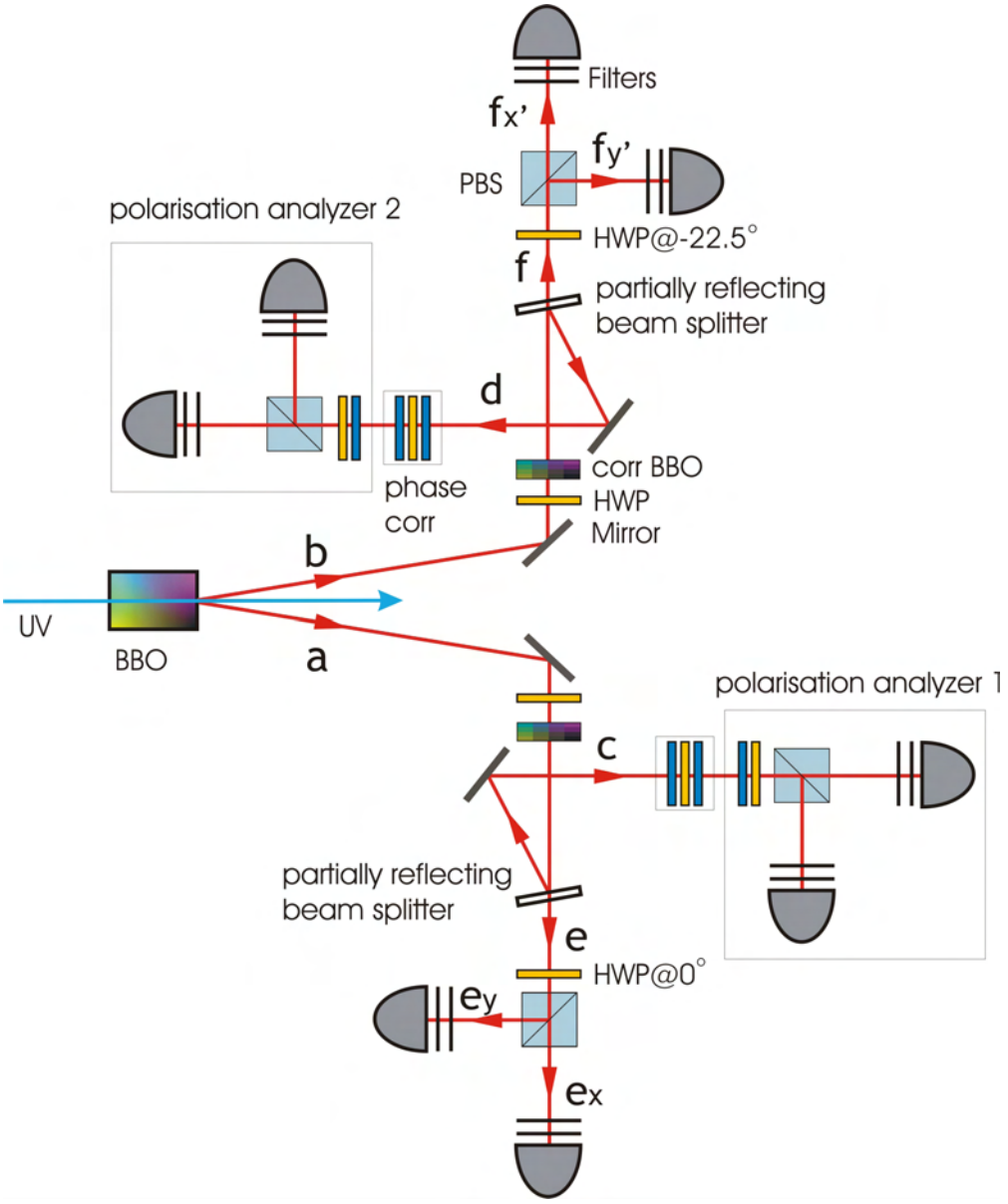

Figure 3.2: *The experimental setup for the heralded entanglement source. Sending the pulsed high-intensity ultraviolet (UV) laser through one β-Barium-Borate (BBO) crystal we generate three polarization entangled photon pairs via third order type-II SPDC process. The longitudinal and spatial walk off of the photons in mode $\hat{a}$ and $\hat{b}$ will be corrected by a half wave plate and a correction BBO before the photons are redirected onto the partially reflecting beam splitters. The transmitted photons are going into the trigger detectors in modes $\hat{e}$ and $\hat{f}$ and the reflected photons are going to the polarization state analyzers installed in the output modes $\hat{c}$ and $\hat{d}$. To control the additional phase introduced by the partial reflecting beam splitters (BS) we employed a combination of two half wave plates and one quarter wave plate. All photons are filtered by narrow bandwidth filters ($\Delta\lambda = 3.2$ nm) and are monitored by silicon avalanche photon detectors. Coincidences are recorded by a laser clocked FPGA based coincidence unit.*

splitters we have chosen three different reflection/transmission ratios: 50/50, 60/40 and 70/30. From the experimental setup given in Fig. 3.2 it can be seen that the partial reflecting mirrors can be exchanged conveniently in order to vary the number of photons transmitted into the trigger modes. The trigger photons are detected in modes ($\hat{e}_x$ and $\hat{e}_y$) in the computational basis and in modes ($\hat{f}_{x'}$ and $\hat{f}_{y'}$) in the diagonal basis. The signal photons in modes ($\hat{c}$ and $\hat{d}$ are detected by polarization analyzers as described in Chapter 2.5.1. Before the detection we had to correct the additional phase introduced by the partial reflecting BSs with the help of a combination of two HWPs and a QWP. As a result from the different distances between the couplers and the BBO, we reach a mean detection efficiency of $\eta_{trig} = 18.2\%$ for the trigger detectors and $\eta_{sig} = 13.7\%$ for the signal detectors.

3.4 Experimental Results

The dependence of the preparation efficiency on the variation of the amplitude transmission coefficient is shown in Fig. 3.3. It can be clearly seen that the danger of under counting photons can be reduced by decreasing the amplitude transmission coefficient and that it is such possible to increase the preparation efficiency of the desired state. The solid line represents the theoretical state preparation efficiency based on third order contribution and assuming a mean detection efficiency of all detectors of 15 %. It can clearly be seen, that by choosing a high enough beam splitting ratio the proposed source is able to reach the deterministic region. To better take our experimental conditions into account, we accustomed the theoretical predictions by taking the different detection efficiencies for the trigger an the signal detectors into account. The results are shown by the dots marked as 'Accustomed theory'. Our experimental results definitely follow the theoretical predictions. The given errors are statistical. The deviation of the performance of the experiment from the theoretical prediction mainly results from differences in the quality of the alignment. With our setup we achieve to significantly improve the preparation efficiency in comparison to the efficiency provided by the standard procedure of preparing single pairs by SPDC, where the efficiency is determined by the number of emitted pairs per UV pulse [40]. However, enhancing the preparation efficiency in this way will lower the over all preparation rate. To still obtain a reasonable over all preparation rate one could employ a laser with a higher pulse repetition rate.

Note, that increasing the input power of UV light into the BBO will lower the fidelity of the generated photon pairs significantly, so that the contributions from imperfectly created pairs cannot be omitted anymore. For perfectly created pairs negative two-photon interference effects [78] will delete the contribution of two pair emission to the trigger signal. Four-pair emission will contribute, not only to the triggers but also to the signal. The experimentally estimated creation probability for a four-pair emission is only of the order of $p \approx 5 \times 10^{-6}$ per pulse. But since we again face the problem of under counting photons, four-pair contribution will lead to

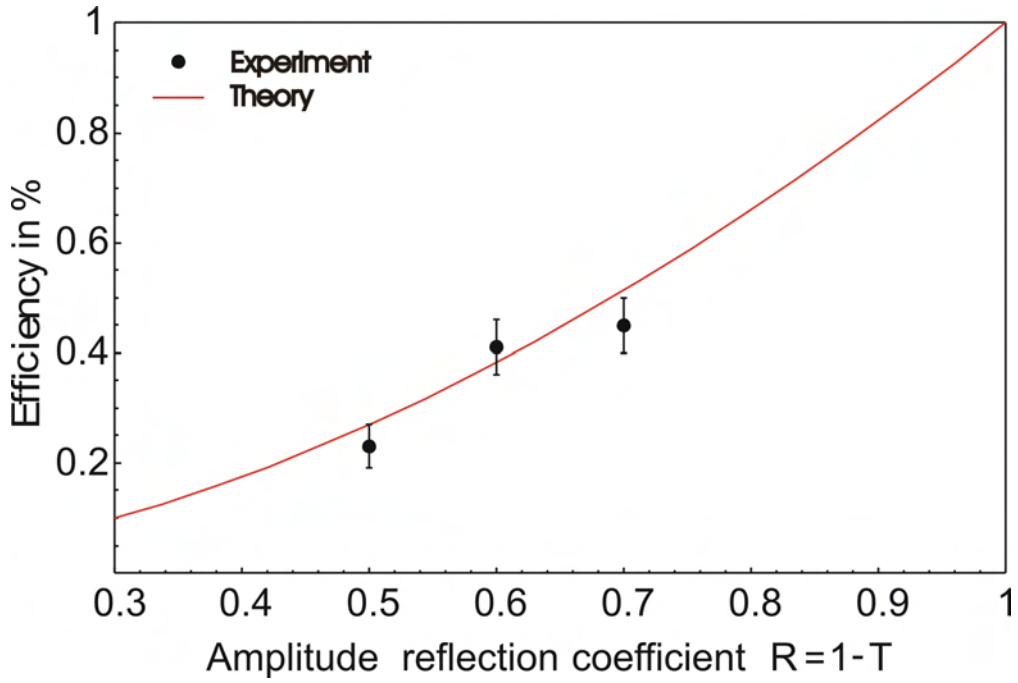

Figure 3.3: *Theoretical and experimental values of the state preparation efficiency for the three amplitude transmission coefficients* $T_a = 0.5, 0.4$ *and 0.3. The solid line represents the theoretical state preparation efficiency based on third order contribution and assuming a mean detection efficiency of all detectors of 15 %. It can clearly be seen, that by choosing a high enough beam splitting ratio the proposed source is able to reach the deterministic region. The theoretical predictions shown by the dots marked as 'Accustomed theory' are taking the different detection efficiencies for the trigger an the signal detectors into account. Our experimental results definitely follow the theoretical predictions. The errors of the experimental data are statistical and the fluctuations mainly result from the quality and stability of our alignment and the laser.*

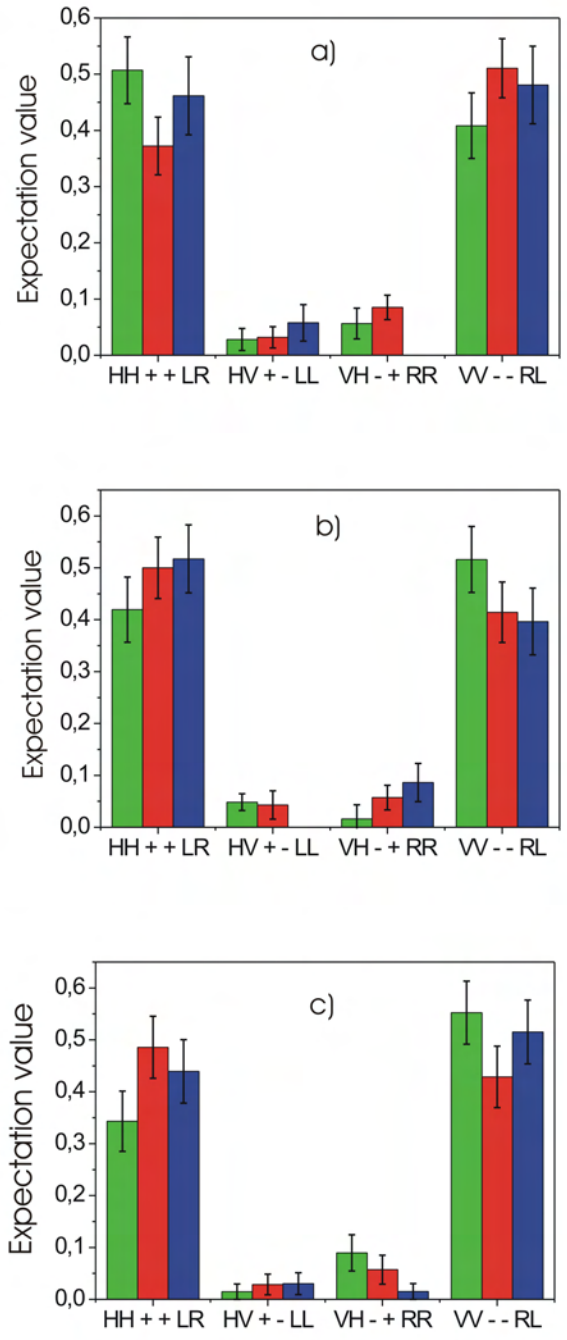

Figure 3.4: *Experimental results for the expectation values of the entangled state of the heralded photons in the output modes for the three different splitting ratios R/T a) 50/50, b) 60/40 and c) 70/30 of the partial reflecting beam splitters. Three complementary basis were used:* $|H\rangle/|V\rangle$, $|+\rangle/|-\rangle$ *and* $|R\rangle/|L\rangle$ *corresponding to the three different local measurements* $\hat{\sigma}_z\hat{\sigma}_z$, $\hat{\sigma}_x\hat{\sigma}_x$ *and* $\hat{\sigma}_y\hat{\sigma}_y$. *Measuring a* $|HH\rangle$ *or* $|VV\rangle$ *(*$|HV\rangle$ *or* $|VH\rangle$*) coincidence for the* $\hat{\sigma}_z\hat{\sigma}_z$ *setting,* $|++\rangle$ *or* $|--\rangle$ *(*$|+-\rangle$ *or* $|-+\rangle$*) for the* $\hat{\sigma}_x\hat{\sigma}_x$ *and* $|RR\rangle$ *or* $|LL\rangle$ *(*$|RL\rangle$ *or* $|LR\rangle$*) for the* $\hat{\sigma}_y\hat{\sigma}_y$ *respectively, the result is equivalent to* $+1$ (-1). *For each basis we measured* ≥ 50 *desired six-fold coincidences.*

an error of the calculated theoretical value of the expected preparation efficiency of 4.5%. Here, the four-pair contribution is evaluated in the same way as the three-pair state, where the limited detection efficiency of the trigger detectors is considered in the calculation.

To evaluate the quality of the entanglement of the output photons we have determined the fidelity of the state by analyzing the polarization state of the photons in modes $\hat{c}$ and $\hat{d}$ with the help of polarization state analyzers. The fidelity of the output state is defined as

$$\begin{aligned} F &= Tr[\hat{\rho}|\Phi^+\rangle\langle\Phi^+|] \\ &= \frac{1}{4}(1 - \langle\hat{\sigma}_x\hat{\sigma}_x\rangle - \langle\hat{\sigma}_y\hat{\sigma}_y\rangle - \langle\hat{\sigma}_z\hat{\sigma}_z\rangle), \end{aligned} \tag{3.8}$$

where $\hat{\rho}$ is the density matrix of the output state and $|\Phi^+\rangle\langle\Phi^+| = \frac{1}{4}(\hat{I} - \hat{\sigma}_x\hat{\sigma}_x - \hat{\sigma}_y\hat{\sigma}_y - \hat{\sigma}_z\hat{\sigma}_z)$. $\hat{\sigma}_x, \hat{\sigma}_y$ and $\hat{\sigma}_z$ are the Pauli matrices. Eq. (3.8) implies that we can obtain the fidelity of the prepared state by consecutively carrying out three local measurements $\hat{\sigma}_x\hat{\sigma}_x$, $\hat{\sigma}_y\hat{\sigma}_y$ and $\hat{\sigma}_z\hat{\sigma}_z$ on the photons in the modes $(\hat{c}_x, \hat{c}_y)$ and $(\hat{d}_x, \hat{d}_y)$.

The experimental results are shown in Fig. 3.4. For all three splitting ratios we measured more than 50 desired counts for each basis. For all three amplitude transmission coefficient $T = 0.3, 0.4, 0.5$ we were able to achieve a preparation fidelity of 0.870, which is sufficient to violate CHSH-type Bell's Inequality [81] for Werner states by three standard deviations. All theoretical and experimental values for the efficiencies and the measured fidelities can be viewed in Table I.

3.5 Discussion

In conclusion we have shown that the Śliwa's and Banaszek's scheme is indeed suitable to implement a heralded source for polarization entangled photon pairs. We have totally realized the proposed scheme, which was considered to be experimentally challenging under the limiting conditions of the present technical standard.

The experiment is based on the well known technique of type-II SPDC, which is robust, stable and involves modest experimental demands. Photon number resolving

Table 3.1: Experimental data for the preparation efficiency and the fidelity of the entangled state in comparison to the theoretically predicted efficiency for the three amplitude transmission coefficients T_a. The theoretical values are calculated solely from third order contributions.

T_a	eff_{theory}[%]	eff_{exp}[%]	fidelity
0.5	27	23 ± 1	0.870 ± 0.028
0.4	39	41 ± 2	0.875 ± 0.030
0.3	52	46 ± 2	0.873 ± 0.030

detectors are not involved in the setup, and therefore we do not face the restriction inherent to other schemes for implementing heralded entanglement sources [68, 71]. We have shown that by appropriately picking the trigger photons from the emission modes we will indeed obtain an entangled photon pair in the output modes. Altogether, only using standard techniques, we have proven the possibility to build a heralded source of entangled photons to overcome the probabilistic nature of spontaneous parametric down conversion sources. To evaluate the performance of our source, we have measured a fidelity of the output state of better than 87 %, and demonstrated the correlation between the transmission coefficient of the used beam splitter and the preparation efficiency of the source, which can even exceed 52 % by choosing an even lower transmission coefficient. This is a significant improvement compared with previous experiments for on-demand sources.

For future applications, the simple optical circuit of our source could be miniaturized by an integrated optics architecture on a chip using a silica-on-silicon technique [82]. Using wave guides instead of bulk optics would improve stability, performance and scalability [83, 77]. Therefore, the demonstrated source might be of promising use in essential photon based quantum information tasks.

Chapter 4

Quantum Teleportation of a Two-Qubit Composite System

4.1 Introduction

In Science Fiction literature a great dream of human kind has been realized already long time ago: the ability to travel by simply disappearing and then reappearing at some distant location (nowadays the most famous: Star Trek). To create a copy of an object at a distant location one does not need the original parts and pieces. The object to be transferred or *teleported* can be fully characterized by its properties, which in classical physics can be determined by measurement. Therefore all that is needed is to send the scanned information so that it can be used for reconstructing the object. But how precisely can this be an exact copy of the original? What happens to the individual quantum properties of the particles, which according to Heisenberg's uncertainty principle cannot be measured with arbitrary precision?

Bennett et al. [32] have suggested that it is possible to transfer the quantum state of a particle onto another particle at a distant location - the process of quantum teleportation - provided one does not get any information about the state in the course of this transformation. This requirement can be fulfilled by using quantum entanglement.

As we will see quantum teleportation is indeed as well a critical component of quantum computation and communication, as its experimental realization also allows new studies of the fundamentals of quantum theory. Therefore it is certainly one of those keystones of QIP [14] and thus central to a number of QIP protocols [21, 55, 29, 84].

4.2 Theory of Quantum Teleportation

The idea of teleportation is illustrated in Fig. 4.1. Alice wants to teleport particle 1, which is in the initial state ($|\chi\rangle_1 = \alpha\,|H\rangle_1 + \beta\,|V\rangle_1$) to Bob. A key role in the

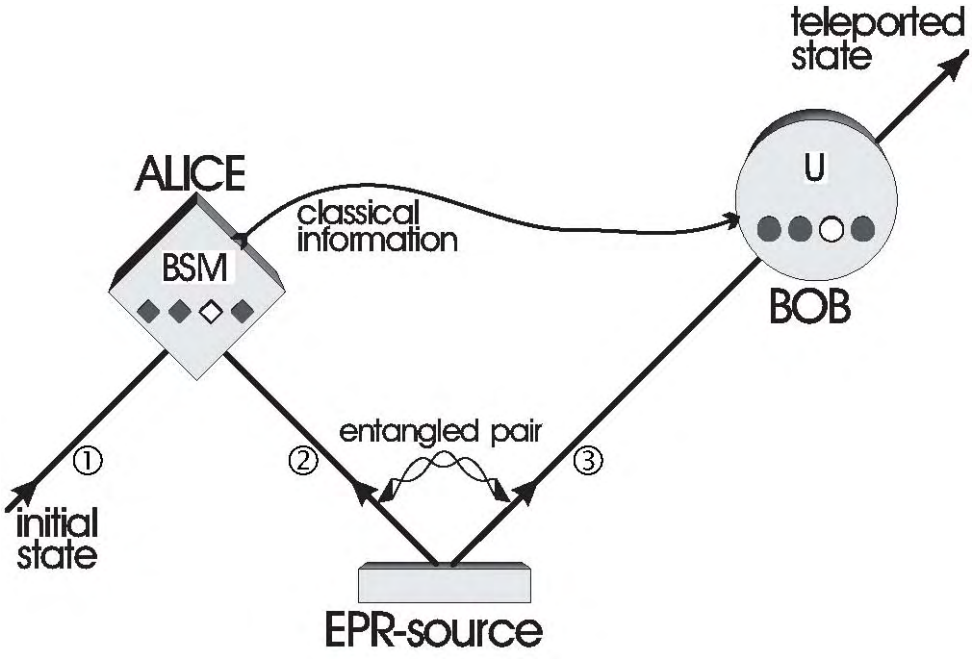

Figure 4.1: *Scheme showing the principle of quantum teleportation. Alice has a quantum system, particle 1, in an initial state, which she wants to teleport to Bob. Alice and Bob also share an ancillary entangled pair of particles 2 and 3 emitted by an EPR source. Alice then performs a joint Bell-state measurement (BSM) on the initial particle and one of the ancillaries, projecting them onto an entangled state. After she has sent the result of her measurement as classical information to Bob, he can perform a unitary transformation (U) on the other ancillary particle resulting in it being in the state of the original particle.*

teleportation scheme is played by an 'ancillary pair' of particles 2 and 3, which is in a maximally entangled Bell state, and is initially shared by Alice and Bob. This entangled state contains no information on the individual particles; it only indicates that the two particles will be in opposite states. As a tribute to Einstein, Podolsky and Rosen, these pairs are often called EPR pairs.

$$\left|\Phi^{+}\right\rangle_{23} = \frac{1}{\sqrt{2}}(\left|H\right\rangle_{2}\left|V\right\rangle_{3} - \left|V\right\rangle_{2}\left|H\right\rangle_{3}). \tag{4.1}$$

This entangled pair, emitted by an EPR source, is a single quantum system in an equal superposition of the states $|H\rangle_2|V\rangle_3$ and $|V\rangle_2|H\rangle_3$.

The essential point to achieve teleportation is to perform a joint BSM on particles 1 and 2 which projects them onto one of the four Bell states of Eq's. (2.9). Alice performs a BSM on 'her' particle 1, initially in the state $|\Psi\rangle_1$, and the ancillary particle 2, which is entangled with the other ancillary particle 3 in the hands of Bob. Although this establishes the possibility of nonclassical correlations between Alice and Bob, the entangled pair at this stage contains no information about $|\Psi\rangle_1$. Indeed the entire system, comprising Alice's unknown particle 1 and the entangled pair is in a pure product state, $|\Psi\rangle_1\left|\Phi^{+}\right\rangle_{23}$, involving neither classical correlation nor quantum entanglement between the unknown particle and the entangled pair. Therefore no measurement on either member of the entangled pair, or both together, can yield any information about $|\Psi\rangle_1$. The complete state of the three particles before Alice's measurement is

$$\begin{aligned} \left|\Psi\right\rangle_{123} \;=\; \left|\Psi\right\rangle_{1}\left|\Phi^{+}\right\rangle_{23} \;=\; & \tfrac{\alpha}{\sqrt{2}}\left(\left|H\right\rangle_{1}\left|H\right\rangle_{2}\left|V\right\rangle_{3} - \left|H\right\rangle_{1}\left|V\right\rangle_{2}\left|H\right\rangle_{3}\right) \\ + \; & \tfrac{\beta}{\sqrt{2}}\left(\left|V\right\rangle_{1}\left|H\right\rangle_{2}\left|V\right\rangle_{3} - \left|V\right\rangle_{1}\left|V\right\rangle_{2}\left|H\right\rangle_{3}\right). \end{aligned} \tag{4.2}$$

In the above equation particles 1 and 2 are represented in the computational basis. However, we can express the combined state in the Bell basis and can thus rewrite Eq. (4.2) as:

$$\begin{aligned} \left|\Psi\right\rangle_{123} \;=\; & \tfrac{1}{2}[\left|\Psi^{-}\right\rangle_{12}\left(-\alpha\left|H\right\rangle_{3} - \beta\left|V\right\rangle_{3}\right) \\ & + \left|\Psi^{+}\right\rangle_{12}\left(-\alpha\left|H\right\rangle_{3} + \beta\left|V\right\rangle_{3}\right) \\ & + \left|\Phi^{-}\right\rangle_{12}\left(\alpha\left|V\right\rangle_{3} + \beta\left|H\right\rangle_{3}\right) \\ & + \left|\Phi^{+}\right\rangle_{12}\left(\alpha\left|V\right\rangle_{3} - \beta\left|H\right\rangle_{3}\right)] \end{aligned} \tag{4.3}$$

Note that particle 1 is still completely separable from particles 2 and 3, since the state in Eq. (4.3) is still the same as in Eq. (4.2). During the teleportation Alice will destroy the quantum state at hand while Bob receives the quantum state, with neither Alice nor Bob obtaining information about the state $|\Psi\rangle$.

Eq. (4.3) implies that the four BSM outcomes are equally likely, each occurring with probability 1/4. Quantum physics predicts that once particles 1 and 2 are

projected into one of the four entangled states, particle 3 is instantaneously projected into one of the four pure states superposed in Eq. (4.3)

$$-|\chi\rangle_3 \quad , \quad -\hat{z}|\chi\rangle_3 \quad , \quad \hat{x}|\chi\rangle_3 \quad , \quad \hat{x}\hat{z}|\chi\rangle_3 \tag{4.4}$$

Each of these possible resultant states for Bob's EPR particle 3 is related in a simple way to the original state $|\Psi\rangle_1$ which Alice sought to teleport. In the case of the first outcome ($|\Phi^+\rangle$) the state of particle 3 is the same as the initial state of particle 1, so Bob needs do nothing further to produce a replica of Alice's unknown state. In the other three cases, Bob could accordingly apply one of the unitary Pauli transformations in Eq. (2.10) to convert the state of particle 3 into the original state of particle 1, after receiving via a classical communication channel the information which one of the four BSM results was obtained by Alice.

After Bob's unitary operation, the final state of particle 3 is therefore

$$|\Psi\rangle_3 = \alpha\,|0\rangle_3 + \beta\,|1\rangle_3\,. \tag{4.5}$$

Note that during the BSM particle 1 loses its identity because it becomes entangled with particle 2. Therefore the state $|\Psi\rangle_1$ is destroyed on Alice's side during teleportation. Performing BSM does not reveal any information on the properties of any of the particles. The fact that no information whatsoever on either particle is gained is also the reason why quantum teleportation escapes the verdict of the no-cloning theorem [85]. After successful teleportation particle 1 is not available in its original state anymore, and therefore particle 3 is not a clone but really the result of teleportation.

The transfer of quantum information from particle 1 to particle 3 can happen over arbitrary distances, hence the name teleportation. Experimentally, quantum entanglement has been shown to survive over a distance of 144 km [20]. We note that in the teleportation scheme it is not necessary for Alice to know where Bob is. Furthermore, the initial state of particle 1 can be completely unknown not only to Alice but to anyone. It could even be quantum mechanically completely undefined at the time the Bell-state measurement takes place. This is the case when, as already remarked by Bennett et al. [32], particle 1 itself is a member of an entangled pair and therefore has no well-defined properties on its own. This ultimately leads to entanglement swapping [80, 86] which will be discussed in more detail in C hapter 5.

Experimental demonstrations of teleportation have been implemented with photons [33, 87, 59] and ions [88, 89]. Very recently long-distance teleportation [90, 91] and open-destination teleportation [54] have also been realized. However, the teleportation of single qubits is insufficient for a large-scale realization of quantum communication and computation [21, 55, 29, 84]. The teleportation of a composite system containing two or more qubits has thus been seen as a long-standing goal in quantum information science.

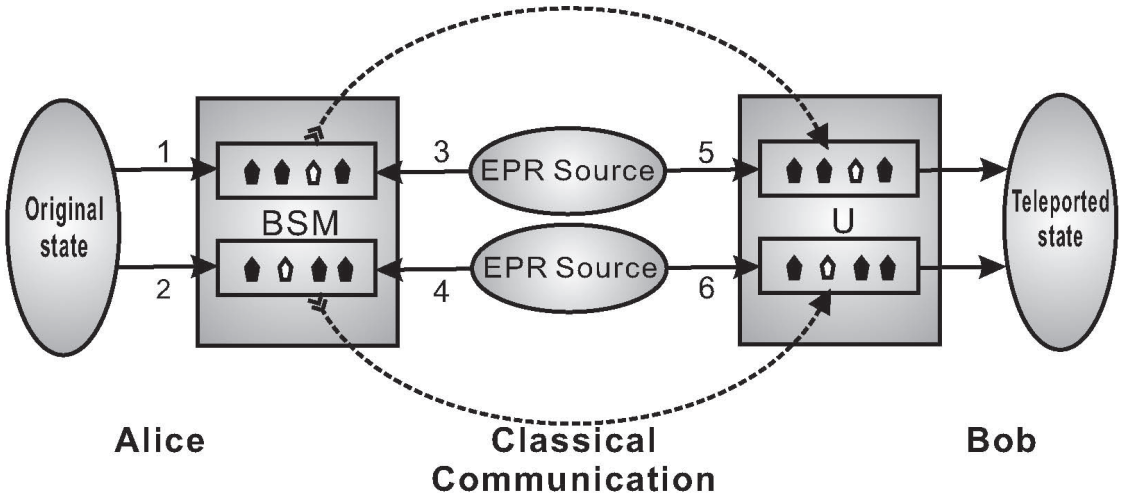

Figure 4.2: *Schematic diagram showing the principle of two-qubit teleportation. Alice wants to teleport an unknown state of a system composed of photon 1 and 2 to Bob. To do so, Alice and Bob first share two entangled photon pairs (EPR source), photon pairs 3-5 and 4-6. Alice then carries out a joint Bell-state measurement (BSM) both on photons 1 and 3 and on photons 2 and 4, respectively. On receiving Alice's BSM results via classical communication, Bob can then carry out a corresponding unitary transformation (*U*) on both photons 5 and 6 to convert them into the original state of photons 1 and 2.*

4.3 Teleportation of a Two-Qubit System

In this chapter we will discuss the first experimental demonstration of a two-photon quantum teleportation. In the experiment, we develop and exploit a six-photon interferometer to teleport an arbitrary polarization state of two photons. Not only does our six-photon interferometer provide an important step towards teleportation of a complex system, it will also enable future experimental investigations on a number of fundamental quantum communication and computation protocols [55, 92, 93, 94]. The concept of two-qubit teleportation and the experimental six-photon setup described in this chapter furthermore constitute the basis for the experiments of the following chapters (5,6).

Although there exist other ways to achieve teleportation of a composite system [95, 96], our experimental scheme [29, 97] closely follows the original proposal for teleportation of single qubits (chapter 4.2). In the two-qubit teleportation, the sender, Alice, wants to send an unknown state of a system composed of qubits 1 and 2,

$$|\chi\rangle_{12} = \alpha\,|H\rangle_1\,|H\rangle_2 + \beta\,|H\rangle_1\,|V\rangle_2 + \gamma\,|V\rangle_1\,|H\rangle_2 + \delta\,|V\rangle_1\,|V\rangle_2\,, \tag{4.6}$$

where α, β, γ and δ are four arbitrary complex numbers satisfying $|\alpha|^2+|\beta|^2+|\gamma|^2+|\delta|^2 = 1$, to a distant receiver, Bob (Fig. 4.2). In order to achieve teleportation, Alice

and Bob first have to share two ancillary entangled photon pairs (photon pairs 3-5 and 4-6) which are prepared in the Bell state $|\Phi^+\rangle$ (see Eq. 2.9). The two-qubit teleportation scheme then works as follows.

Alice first teleports the state of photon 1 to photon 5 following the standard teleportation protocol. In terms of the four Bell-states of photons 1 and 3,

$$\begin{aligned} |\Phi^{\pm}\rangle_{13} &= \frac{1}{\sqrt{2}}(|H\rangle_1|H\rangle_3 \pm |V\rangle_1|V\rangle_3) \\ |\Psi^{\pm}\rangle_{13} &= \frac{1}{\sqrt{2}}(|H\rangle_1|V\rangle_3 \pm |V\rangle_1|H\rangle_3), \end{aligned} \tag{4.7}$$

the combined state of photons 1, 2, 3 and 5 can be rewritten as

$$\begin{aligned} |\chi\rangle_{12}|\Phi^+\rangle_{35} =& \frac{1}{2}(|\Phi^+\rangle_{13}|\chi\rangle_{52} + |\Phi^-\rangle_{13}\hat{\sigma}_{5z}|\chi\rangle_{52} \\ &+ |\Psi^+\rangle_{13}\hat{\sigma}_{5x}|\chi\rangle_{52} + |\Psi^-\rangle_{13}(-i\hat{\sigma}_{5y})|\chi\rangle_{52}), \end{aligned} \tag{4.8}$$

where $\hat{\sigma}_x$, $\hat{\sigma}_y$ and $\hat{\sigma}_z$ are the well-known Pauli operators. Eq. (4.8) implies, that by performing a joint Bell state measurement (BSM) on qubits 1 and 3, Alice projects the state of qubits 5 and 2 onto one of the four corresponding states. After she has told Bob her BSM result via a classical communication channel, Bob can convert the state of qubits 5 and 2 into the original state $|\chi\rangle_{52}$ by applying to photon 5 a corresponding local unitary transformation ($\hat{I}$, $\hat{\sigma}_x$, $\hat{\sigma}_y$, $\hat{\sigma}_z$), independent of the original state.

Similarly, the combined state of photons 2, 4, 5 and 6 can be rewritten in terms of the four Bell-states of photons 2 and 4 as

$$\begin{aligned} |\chi\rangle_{52}|\Phi^+\rangle_{46} =& \frac{1}{2}(|\Phi^+\rangle_{24}|\chi\rangle_{56} + |\Phi^-\rangle_{24}\hat{\sigma}_{6Z}|\chi\rangle_{56} \\ &+ |\Psi^+\rangle_{24}\,\hat{\sigma}_{6X}\,|\chi\rangle_{56} + |\Psi^-\rangle_{24}\,(-i\hat{\sigma}_{6Y})\,|\chi\rangle_{56}). \end{aligned} \tag{4.9}$$

Following the above procedure, Alice can also teleport the state of photon 2 to photon 6. First, Alice performs a joint BSM on photons 2 and 4 and sends the BSM result to Bob. Upon the BSM result received, by applying to photon 6 a corresponding local unitary transformation ($\hat{I}$, $\hat{\sigma}_x$, $\hat{\sigma}_y$, $\hat{\sigma}_z$), Bob can convert the state of qubits 5 and 6 into the original state

$$|\chi\rangle_{56} = \alpha|H\rangle_5|H\rangle_6 + \beta|H\rangle_5|V\rangle_6 + \gamma|V\rangle_5|H\rangle_6 + \delta|V\rangle_5|V\rangle_6 \tag{4.10}$$

to accomplish the task of the most general two-qubit teleportation.

The above scheme has a remarkable feature: it teleports the two photonic qubits, 1 and 2 individually. This way, neither the two original qubits nor the teleported qubits have to be in the same place. Such a flexibility is desired in distributed quantum information processing, such as quantum telecomputation [84] and quantum secret sharing [53, 98]. Moreover, the above method of teleporting each qubit of a composite system individually can be easily generalized to teleport a N-qubit complex system.

4.4 Experimental Setup

A schematic diagram of our experimental setup is shown in Fig. (4.3). The developed high-intensity ultraviolet laser successively passes through two BBO crystals to generate three polarization-entangled photon pairs [30]. The ultraviolet laser beam is circularized and has a central wavelength of 390 nm, a pulse duration of 180 fs, a repetition rate of 76 MHz and an average power of 1.0 W. All three photon pairs are originally prepared in the Bell state $|\Phi^+\rangle = (|HH\rangle + |VV\rangle)/\sqrt{2}$. Following the efforts described in the above section, we managed to observe on average 10^5 photon pairs per second from each source. This is almost five times brighter than the source achieved in a recent teleportation experiment [54]. With this high-intensity entangled photon source we could obtain in total 10 six-photon events per minute. This is two orders of magnitude higher than any former photonic teleportation experiment could have achieved.

With the help of wave plates and polarizers, we prepared photon pair 1-2 in the desired two-qubit state $|\chi\rangle_{12}$ that is to be teleported. Photon pairs 3-5 and 4-6, which are in the state $|\Phi^+\rangle$, are used as the two ancillary pairs.

To implement two-qubit teleportation, it is necessary to perform a joint BSM on photons 1 and 3 and photons 2 and 4, respectively. To demonstrate the working principle of two-qubit teleportation it is sufficient to identify one of the four Bell-states in both BSMs, although this will result in a reduced efficiency - the fraction of success - of 1/16. In the experiment, we decide to analyze the Bell-state $|\Phi^+\rangle$ (see chapter 2.5.1). This is achieved by interfering photons 1 and 3 and photons 2 and 4 on the polarizing beam-splitters, PBS_{13} and PBS_{24}, respectively. To interfere photons 1 and 3 (photons 2 and 4) on the PBS_{13} (PBS_{24}), it has to be guaranteed that the two photons have good spatial and temporal overlap at the PBS such that they are indistinguishable. To achieve this, the two outputs of the PBSs are spectrally filtered ($\Delta\lambda_{FWHM} = 2.8nm$) and monitored by fiber-coupled single-photon detectors [79]. Moreover, perfect temporal overlap is accomplished by adjusting the path length of photon 3 (photon 2) by a delay prism 1 (prism 2) to observe "Hong-Ou-Mandel"-type interference fringes (HOM) [99, 78] behind the PBS_{13} (PBS_{24}) in the diagonal ($|+\rangle/|-\rangle$) basis [100]. These interferometers are sensitive only to length changes on the order of the coherence length of the detected photons ($\sim$110 μm) and stay stable for weeks. With the help of polarizers at 45°, the required projection of photons 1 and 3 (2 and 4) onto $|\Phi^+\rangle$ can then be achieved by detecting behind PBS_{13} (PBS_{24}) a $|+\rangle|+\rangle$ or $|-\rangle|-\rangle$ coincidence between detectors D1 and D3 (D2 and D 4) [100], as we have described in detail in chapter (2.5.1). Note that, in the experiment, only the $|+\rangle|+\rangle$ coincidence is registered, which further reduces the teleportation efficiency to 1/64. However, by inserting one PBS and two detectors behind each output of PBS13 and PBS24, respectively, both $|\Phi^+\rangle$ (by detecting a $|+\rangle|+\rangle$ or $|-\rangle|-\rangle$ coincidence) and $|\phi^-\rangle$ (by detecting a $|+\rangle|-\rangle$ or $|-\rangle|+\rangle$ coincidence) can be identified and thus the efficiency can be increased up to 1/4 [49].

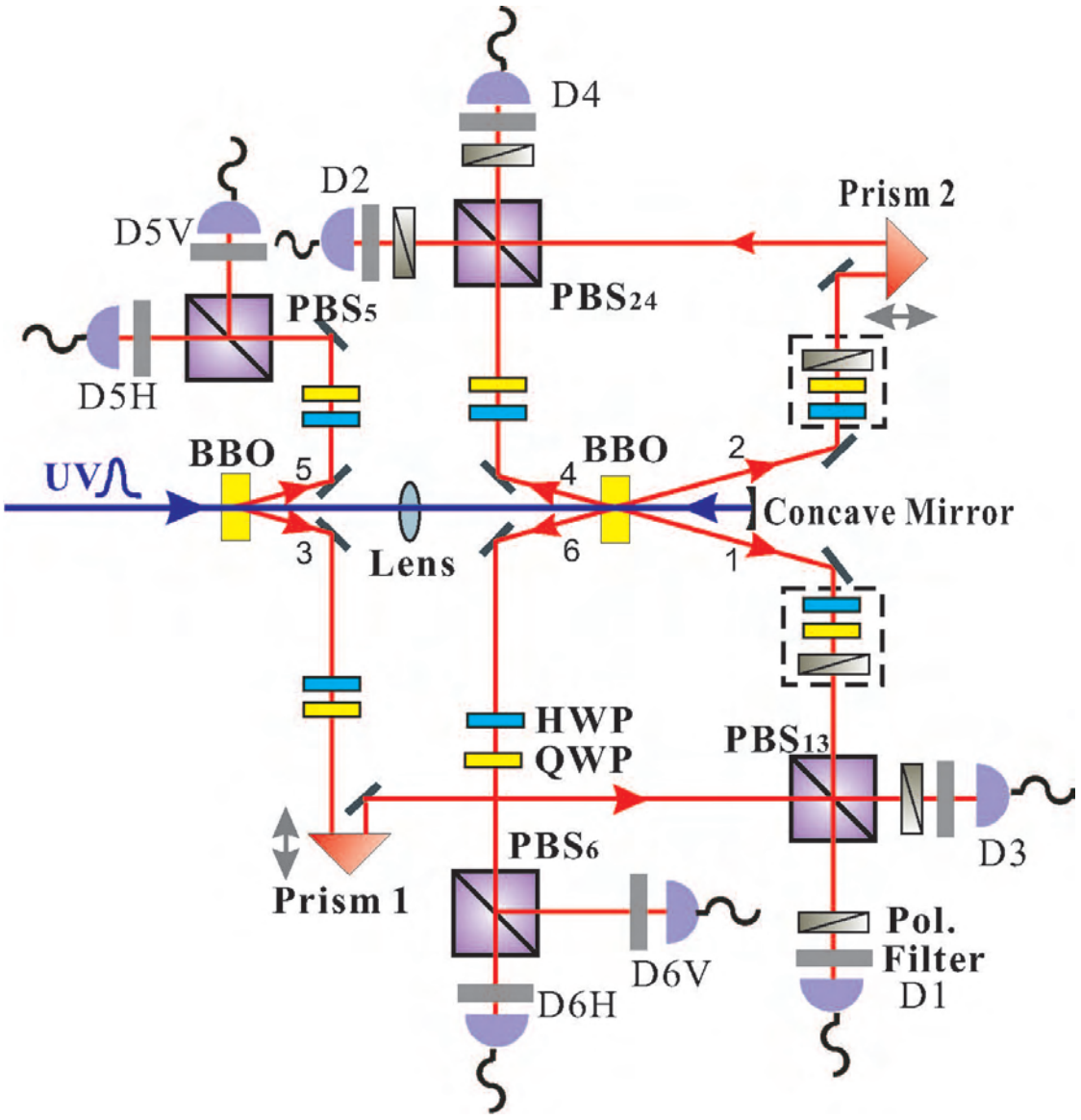

Figure 4.3: *A schematic diagram of the experimental setup. The ultraviolet pulse passes through a BBO crystal to generate a polarization-entangled photon pair in modes 3 and 5 (i.e. the first ancillary entangled photon pair). After the first BBO, a 10-cm-focus lens is introduced to refocus the ultraviolet pulse onto the second BBO to produce another entangled photon pair in modes 1 and 2 (to prepare the two qubits to be teleported). Reflected by a concave mirror, the ultraviolet pulse pumps once more into the second BBO and generates the third entangled photon pair in modes 4 and 6 (that is, the second ancillary photon pair). Prisms 1 and 2, both mounted on step motors, are used to compensate the time delay for the interference on polarizing beam splitters PBS13 and PBS24, respectively. PBS5 and PBS6 are used to verify the teleported state with the help of wave plates in front of them. The photons are all detected by silicon avalanched single-photon detectors. Coincidences are recorded with a coincidence unit clocked by the infrared laser pulses. Pol. are linear polarizers and Filter labels the narrow band filter with* $\Delta\lambda_{FWHM} = 2.8nm$.

As shown in Eq. (4.8) and Eq. (4.9), the projection measurements onto $|\Phi^+\rangle_{13}$ and $|\Phi^+\rangle_{24}$ leave photons 5 and 6 in the state $|\chi\rangle_{56}$, i.e. the original state of photons 1 and 2. To demonstrate that our two-qubit teleportation protocol works for a general unknown polarization state of photons 1 and 2, we decide to teleport three different initial states:

$$\begin{aligned} |\chi\rangle_A &= |H\rangle_1|V\rangle_2 \\ |\chi\rangle_B &= \tfrac{1}{2}\left(|H\rangle_1 + |V\rangle_1\right)\left(|H\rangle_2 - i|V\rangle_2\right) \\ |\chi\rangle_C &= \tfrac{1}{\sqrt{2}}\left(|H\rangle_1|V\rangle_2 - |V\rangle_1|H\rangle_2\right) \end{aligned} \tag{4.11}$$

$|\chi\rangle_A$ is simply one of the four computational basis vectors in the two-qubit Bloch sphere (Fig. 2.1); $|\chi\rangle_B$ is composed of a linear polarization state and a circular polarization state, which is also a superposition of all the four computational basis vectors; and $|\chi\rangle_C$ is a maximally entangled Bell state.

4.5 Experimental Results

We quantify the quality of our teleportation experiment by looking at the fidelity of the teleported state as defined in Eq. (2.35). To measure the fidelity of two-qubit teleportation, two PBSs (PBS_5 and PBS_6) and corresponding wave plates (HWP and QWP), as shown in Fig. (4.3), are combined properly to analyze the teleported state of photons 5 and 6.

The fidelity measurements for the $|\chi\rangle_A$ and $|\chi\rangle_B$ teleportation are straight forward. Conditioned on detecting a $|+\rangle|+\rangle$ coincidence between D1 and D3, D2 and D4, respectively, we analyze the teleported state of photons 5 and 6 in the computational basis for the $|\chi\rangle_A$ teleportation; whereas we analyze photon 5 in the diagonal basis and photon 6 in the circular basis for the $|\chi\rangle_B$ teleportation. As the above state analysis only involves orthogonal measurements on individual qubits, the fidelity of the teleported state is directly given by the fraction of observing a $|\chi\rangle_A$ or $|\chi\rangle_B$ state at detectors D5 and D6. The measurement results are shown in Fig. (4.4). The experimental integration time for each fidelity measurement was about 60 hours and we recorded about 100 desired two-qubit teleportation events. The integration time is slightly longer than would be expected from the original source rate, due to the additional losses at the interference PBSs. On the basis of our original data, we conclude that the fidelity for $|\chi\rangle_A$ and $|\chi\rangle_B$ is 0.86 ± 0.03 and 0.75 ± 0.02, respectively.

The measurement on the fidelity of the $|\chi\rangle_C$ teleportation is a bit more complex, since a complete Bell state analysis on photons 5 and 6 usually requires nonlinear interaction between them. Fortunately, the fidelity can still be determined by local measurements on individual qubits. To see this, we write the density matrix of $|\chi\rangle_C$ in terms of the Pauli matrices:

$$|\chi\rangle_{CC}\langle\chi| = |\Psi^-\rangle\langle\Psi^-| = \frac{1}{4}\left(\hat{I} - \hat{\sigma}_x\hat{\sigma}_x - \hat{\sigma}_y\hat{\sigma}_y - \hat{\sigma}_z\hat{\sigma}_z\right) \tag{4.12}$$

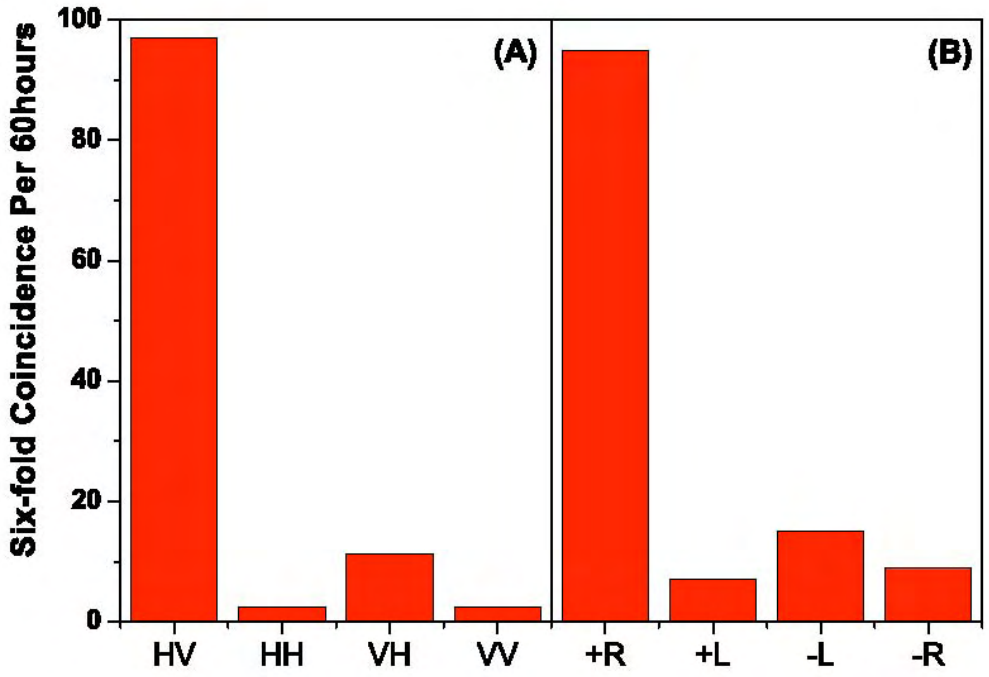

Figure 4.4: *Experimental results for the teleportation of the $|\chi\rangle_A$ state and the $|\chi\rangle_B$ state. Each measurement took 60 h.* ***(A)*** *The $|\chi\rangle_A$ state. We measured photon 5 and 6 in the computational basis.* ***(B)*** *The $|\chi\rangle_B$ state. We measured photon 5 in the diagonal and photon 6 in the circular basis. The fraction of $|H\rangle|V\rangle$ ($|+\rangle|R\rangle$) to the sum of all counts shows the fidelity for the teleportation of the $|\chi\rangle_A$ ($|\chi\rangle_B$) state in A (B).*

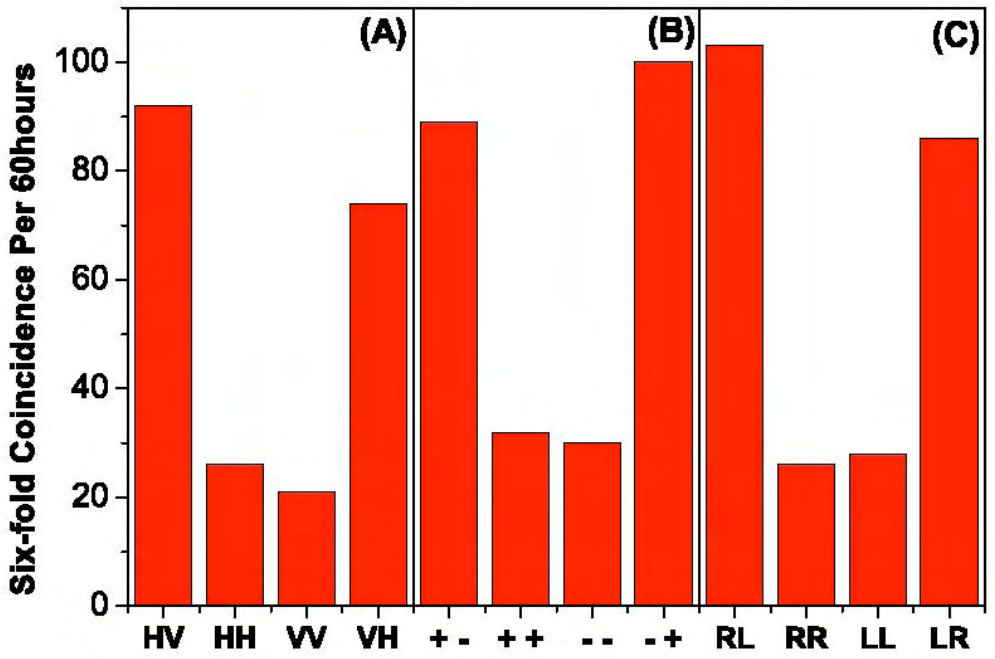

Figure 4.5: *Experimental results for the $|\chi\rangle_C$ teleportation. Three complementary bases were used: (**A**) computational, (**B**) diagonal and (**C**) circular basis, corresponding to the three different local measurements $\langle\hat{\sigma}_x\hat{\sigma}_x\rangle$, $\langle\hat{\sigma}_y\hat{\sigma}_y\rangle$ and $\langle\hat{\sigma}_z\hat{\sigma}_z\rangle$. Each measurements took 60 hours. In A whenever there is a $|H\rangle|H\rangle$ or $|V\rangle|V\rangle$ coincidence, the result of $\hat{\sigma}_x\hat{\sigma}_x$ is $+1$, whereas $|H\rangle|V\rangle$ or $|V\rangle|H\rangle$ represents -1. In B, $|+\rangle|+\rangle$ or $|-\rangle|-\rangle$ represents $+1$, whereas $|+\rangle|-\rangle$ or $|-\rangle|+\rangle$ represents -1. In C, $|R\rangle|R\rangle$ or $|L\rangle|L\rangle$ displaces $+1$, whereas $|R\rangle|L\rangle$ or $|L\rangle|R\rangle$ displaces -1.*

Original States	Fidelities	Fidelities after subtraction of noise
$\|H\rangle\|V\rangle$	0.86 ± 0.03	0.97 ± 0.03
$(\|H+V\rangle\|H-iV\rangle)/2$	0.75 ± 0.02	0.83 ± 0.02
$(\|H\rangle\|V\rangle - \|V\rangle\|H\rangle)/\sqrt{2}$	0.65 ± 0.03	0.77 ± 0.03
Average	0.75 ± 0.03	0.86 ± 0.03

Table 4.1: Fidelities of quantum teleportation of a two-qubit composite system.

With Eq. (4.12) we can expand the fidelity to

$$F = Tr\left(\hat{\rho}|\Psi^-\rangle\langle\Psi^-|\right) = \frac{1}{4}Tr\left[\hat{\rho}\left(\hat{I} - \hat{\sigma}_x\hat{\sigma}_x - \hat{\sigma}_y\hat{\sigma}_y - \hat{\sigma}_z\hat{\sigma}_z\right)\right]. \tag{4.13}$$

This implies that we can obtain the fidelity of the $|\chi\rangle_C$ teleportation by consecutively carrying out three local measurements $\langle\hat{\sigma}_x\hat{\sigma}_x\rangle$, $\langle\hat{\sigma}_y\hat{\sigma}_y\rangle$ and $\langle\hat{\sigma}_z\hat{\sigma}_z\langle$ on the two teleported qubits. The measurement results for the three operators are shown in Fig. (4.5), each of which took about 60 hours. Using Eq. (4.13) we determine an experimental fidelity of 0.65 ± 0.03.

As can be seen from the above experimental results, all the teleportation fidelities are well beyond the state estimation limit of 0.40 for a two-qubit composite system [101], hence successfully demonstrating quantum teleportation of a two-qubit composite system. The imperfection of the fidelities is mainly due to the noise caused by emission of two pairs of down-converted photons by a single source [33]. In our experiment, this noise contributes around 10 spurious six-fold coincidences in 60 hours and was not subtracted in the fidelity estimation. Table (4.1) clearly shows that by subtracting this noise, as it was done in a previous experiment [33], the fidelities improve strongly. Besides the double pair emission, the limited interference visibility and imperfect entangled state also reduce our teleportation fidelities. We notice that the fidelities of $|\chi\rangle_B$ and $|\chi\rangle_C$ teleportation are worse than those of $|\chi\rangle_A$. This is because the fidelities of $|\chi\rangle_B$ and $|\chi\rangle_C$ teleportation depend on the interference visibility on PBS13 and PBS24, while the $|\chi\rangle_A$ teleportation fidelity does not. Moreover, as the quality of the initial entangled state $|\chi\rangle_C$ is not as good as for the disentangled states $|\chi\rangle_A$ and $|\chi\rangle_B$, the fidelity of $|\chi\rangle_C$ teleportation is worse than that of the other two.

4.6 Discussion

In this chapter, we have discussed the development and exploration of a six-photon interferometer to report the first experimental demonstration of a two-qubit composite system. Not only does our experiment present an important step towards teleportation of a complex system, the techniques developed also enable immediate experimental investigations on novel quantum communication and computation

protocols, which will become more apparent in the following Chapters 5 and 6: Our six-photon interferometer allows the demonstration of a multiple swapping operation of an entangled state – in combination with quantum memory an indispensable prerequisite for large scale quantum communication networks. Using a slightly modified setup, photons 3,4,5 and 6 can first be prepared in a four-photon cluster state, which can further be exploited to demonstrate a teleportation-based controlled-NOT operation on photons 1 and 2 – this operation constitutes the kernel of fault tolerant quantum computation.

Chapter 5

Multistage Entanglement Swapping

5.1 Introduction

There exists an alternative way to create entanglement between two particles: it employs the projective Bell-State measurement (BSM) of the state of two particles onto an entangled state. If now these two particles, on which the BSM is performed, are taken from already entangled pairs, meaning each of the particles have a partner particle, then these remaining partner particles will automatically also collapse into an entangled state. This striking application of the projection postulate is called entanglement swapping[80].

Entanglement swapping thus provides a method of entangling distant particles, that never interacted and do not share a common past. The original idea was to use entanglement swapping for the so called 'event-ready detection' of entangled pairs. But moreover it became one of the most important ingredients for many concepts and protocols, which lay at the heart of quantum communication [21, 22, 92, 102, 103].

In photonic quantum communication, the distance over which information can be transferred is largely limited due to de-coherence from coupling to the environment and an increasing loss of photons in a quantum channel. This leads to an exponential fidelity decay of quantum information. This problem can be solved by subdividing larger distances into smaller sections over which entanglement or quantum states can be distributed. The sections are then bridged by entanglement swapping processes [21, 22, 92, 102]. The swapping procedure therefore constitutes one of the key elements for a quantum relay, and a full quantum repeater if combined with quantum purification [104, 105, 106, 107] and quantum memory [108, 109, 76]. As a result, quantum communication becomes feasible despite of realistic noise and imperfections. At the same time, the overhead for the used resources and communication time only increase polynomially with the distance [21, 22, 92, 102, 103].

When dividing a quantum channel into many segments, with the length of each

segment comparable to the channel loss length, one can achieve reliable and robust long-distance quantum communication by connecting two adjacent segments through entanglement swapping. Experimentally, photonic entanglement swapping has so far successfully been achieved for the case of discrete variables [59, 110, 111], and for continuous variables [112, 113, 114], both via a single stage process. However, only after successful multiple swapping, we are able to have a fully functional quantum repeater. For quantum information carriers possessing mass, multiple swapping processes can speed up the distribution of entanglement by a factor that is proportional to the number of segments used [86]. Moreover, multistage entanglement swapping can improve the protection of quantum states against noise suffered from amplitude errors [86].

In this chapter we discuss an experimental demonstration of entanglement swapping over two stages. Employing three highly bright and spatially independent pairs of polarization entangled photons, and performing BSMs among the three segments finally yields a maximally entangled pair distributed between the two distant parties. To quantitatively evaluate the performance, we have observed the quality of the output state by the characterization of an entanglement witness, which confirms genuine entanglement generation. Our experiment implements an entanglement distribution over two distant stations which are initially independent of each other and have never physically interacted in the past. This proof-of-principle demonstration constitutes an important step towards robust long-distance quantum relays, quantum repeaters and related quantum protocols based on multiple entanglement swapping.

5.2 Multistage Entanglement Swapping

The principle for multistage entanglement swapping is sketched in Fig. (5.1). Consider three independent sources, simultaneously emitting each a pair of maximally entangled photons (EPR pair). In anticipation of our experiments we assume that these are polarization entangled photons in the state

$$|\Psi\rangle_{123456} = |\Psi^-\rangle_{12} \times |\Psi^-\rangle_{34} \times |\Psi^-\rangle_{56}, \tag{5.1}$$

where $|\Psi^-\rangle_{ij}$ is one of the four maximally entangled Bell states of Eq. (2.9). Note that photon pairs 1-2, 3-4 and 5-6 are entangled in the antisymmetric polarization state, respectively. However, the states of the three pairs are factorizable from each other, namely there is no entanglement among any photons from different pairs.

As a first step we perform a joint BSM on photons 2 and 3, i.e. photons 2 and 3 are projected onto one of the four Bell states. Moreover, this measurement also projects photons 1 and 4 onto a Bell state, in a form depending on the result of the BSM of photons 2 and 3. Close inspection shows that for the initial state given in Eq. (5.1), the emerging state of photons 1 and 4 is identical to the one that photons 2 and 3 collapse into. This is a consequence of the fact that the state of Eq. (5.1)

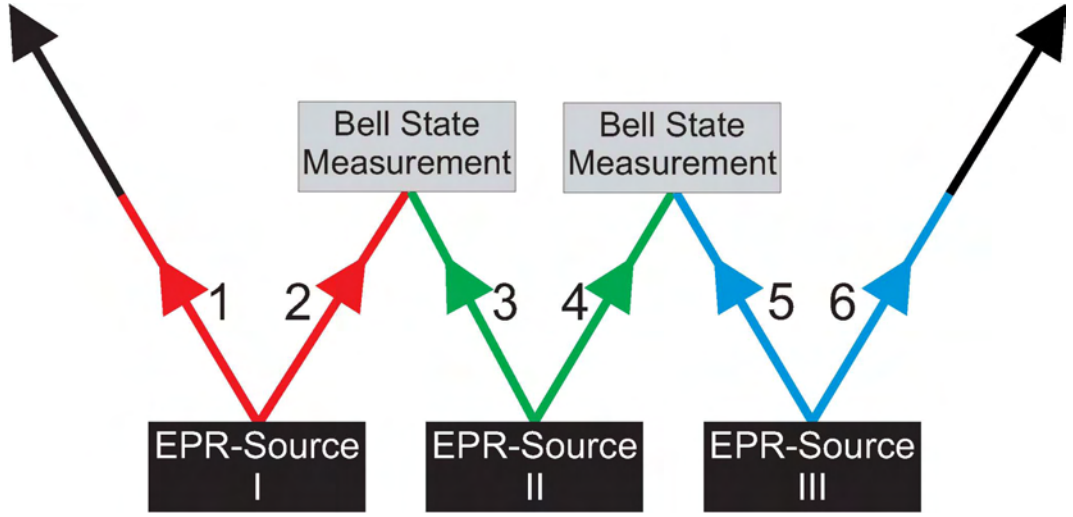

Figure 5.1: *Principle of multistage entanglement swapping. Three Einstein Podolsky Rosen (EPR) sources produce pairs of entangled photons 1-2, 3-4 and 5-6. Photon 2 from the inial state and photon 3 from the first ancillary pair are subjected to a joint BSM, and so are photon 4 from the first ancillary and photon 5 from the second ancillary pair. The two BSMs project outgoing photons 1 and 6 onto an entangled state. Thus the entanglement of the initial pair is swapped to an entanglement between photons 1 and 6.*

can be rewritten as

$$\begin{aligned} |\Psi\rangle_{123456} \quad = \quad & \tfrac{1}{2}[|\Psi^+\rangle_{14}|\Psi^+\rangle_{23} - |\Psi^-\rangle_{14}|\Psi^-\rangle_{23} \\ & -|\Phi^+\rangle_{14}|\Phi^+\rangle_{23} + |\Phi^-\rangle_{14}|\Phi^-\rangle_{23}] \\ & \times|\Psi^-\rangle_{56} \end{aligned} \tag{5.2}$$

In all cases photons 1 and 4 emerge entangled despite the fact that they never interacted with one another in the past. After the joint measurement of photons 2 and 3 one knows immediately about the entanglement type between photons 1 and 4.

Without loss of generality, we assume in the first step that photons 2 and 3 have collapsed into the state $|\Phi^+\rangle_{23}$ as a result of the first BSM. The remaining four-photon state is then of the form

$$\begin{aligned} |\Psi\rangle_{1456} \quad = \quad & \tfrac{1}{2}\ [|\Psi^+\rangle_{16}|\Phi^-\rangle_{45} + |\Psi^-\rangle_{16}|\Phi^+\rangle_{45} \\ & -|\Phi^+\rangle_{16}|\Psi^-\rangle_{45} - |\Phi^-\rangle_{16}|\Psi^+\rangle_{45}] \end{aligned} \tag{5.3}$$

In a similar manner we perform a second BSM on photons 4 and 5. Again a detection of the state $|\Phi^+\rangle_{45}$ results in projecting the remaining photons 1 and 6 onto the Bell state

$$|\Psi^-\rangle_{16} = \frac{1}{\sqrt{2}}(|H\rangle_1|V\rangle_6 - |V\rangle_1|H\rangle_6) \tag{5.4}$$

5.3 Experimental Setup

A schematic diagram of our setup for multistage entanglement swapping is illustrated in Fig. (5.2). The used setup is very similar to the one used in the previous chapter (4). The pulsed high-intensity ultraviolet (UV) beam successively passes through three β-Barium-Borate (BBO) crystals to generate three polarization entangled photon pairs via type-II parametric down conversion [30]. For the joint BSM of photons 2 and 3 (photons 4 and 5), we choose to analyze the case of detecting the projection onto a $|\Phi^+\rangle$ state. Using once again the method of chapter (2.5.1) the Bell state analyzer allows the projection of photons 2 and 3 (4 and 5) onto the state $|\Phi^+\rangle$ upon the detection of a $|+\rangle|+\rangle$ or $|-\rangle|-\rangle$ coincidence at detectors D2 and D3 (D4 and D5). Again, only the $|+\rangle|+\rangle$ coincidences are registered, which yields an overall success efficiency of 1/64. The resulting state of photons 1 and 6 is polarization analyzed behind PBS1 and PBS6, respectively.

5.4 Experimental Results

As shown in equations Eq. (5.2, 5.3, 5.4) the projection measurements onto $|\Phi^+_{23}\rangle$ and $|\Phi^+_{45}\rangle$ leave photons 1 and 6 in the maximally entangled state $|\Psi^-_{16}\rangle$. In contrast to quantum state tomography, the measurement of witness operators does not provide a complete reconstruction of the original quantum state, it however allows to check with a minimal number of local measurements for an entanglement character of a quantum state (see section 2.5.2). To verify that the two photons really result in an entangled state, and thus the swapping operation is successful, the expectation value of the corresponding witness operator [61, 115] is expected to take a value between -1 and 0. In our case, the applied witness operator W is the most efficient one since it involves only the minimal number of local measurements [61]. It can be measured locally by choosing correlated measurement settings, that involve only the simultaneous detection of linear, diagonal and circular polarizations for both photons. We have performed local measurements on the outgoing state of photons 1 and 6 in the three complementary bases; linear (computational) ($|H\rangle/|V\rangle$), diagonal ($|+\rangle/|-\rangle$) and circular ($|R\rangle/|L\rangle$).

The entanglement witness is given by

$$\begin{aligned}\hat{\mathcal{W}} \;=\; & \tfrac{1}{2}\,(|HH\rangle\langle HH| + |VV\rangle\langle VV| + |++\rangle\langle ++| \\ & +|--\rangle\langle --| - |RL\rangle\langle RL| - |LR\rangle\langle LR|).\end{aligned} \tag{5.5}$$

In the experiment, we perform measurements for each correlation function of the entanglement witness. The expectation values are shown in Fig. (5.3). Experimental integration time for each local measurement took about 60 hours and we recorded about 180 events of desired two-qubit coincidences. Every expectation value for a correlation function is obtained by making a von Neumann measurement along a specific basis and compute the probability over all the possible events. For example,

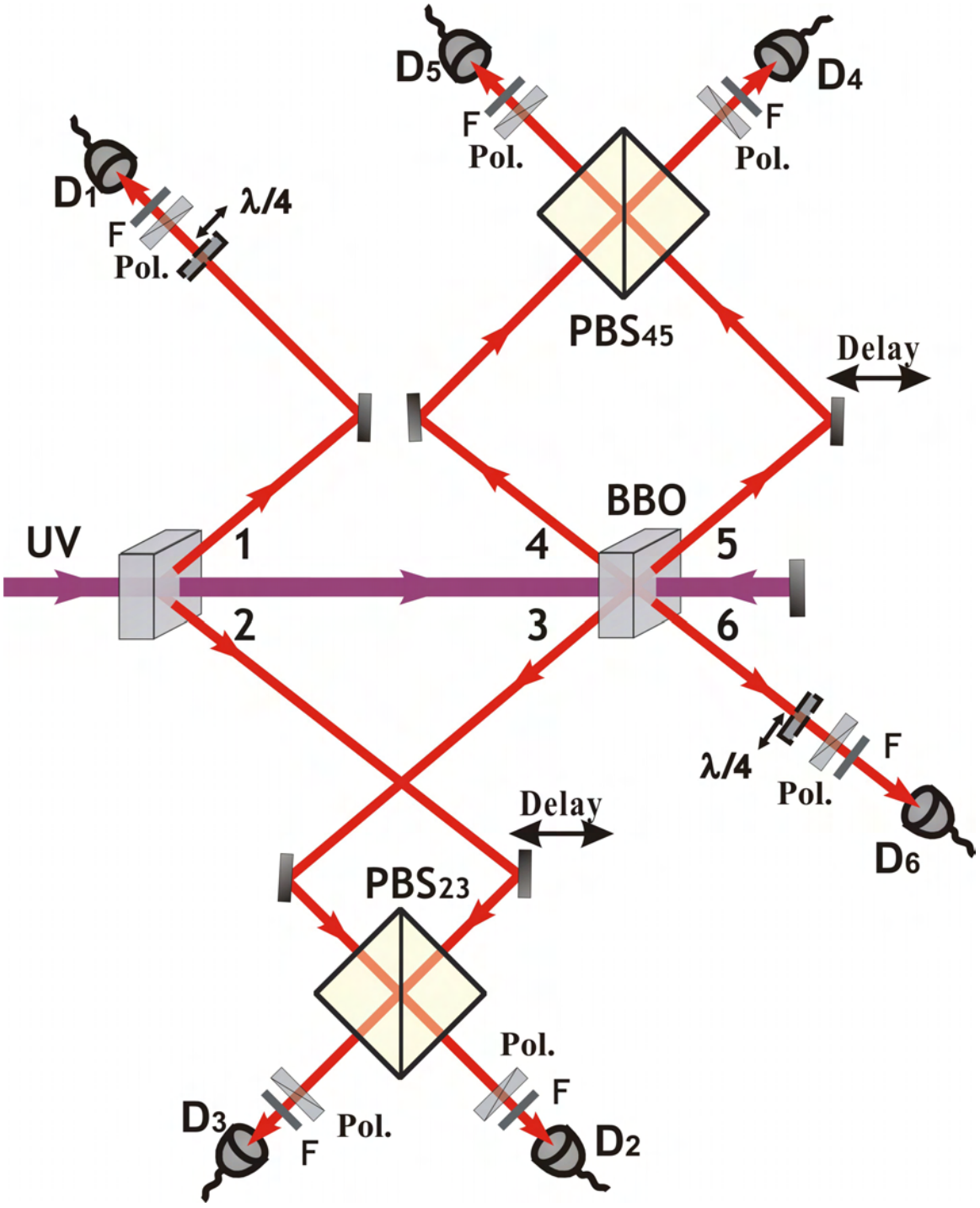

Figure 5.2: *A schematic diagram of the experimental setup. The focused ultraviolet laser beam passes through the first BBO generating photon pair 1-2. Refocussed, it passes through the second BBO generating the ancillary pair 3-4. After reflection it again passes through the second BBO generating pair 5-6. In order to perform a BSM of photons 2 and 3 (4 and 5), they are interfered at PBS23 (PBS45) and analyzed with polarizers at 45°. PBS1 and PBS6 are polarization analyzers for the swapped entangled state.*

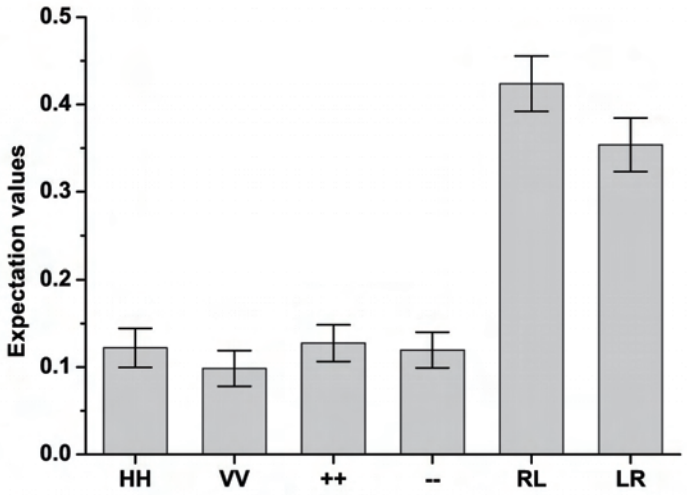

Figure 5.3: *Experimental expectation values for every correlation function of the entanglement witness for the swapped state. The results are derived by twofold coincidence measurements along three complementary common bases* ***(a)*** $|H\rangle|V\rangle$, ***(b)*** $|+\rangle|-\rangle$ *and* ***(c)*** $|R\rangle|L\rangle$, *conditioned on a fourfold coincidence event in* $|++++\rangle$ *for detectors D2-D3-D4-D5 which ensures two successful Bell state measurements.*

for a HH correlation $\mathrm{Tr}(\hat{\rho}|HH\rangle\langle HH|)$, we perform measurements along the linear (computational) basis. Then its value is given by the number of coincidence counts of HH over the sum of all coincidence counts of HH, HV, VH and VV. We proceed likewise for the other correlation settings. The witness can then directly be evaluated to

$$\mathrm{Tr}(\hat{\rho}\hat{\mathcal{W}}) = -0.16 \pm 0.03. \tag{5.6}$$

The negativity of the measured witness implies clearly that the original entanglement has indeed been swapped. The imperfection of our data is due to the non-ideal quality of entangled states generated from the high power UV beam, as well as the partial distinguishability of independent photons at PBS23 and PBS45, which leads to non-perfect interferences and a degrading of the entanglement output quality [116, 117]. Moreover, double pair emission by a single source causes noise of an order of 10 spurious six-fold coincidences in 60 hours and was not subtracted in calculating the expectation value of the witness operator.

To ensure that there is no entanglement between photons 1 and 6 before neither of the entanglement swapping process, we have performed a complete quantum state tomography of the combined state. The experimental expectation values for various bases are illustrated in Fig. (5.4). Concurrence [118] is a monotone function of entanglement, ranging from 0 for a separable state to 1 for a maximally

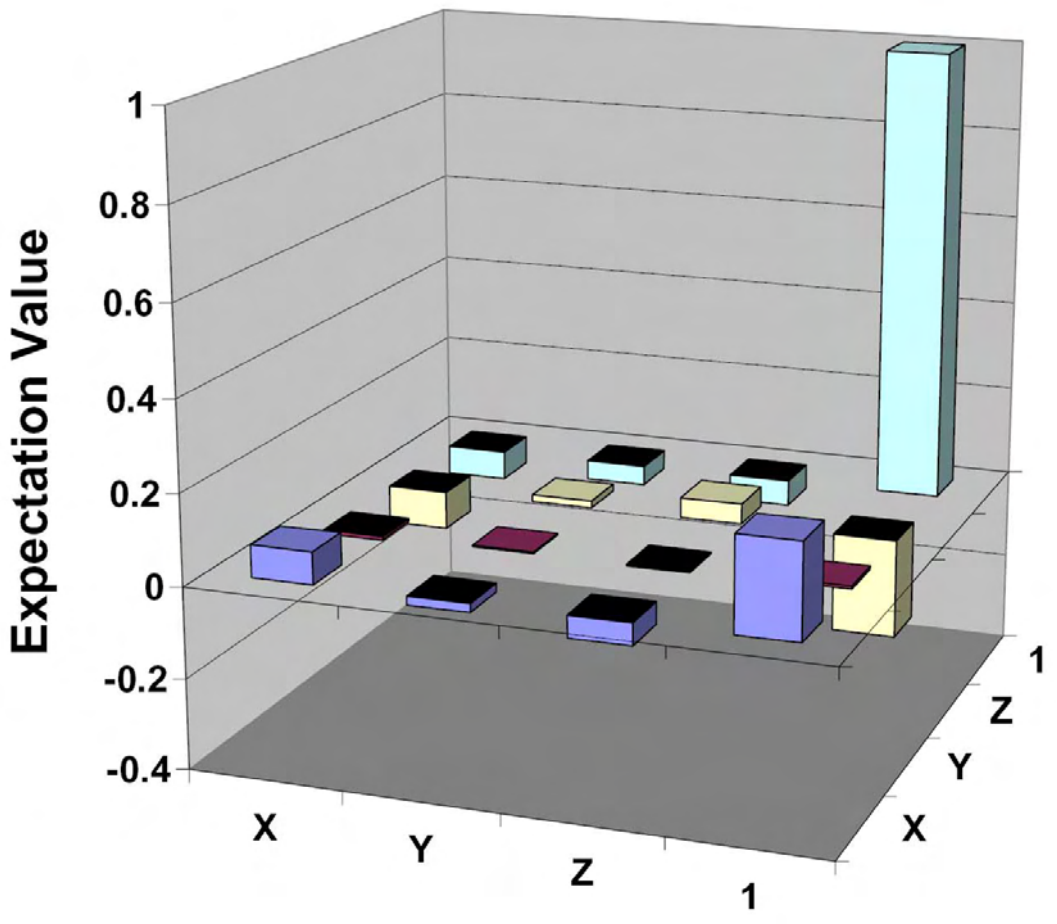

Figure 5.4: *Complete quantum state tomography on photons 1 and 6 before entanglement swapping. Label X corresponds to measurement setting $\hat{\sigma}_x$, while Y and Z are for $\hat{\sigma}_y$ and $\hat{\sigma}_z$, respectively. The result shows that the photons didn't reveal any entanglement whatsoever before the swapping operation.*

entangled state. In terms of concurrence, we can thus quantify the degree of entanglement through a reconstructed density matrix ρ_{init} for the initial combined state from the data shown in Fig. (5.4). The concurrence C_{init} derived from ρ_{init} is $C_{init} = \max(0, -0.39 \pm 0.01) = 0$. As expected, the concurrence C is exactly 0, which shows that photons 1 and 6 were independent and did not reveal any entanglement whatsoever before the swapping. Ideally, for a completely mixed state the expectation value for all local measurements should be 0, except for the unity operator, which should be 1. The contributions of the measurement settings other than the unity operator are mainly due to noise caused by scattered light of the UV beam at the BBO crystal. After the two-stage entanglement swapping, entanglement arises as unambiguously confirmed by the witness measurement of Eq. (5.6).

5.5 Discussion

In this chapter, we have discussed the first demonstration of a proof-of-principle implementation of a two-stage entanglement swapping using photonic qubits. The feasibility and effectiveness of this process has been verified by a successful distribution of genuine entanglement after two simultaneously independent swapping processes. This result yields the possibility of immediate near-future applications of various practical QIP tasks. If combined with narrow-band entanglement sources, the implementation of quantum relays (without quantum memory) and quantum repeaters (with quantum memory) for either free space or fiber-based entanglement distribution could become within current reach, as well as quantum state transfer and quantum cryptography networks in a more efficient way and over much larger distances of around hundreds of kilometers. Our demonstration also allows for the possibility of utilizing multi-party, multiple stages entanglement swapping to achieve global quantum communication networks, though with significant challenges ahead [86].

Chapter 6

Teleportation-Based Controlled-NOT Gate for Fault-Tolerant Quantum Computation

6.1 Introduction

Quantum computers promise a dramatic speed up for many computational tasks and, in theory, can outperform their classical counterparts in various computational applications such as searching an unsorted data base [46] or factorizing large numbers [23]. They further promise efficient simulation of dynamics of complex quantum systems, which is not possible with conventional computers [12].

For large-scale quantum computation however, the inevitable coupling of physical qubits to the noisy environment and residual imperfections in physical systems [119, 120, 121] impose a major challenge to a practical implementation. Namely, this coupling can lead to errors among the processed qubits making quantum error correction schemes necessary. Several algorithms to encode a logic qubit onto a number of physical qubits have been developed [93, 104, 122, 123, 124, 125]. These codes are able to correct for any single qubit error, as long as maximally one of the physical qubits has been altered. After decryption one is able to recover the unaltered, original logic qubit. A next problem arises once we want to perform quantum gates, i.e. to perform logic operations on the protected data. Since the logic qubit has been encoded, we need to perform corresponding operations on the physical qubits. Depending on the characteristics of the chosen code and gate (in particular conditional gates), errors may then not only propagate between blocks of encoded qubits but also within them. This can compromise the code's ability to correct for these errors. The solution are the so-called "fault-tolerant quantum gates". A procedure is called fault-tolerant if its failing components do not spread more errors in the block

of encoded output qubits than the code can correct. In a seminal paper, Gottesman and Chuang (GC) introduced a novel protocol to implement any quantum gate needed for quantum computation in a fault-tolerant manner [55]. A procedure is fault-tolerant if its failing components (this includes the input) do not spread more errors in the block of encoded output qubits than the code can correct.

In this chapter we present the non-trivial realization of the GC scheme. We implemented the proposed architecture by performing a teleportation-based two-qubit controlled-NOT gate through linear optics with a high-fidelity six-photon interferometerby combining the techniques of quantum teleportation of a composite system [126] and the creation of a four-qubit photon cluster state [127]. In the experiment, we chose to implement a teleportation-based controlled-NOT (C-NOT) gate, which, together with very easy to implement single qubit operations, is sufficient to perform all logic operations needed for quantum computation [128, 129]. The obtained results clearly prove the involved working principles and the entangling capability of the gate. Our experiment represents an important step towards the feasibility of realistic quantum computers and triggered many further applications in linear optics quantum information processing, such as one-way quantum computation [94] and linear optics quantum computation [29].

6.2 The Teleportation-Based C-NOT gate

The approach of Gottesman and Chuang, a generalization of quantum teleportation [32, 33] (see chapter 4.2), is straight forward and requires only a minimum of resources. A key element of their work is the C-NOT gate, which acts on two qubits, a control and a target qubit. The logic table of the C-NOT operation (U^{C-NOT}) is given by (see chapter 2.2.3)

$$\begin{aligned} |H\rangle_i|H\rangle_j &\rightarrow |H\rangle_i|H\rangle_j \quad , \\ |H\rangle_i|V\rangle_j &\rightarrow |V\rangle_i|V\rangle_j \quad , \\ |V\rangle_i|H\rangle_j &\rightarrow |V\rangle_i|H\rangle_j \quad \text{and} \\ |V\rangle_i|V\rangle_j &\rightarrow |H\rangle_i|V\rangle_j \quad , \end{aligned}$$

where we have used the photon polarization degree of freedom to encode our qubits.

Instead of directly performing complicated gate operations on the input qubits, we prepare a two-photon input

$$|\Psi_{in}\rangle_{ij} = \alpha|H\rangle_i|H\rangle_j + \beta|H\rangle_i|V\rangle_j + \gamma|V\rangle_i|H\rangle_j + \delta|V\rangle_i|V\rangle_j \qquad (6.1)$$

$|\Psi_{in}\rangle_{ij}$ can be in a completely random state, in which qubit j acts as the control bit $|C\rangle_j$ and qubit i as the target bit $|T\rangle_i$ and the pre-factors α, β, γ and δ are four arbitrary complex numbers satisfying $|\alpha|^2 + |\beta|^2 + |\gamma|^2 + |\delta|^2 = 1$. Serving as a C-NOT gate the entangling properties of our four-photon cluster state $|\chi\rangle$ have to fulfill the condition, that the output state is equivalent to the input state up to the

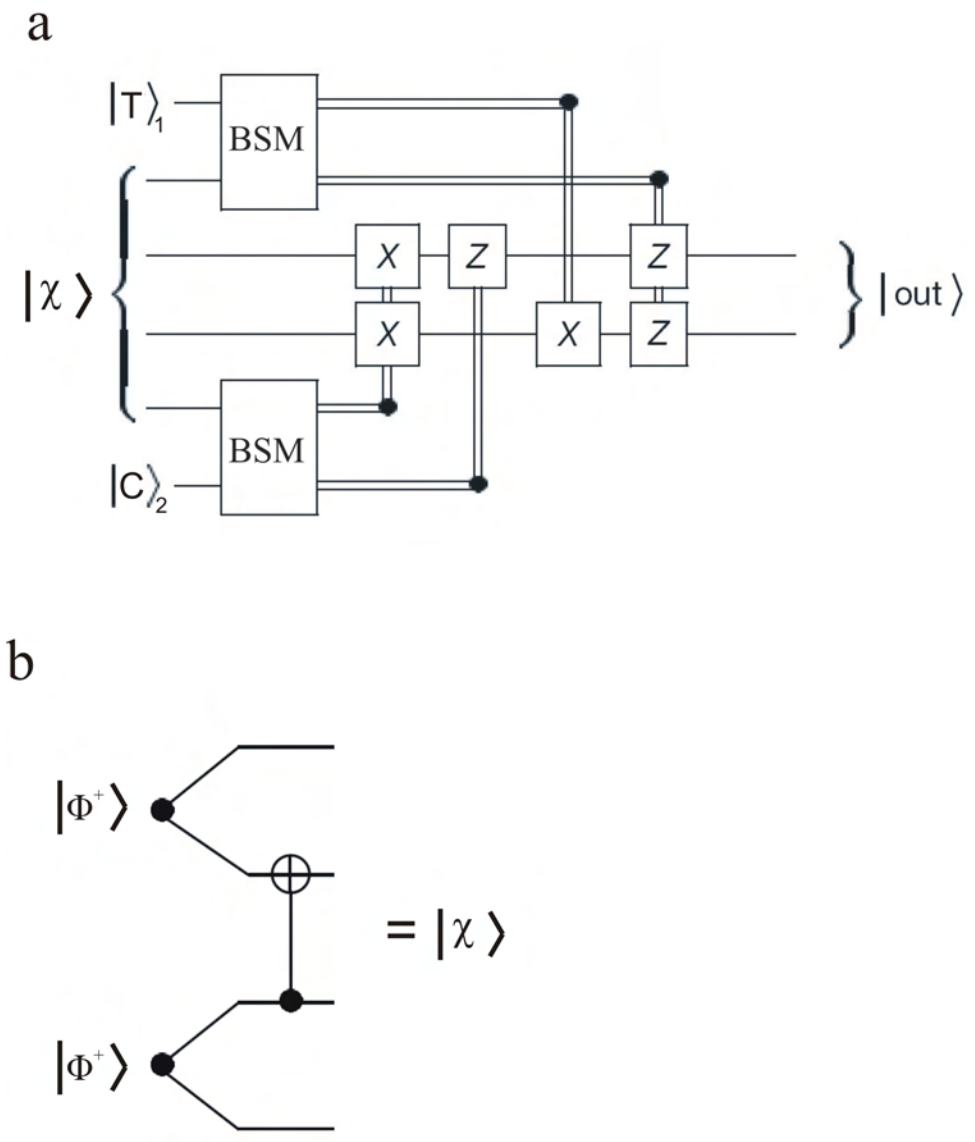

Figure 6.1: ***(a)*** *Quantum circuit for teleporting two qubits through a C-NOT gate. Time flow is from left to right. The input consisting of the target qubit* $|T\rangle_1$ *and control qubit* $|C\rangle_2$ *can be arbitrarily chosen. Bell State Measurements (BSMs) are performed between the input states and the outer qubits of the special entangled state* $|\chi\rangle$*. Depending on the outcome of the BSMs, local unitary operations (X, Z) are conducted on the remaining qubits of* $|\chi\rangle$*, which then form the output* $|out\rangle = U^{C-NOT}|T\rangle_1|C\rangle_2$*. Single lines correspond to qubits and double lines represent classical bits.* ***(b)*** *The special entangle state* $|\chi\rangle$ *can be constructed by performing a C-NOT gate on two EPR pairs, with* $|\Phi^+\rangle = \frac{1}{\sqrt{2}}(|H\rangle|H\rangle + |V\rangle|V\rangle)$*.*

following unitary transformation

$$|\Psi_{out}\rangle_{ij} \quad = \quad \hat{U}^{C-NOT}|\Psi_{in}\rangle_{ij} \tag{6.2}$$

. As sketched in Fig. 6.1a) the four-qubit photon cluster state $|\chi\rangle$ we will construct beforehand. After the creation of $|\chi\rangle$ one transfers the data of the two input qubits, the target bit $|T\rangle_i$ and the control bit $|C\rangle_j$, onto $|\chi\rangle$ by quantum teleportation. This is done by successively performing a joint "Bell-State-Measurement" (BSM) between the target (control) qubit and the two outer qubits of $|\chi\rangle$. As a direct consequence of the projective BSMs and the four-partite entanglement of $|\chi\rangle$, the remaining two (output) qubits

$$|\Psi_{out}\rangle_{ij} \quad = \quad \alpha|H\rangle_i|H\rangle_j + \beta|V\rangle_i|V\rangle_j + \gamma|V\rangle_i|H\rangle_j + \delta|H\rangle_i|V\rangle_j \tag{6.3}$$

already posses the information originally carried by the input qubits. The target qubit i of the output state is flipped on the condition that the control qubit j is in the state $|V\rangle$. Finally, we need to apply single qubit (Pauli) operations to the output qubits, depending on the outcome of the BSMs.

Note, that in the above scheme all qubits are logic qubits. However, the scheme generalizes in a straight forward manner when we use a larger number of physical qubits to encode our logic qubits. The procedure is then fault-tolerant since all operations are transversal, i.e. qubits of one block of encoded qubits interact only with corresponding qubits in other code blocks. A further advantage is the fact that only classically controlled single-qubit operations and BSMs are needed to perform the actual gate and that the resource of the special entangled state $|\chi\rangle$ can be constructed in forehand. If its generation fails nothing is lost by discarding it and trying again until successful generation. We would like to emphasize two aspects: First, the setup can be used to process any unknown input state and second, several other quantum gates can be implemented by this scheme. The choice of gate only depends on the form of the ancillary state $|\chi\rangle$.

In the following, we will give a step by step analysis of the teleportation-based C-NOT gate, as implemented in our setup given in Fig. 6.2: We align each β-barium borate (BBO) crystal carefully to produce two pairs of polarization entangled photons 3,4 and 5,6 in the state

$$|\Psi^+\rangle = \frac{1}{\sqrt{2}}\left(|H\rangle|H\rangle + |V\rangle|V\rangle\right) \tag{6.4}$$

According to the method described by Kiesel et al. [127], to prepare the cluster state $|\chi\rangle$ we now direct photons 4 and 6 to the two input modes of a polarization dependent beam splitter (PDBS), respectively. The transmission T_H (T_V) of

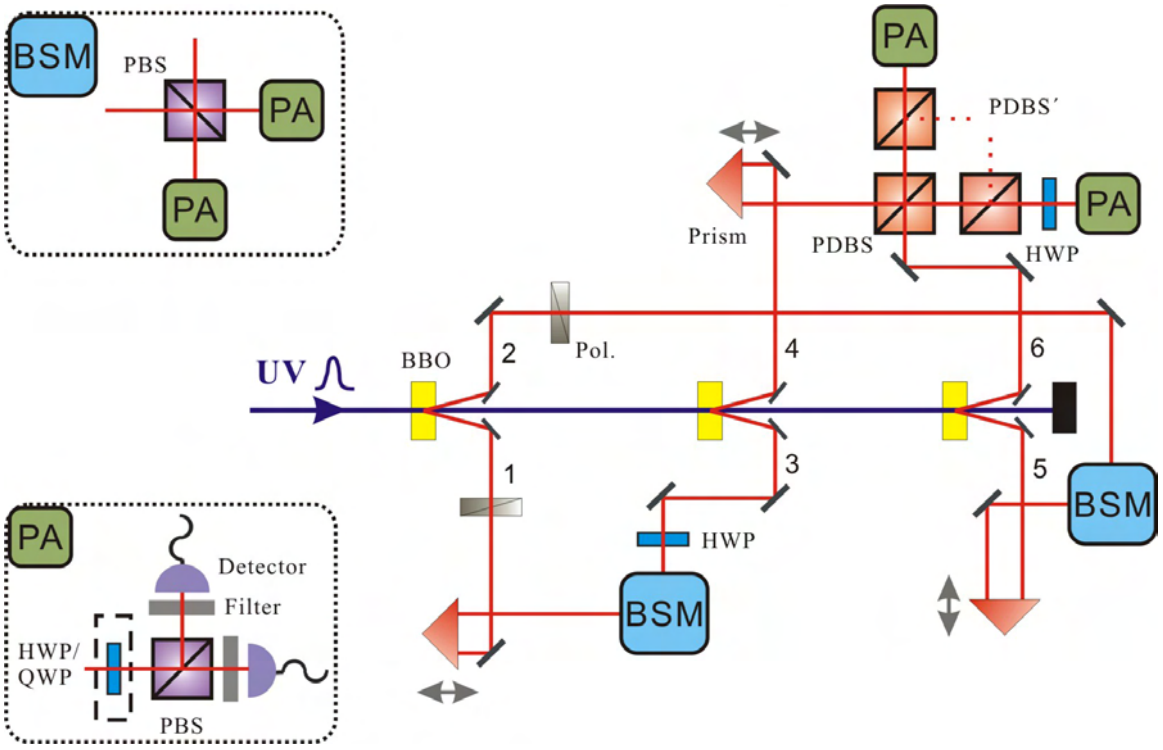

Figure 6.2: *A schematic diagram of the experimental setup. A high-intensity pulsed ultraviolet laser beam (UV) passes through three β-barium borate (BBO) crystals to generate three polarization entangled photon pairs via SPDC (see chapter 2.3.1). At the first BBO the UV generates a photon pair in modes 1 and 2 (that is, the input consisting of the target and control qubit). After the crystal, the UV is refocused onto the second BBO to produce another entangled photon pair in modes 3 and 4 and correspondingly for modes 5 and 6. Photons 4 and 6 are then overlapped at a PDBS and together with photons 3 and 5 constitute the cluster state. Two PDBS' are used for state normalization. The prisms are mounted on step motors and are used to compensate the time delay for the interference at the PDBS and the BSMs. A BSM is performed by overlapping two incoming photons on a PBS and two subsequent polarization analyses (PA). A PA projects the photon onto an unambiguous polarization depending on the basis determined by the choice of HWP or QWP. The photons are detected by silicon avalanched single-photon detectors. Coincidences are recorded with a coincidence unit clocked by the infrared laser pulses. Pol. are polarizers to prepare the input state and Filter label the narrow band filters with* $\Delta_{FWHM} = 3.2$ *nm.*

horizontally (vertically) polarized light at the PDBS is 1 (1/3), and we thus get

$$\begin{aligned}\rightarrow\ & \frac{1}{2}\big(|H\rangle_3|H\rangle_{4'}|H\rangle_5|H\rangle_{6'}+\frac{1}{\sqrt{3}}|H\rangle_3|H\rangle_{4'}|V\rangle_5|V\rangle_{6'}\\ & +\frac{1}{\sqrt{3}}|V\rangle_3|V\rangle_{4'}|H\rangle_5|H\rangle_{6'}\\ & -\frac{1}{3}|V\rangle_3|V\rangle_{4'}|V\rangle_5|V\rangle_{6'}\big).\end{aligned} \tag{6.5}$$

Here we have neglected terms with more than one photon in a single output mode of the PDBS, since in the experiment we post select only terms that lead to a six-fold coincidence.

In order to symmetrize the state we place a PDBS' ($T_H = 1/3, T_V = 1$) in each output mode of the PDBS and receive

$$\begin{aligned}\rightarrow\ & \frac{1}{6}\big(|H\rangle_3|H\rangle_{4''}|H\rangle_5|H\rangle_{6''}+|H\rangle_3|H\rangle_{4''}|V\rangle_5|V\rangle_{6''}\\ & +|V\rangle_3|V\rangle_{4''}|H\rangle_5|H\rangle_{6''}-|V\rangle_3|V\rangle_{4''}|V\rangle_5|V\rangle_{6''}\big).\end{aligned} \tag{6.6}$$

This is already the desired four-qubit cluster state up to local unitary operations. To bring it to the desired form, we place half-wave plates (HWPs) – with an angle of 22.5° between the fast and the horizontal axis – into arms 3 and 4. This yields

$$\begin{aligned}\rightarrow\ & \left(|H\rangle_3|H\rangle_{4''}+|V\rangle_3|V\rangle_{4''}\right)|H\rangle_5|H\rangle_{6''}\\ & +\left(|H\rangle_3|V\rangle_{4''}+|V\rangle_3|H\rangle_{4''}\right)|V\rangle_5|V\rangle_{6''}\\ =\ & |\chi\rangle_{34''56''},\end{aligned} \tag{6.7}$$

where we have neglected the overall pre-factor 1/6 and we arrive at the desired ancillary four-photon cluster state $|\chi\rangle$ described in ref. [55]. Note, that altogether, the probability of having one photon in each desired output, and thus having successfully created the cluster state, is 1/9.

The state given in Eq. 6.7 is a four-particle cluster state [130] of the form

$$|\chi\rangle=\frac{1}{2}\left((|H\rangle|H\rangle+|V\rangle|V\rangle)|H\rangle|H\rangle+(|H\rangle|V\rangle+|V\rangle|H\rangle)|V\rangle|V\rangle\right). \tag{6.8}$$

Due to the special entanglement characteristics of $|\chi\rangle$, after the teleportation the output state is equivalent to the desired unitary transformation of the input state given by

$$|out\rangle=\hat{U}^{C-NOT}|T\rangle_1|C\rangle_2. \tag{6.9}$$

As can be seen in Fig. (6.1b) $|\chi\rangle$ can be created simply by performing a C-NOT operation on two EPR pairs. This C-NOT operation is the essential difference to the original teleportation scheme and is the reason for the fact that the output state is not identical to the input state, but rather in the desired form of Eq. (6.9).

To see this let us now have a look at the teleportation in more detail: Photons 1 and 2 constitute the input to our C-NOT gate. We assume that they are in a most general input state $|\Psi_{in}\rangle_{12}$

$$|\Psi_{in}\rangle_{12} = \alpha|H\rangle_1|H\rangle_2 + \beta|H\rangle_1|V\rangle_2 + \gamma|V\rangle_1|H\rangle_2 + \delta|V\rangle_1|V\rangle_2 \tag{6.10}$$

In this case Eq. (6.9) takes the form

$$\begin{aligned} |\Psi_{out}\rangle_{46} &= \hat{U}^{C-NOT}|\Psi_{in}\rangle_{12} \\ &= \alpha|H\rangle_4|H\rangle_6 + \beta|V\rangle_4|V\rangle_6 + \gamma|V\rangle_4|H\rangle_6 + \delta|H\rangle_4|V\rangle_6 \end{aligned} \tag{6.11}$$

Together with photons 3, 4, 5 and 6 in the cluster state of Eq. (6.8) we can now express the combined state of all six photons in terms of Bell states for photons 1-3 and 2-5 and in terms of the desired output state $|\Psi_{out}\rangle_{46}$ for photons 4-6 with corresponding Pauli operations

$$\begin{aligned} |\Psi_{in}\rangle_{12} \otimes |\chi\rangle_{3456} = \\ |\Phi^+\rangle_{13}|\Phi^+\rangle_{25} \quad & |\Psi_{out}\rangle_{46} \quad + |\Phi^+\rangle_{13}|\Phi^-\rangle_{25} \quad \hat{\sigma}_z^6|\Psi_{out}\rangle_{46} \\ +|\Phi^+\rangle_{13}|\Psi^+\rangle_{25} \quad & \hat{\sigma}_x^4\hat{\sigma}_x^6|\Psi_{out}\rangle_{46} \quad + |\Phi^+\rangle_{13}|\Psi^-\rangle_{25} \quad \hat{\sigma}_x^4\hat{\sigma}_x^6\hat{\sigma}_z^6|\Psi_{out}\rangle_{46} \\ +|\Phi^-\rangle_{13}|\Phi^+\rangle_{25} \quad & \hat{\sigma}_z^4\hat{\sigma}_z^6|\Psi_{out}\rangle_{46} \quad + |\Phi^-\rangle_{13}|\Phi^-\rangle_{25} \quad \hat{\sigma}_z^4|\Psi_{out}\rangle_{46} \\ +|\Phi^-\rangle_{13}|\Psi^+\rangle_{25} \quad & \hat{\sigma}_x^4\hat{\sigma}_z^4\hat{\sigma}_x^6\hat{\sigma}_z^6|\Psi_{out}\rangle_{46} \quad + |\Phi^-\rangle_{13}|\Psi^-\rangle_{25} \quad \hat{\sigma}_x^4\hat{\sigma}_z^4\hat{\sigma}_x^6|\Psi_{out}\rangle_{46} \\ +|\Psi^+\rangle_{13}|\Phi^+\rangle_{25} \quad & \hat{\sigma}_x^4|\Psi_{out}\rangle_{46} \quad + |\Psi^+\rangle_{13}|\Phi^-\rangle_{25} \quad \hat{\sigma}_x^4\hat{\sigma}_z^6|\Psi_{out}\rangle_{46} \\ +|\Psi^+\rangle_{13}|\Psi^+\rangle_{25} \quad & \hat{\sigma}_x^6|\Psi_{out}\rangle_{46} \quad + |\Psi^+\rangle_{13}|\Psi^-\rangle_{25} \quad \hat{\sigma}_x^6\hat{\sigma}_z^6|\Psi_{out}\rangle_{46} \\ +|\Psi^-\rangle_{13}|\Phi^+\rangle_{25} \quad & \hat{\sigma}_x^4\hat{\sigma}_z^4\hat{\sigma}_z^6|\Psi_{out}\rangle_{46} \quad + |\Psi^-\rangle_{13}|\Phi^-\rangle_{25} \quad \hat{\sigma}_x^4\hat{\sigma}_z^4|\Psi_{out}\rangle_{46} \\ +|\Psi^-\rangle_{13}|\Psi^+\rangle_{25} \quad & \hat{\sigma}_z^4\hat{\sigma}_x^6\hat{\sigma}_z^6|\Psi_{out}\rangle_{46} \quad + |\Psi^-\rangle_{13}|\Psi^-\rangle_{25} \quad \hat{\sigma}_z^4\hat{\sigma}_x^6|\Psi_{out}\rangle_{46} \end{aligned} \tag{6.12}$$

From this we can directly see, that two BSMs on photons 1-3 and 2-5, project the output photons 4 and 6 onto a state that is directly correlated to the desired final state given in Eq. (6.11). The only thing left to do is to apply corresponding Pauli operations, depending on the outcome of the BSMs. With the help of polarizing beam splitters, in our experiment we are able to identify the Bell states $|\Phi^\pm\rangle_{13}$ and $|\Phi^\pm\rangle_{25}$, i.e. we project the combined state of photons 1, 2, 3 and 5 onto one of the four possibilities $|\Phi^\pm\rangle_{13}|\Phi^\pm\rangle_{25}$. We thus have to consider four different results of the BSMs

Result of BSMs	Output state
$\|\Phi^+\rangle_{13}\|\Phi^+\rangle_{25}$	$\|\Psi_{out}\rangle_{46}$
$\|\Phi^+\rangle_{13}\|\Phi^-\rangle_{25}$	$\hat{\sigma}_z^6\|\Psi_{out}\rangle_{46}$
$\|\Phi^-\rangle_{13}\|\Phi^+\rangle_{25}$	$\hat{\sigma}_z^4\hat{\sigma}_z^6\|\Psi_{out}\rangle_{46}$
$\|\Phi^-\rangle_{13}\|\Phi^-\rangle_{25}$	$\hat{\sigma}_z^4\|\Psi_{out}\rangle_{46}$

To receive the desired final state of photons 4 and 6, we have to apply corresponding Pauli operations, depending on the outcome of the BSMs.

6.3 Experimental Setup

A schematic diagram of our experimental setup is shown in Fig. 6.2. All three photon pairs are originally prepared in the Bell-state $|\Phi^+\rangle = \frac{1}{\sqrt{2}}(|H\rangle|H\rangle + |V\rangle|V\rangle)$. We observe on average 7×10^4 photon pairs per second from each (EPR) source. With this high-intensity entangled photon source we obtain in total 3.5 six-photon events per minute. This is less than half the count rate of our previous six-photon experiments [126, 131]. Since the new scheme is more complex and involves more interferences, the fidelity requirements are more stringent. Thus, we have to reduce the pump power from 1.0 W to 0.8 W in order to reduce noise contributions that arise from the emission of two pairs of down-converted photons by a single source (double-pair-emission). We are able to achieve a count rate for the four-qubit cluster state $|\chi\rangle_{3456}$ that is two orders of magnitude larger than in a recent experiment [127]. The improvement of the count rate is necessary in order to be able to perform the six-photon experiment in a reasonable amount of time over which the experimental setup can be kept stable.

With the help of wave plates (HWPs) and polarizers, we prepare photon pair 1&2 in the desired two-qubit input state $|\Psi\rangle_{12}$. Photon pairs 3&4 and 5&6, which are both in the state $|\Phi^+\rangle$, are used as a resource to construct the special entangled state $|\chi\rangle_{3456}$ by directing photons 4 and 6 to the two input modes of a polarization dependent beam splitter (PDBS). As can be observed in Fig. 6.2 Photons 4 and 6 are interfered on a beam splitter with a polarization-dependent splitting ratio (PDBS), i.e. the transmission for horizontal (vertical) polarization is $T_H = 1$ ($T_V = 1/3$). In order to balance the transmission for all input polarizations, beam splitters (PDBS') with reversed transmission conditions ($T_H = 1/3$, $T_V = 1$) are placed in each output of the overlapping PDBS. Altogether, the probability of having one photon in each desired output, and thus having successfully created the cluster state, is 1/9. Half wave plates (HWPs) in arms 3 and 4 are used to transform the cluster state to the desired state by local unitary operations. Teleporting the input data of $|\psi\rangle_{12}$ to $|\chi\rangle_{3456}$ requires joint BSMs on photons 1&3 and photons 2&5. To demonstrate the working principle of the teleportation-based C-NOT gate, it is sufficient to identify one of the four Bell states in both BSMs [126, 132]. However, in the experiment we decide to analyse the two Bell states $|\Phi^+\rangle$ and $|\Phi^-\rangle$ to increase the efficiency - the fraction of success - by a factor of 4. This is achieved by interfering photons 1&3 and photons 2&5 on a polarizing beam splitter (PBS) and performing a polarization analysis (PA) on the two outputs [49]. With the help of a HWP, a PBS and fiber-coupled single photon detectors, we are able to project the input photons of the BSM onto $|\Phi^+\rangle$ upon the detection of a $|+\rangle|+\rangle$ or $|-\rangle|-\rangle$ coincidence, and onto $|\Phi^-\rangle$ upon the detection of a $|+\rangle|-\rangle$ or $|-\rangle|+\rangle$ coincidence (where $|\pm\rangle = (|H\rangle \pm |V\rangle)/\sqrt{2}$). The increase in success efficiency compared to [126, 132] allows us to reduce the pump power in order to reduce noise contributions while preserving the overall count rate.

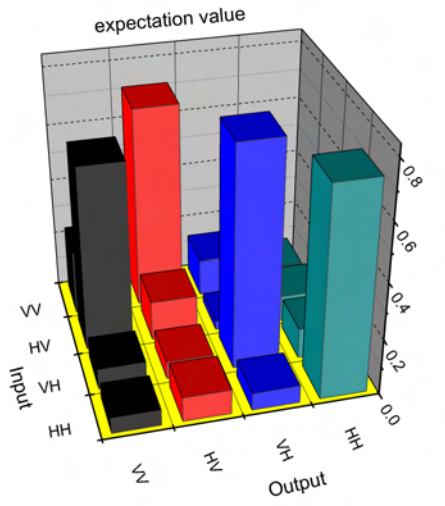

Figure 6.3: Experimental results for truth table of the C-NOT gate. The first qubit is the target and the second is the control qubit. The average fidelity for the truth table is 0.72 ± 0.05.

6.4 Experimental Results

The projective BSMs between the data input photon 1 (2) and photon 3 (5) of the cluster state leave the remaining photons of the cluster state 4&6 up to a unitary transformation in the state $|out\rangle_{46}$. This is the desired final state of having performed a C-NOT operation on photons 1&2. To demonstrate that our teleportation-based C-NOT gate protocol works for a general unknown polarization state of photons 1&2, we decide to measure the truth table of our gate. That is, we measure the output for all possible combinations of the two-qubit input in the computational basis. The fidelity measurements for the truth table are straightforward. Conditional on detecting a fourfold coincidence at the two BSMs, we analyze the output photons 4&6 in the computational H/V basis. Depending on the type of coincidence at the BSM ($|+\rangle|+\rangle$, $|+\rangle|-\rangle$, $|-\rangle|+\rangle$, $|-\rangle|-\rangle$), i.e. depending onto which Bell state the photons have been projected, we analyze the output by taking into account the corresponding unitary transformation. Since this state analysis only involves orthogonal measurements on individual qubits, the fidelity of the output state is directly given by the fraction of observing the desired state. The measurement results are shown in Fig. 6.3.

We quantify the quality of our output state by looking at the fidelity as defined by

$$F = Tr(\hat{\rho}|out\rangle\langle out|),$$

where $|out\rangle$ is the theoretically desired final state and $\hat{\rho}$ is the density matrix of the experimental output state. To analyze the operation and to experimentally measure the fidelity of the two-qubit output, we again use PAs. Depending on the

measurement setting we use quarter wave plates (QWP) or HWP in front of the PBS. A total of 12 single-photon detectors have been used in the experiment. The experimental integration time for each possible combination of the input photons was about 50 hours and we recorded about 120 desired two-qubit events. The overall count rate is reduced by a factor of 1/72 due to the success probability of creating the cluster state (1/9), the success probability of the BSMs (1/4) and due to the loss by initializing the input state with polarizers (1/2). On the basis of our original data, we conduct that the average fidelity for the output states of the truth table is 0.72 ± 0.05.

However, that is not sufficient to show the quantum characteristic of a C-NOT gate. The remarkable feature of a C-NOT gate is its capability of entangling two separable qubits. Thus, to fully demonstrate the successful operation of our protocol, we furthermore choose to perform the entangling operation

$$|H\rangle_T \otimes \frac{1}{\sqrt{2}}(|H\rangle_C + |V\rangle_C) \overset{C-NOT}{\longrightarrow} \frac{1}{\sqrt{2}}(|H\rangle_T|H\rangle_C + |V\rangle_C|V\rangle_C) = |\Phi^+\rangle_{TC}.$$

The determination of the entangling capability is a bit more complex. Since the output state is entangled, we are not able to determine its fidelity by a single measurement setting. However, with three successive local measurements on individual qubits we are still able to accomplish our task. This can be seen by a closer look at the fidelity under scrutiny

$$F = Tr(\hat{\rho}|\Phi^+\rangle\langle\Phi^+|) = \frac{1}{4}Tr\left(\hat{\rho}(\hat{I} + \hat{\sigma}_x\hat{\sigma}_x - \hat{\sigma}_y\hat{\sigma}_y + \hat{\sigma}_z\hat{\sigma}_z)\right)$$

This implies that by measuring the expectation values $\langle\hat{\sigma}_x\hat{\sigma}_x\rangle$, $\langle\hat{\sigma}_y\hat{\sigma}_y\rangle$, $\langle\hat{\sigma}_z\hat{\sigma}_z\rangle$ we can directly obtain the fidelity of the entangled output state. The experimental results for the correlated local measurement settings are shown in Figures 6.4, 6.5 and 6.6, for a more quantitative overview see Table. 6.1. The integration time for the first and last setting was about 60 hours and for the second setting about 80 hours. Using the above equation, we determine from our experimental results an fidelity of 0.575 ± 0.027. This is well beyond the state estimation limit of 0.40 [101]. Furthermore and most importantly, the result proofs genuine entanglement between the two output photons, since it is above the entanglement limit of 0.50 [61].

In addition, we have measured the fidelity of the used four-qubit cluster state $|\chi\rangle_{3456}$ and obtain an experimental result of 0.694 ± 0.003. This measurement has been performed in complete analogy to Kiesel et al. However, at the cost of a bit lower fidelity, we have achieved a count rate that is more than two orders of magnitudes larger.

All experimental results are calculated directly from the original data and no noise contributions have been subtracted. The rather large imperfection of the fidelities has several causes. First of all due to the large pump power double-pair-emission contributes largely to the noise. Furthermore, the interference visibility is limited since the complex phase compensations drift over the long measurement times. Also

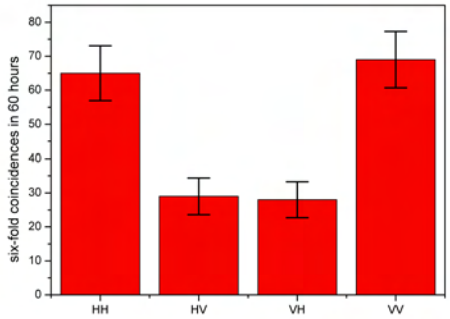

Figure 6.4: *Experimental results for the fidelity measurement of the entangled output state in the* ***computational*** *basis. The measured expectation value for* $\langle \hat{\sigma}_z \hat{\sigma}_z \rangle$ *is* 0.403 ± 0.066.

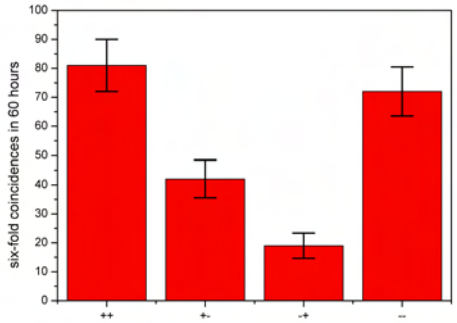

Figure 6.5: *Experimental results for the fidelity measurement of the entangled output state in the* ***diagonal*** *basis. The measured expectation value for* $\langle \hat{\sigma}_x \hat{\sigma}_x \rangle$ *is* 0.462 ± 0.057.

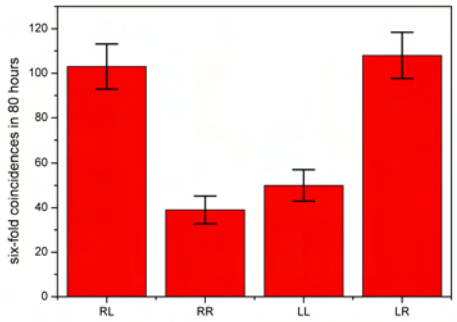

Figure 6.6: *Experimental results for the fidelity measurement of the entangled output state in the* ***circular*** *basis. The measured expectation value for* $\langle \hat{\sigma}_y \hat{\sigma}_y \rangle$ *is* -0.434 ± 0.062.

	00	01	10	11	expectation value
$\sigma_x\sigma_x$	81	42	19	72	0.462 ± 0.057
$\sigma_y\sigma_y$	39	103	108	50	-0.434 ± 0.062
$\sigma_z\sigma_z$	65	29	28	69	0.403 ± 0.066

Table 6.1: Experimental results for fidelity measurement of entangled output state. Three complementary basis are used: **(A)** $\langle\hat{\sigma}_x\hat{\sigma}_x\rangle$ with 0/1 standing for $|+\rangle/|-\rangle$; **(B)** $\langle\hat{\sigma}_y\hat{\sigma}_y\rangle$ with 0/1 standing for $|L\rangle/|R\rangle = \frac{1}{\sqrt{2}}(|H\rangle \pm i|V\rangle)$ and **(C)** $\langle\hat{\sigma}_z\hat{\sigma}_z\rangle$ with 0/1 standing for $|H\rangle/|V\rangle$.

imperfect input states reduce the quality of our output states. Note that we achieve a better fidelity for the truth table than for the entangling case. This is because for the latter one the fidelity depends on the interference visibility at the PBS of the BSM. All given errors are of statistical nature and correspond to ± 1 standard deviations.

6.5 Discussion

Compared to previous six-photon experiments [126, 132] our experimental setup is more complex and involves more interferences, which introduces additional phases that are difficult to control. Various efforts have been made to compensate these phases and to achieve the stringent fidelity requirements and a sufficient six-photon count rate. Although there is fast progress in the theoretical description of quantum information processing, the difficulties in handling quantum systems have not allowed an equal advance in the experimental realization of the new proposals. Up to now, not even a proof-in-principle demonstration of a teleportation-based quantum logic gate, the fundamental building block of the Gottesman-Chuang (GC) scheme, had been realized.

With our setup we have demonstrated the first non-trivial proof-of-principle implementation of the protocol introduced by Gottesman and Chuang. We have experimentally realized a C-NOT gate based on quantum teleportation. With our six-photon architecture we have experimentally demonstrated the ability to entangle two separable qubits and have measured the truth table of the gate. Note however, that strictly speaking we did not show complete fault-tolerance, since in our experiment we did not encode logic qubits onto a larger number of physical qubits. The principle of the scheme, on the other hand, stays exactly the same and the developed techniques of our setup can be readily extended for the case of a larger number of encoded qubits. Although the generation of a large number of qubits, as well as a necessary improvement of the fidelity still requires extensive efforts in the future.

In summary, the teleportation-based scheme proposed by Gottesman and Chuang offers a novel way for scalable quantum computing. Most attractively however, this architecture allows for realizations of universal quantum gates in a fault-tolerant

manner, and in fact serves as an important basis for measurement-based quantum computing. Thus, our experimental demonstration represents an important step towards the realization of resource-efficient, scalable quantum computation.

Chapter 7

Conclusions and Outlook

In this thesis, we have reported our research on the field of quantum information processing. We have used pairs of polarization-entangled photons as produced by pulsed parametric down-conversion to experimentally explore interference phenomena of multi-particle quantum systems.

Within the work of this thesis we have designed and developed a new generation of a high power EPR source, which we have exploited to build an event-ready source for entangled photon pairs:

- (i) We experimentally realized the event-ready entanglement source proposed by Śliwa and Banaszek. Demonstrating a state preparation efficiency of the source up to 52 % at a fidelity better than 87 % is a significant improvement compared with previous experiments for on-demand sources. The working principle presents a substantial advancement over the general methods by using linear optics, so that the demonstrated source might be of promising use in essential photon based quantum information tasks. It is feasible to support on-demand applications and suitable to be integrated into on-chip waveguide quantum circuit applications, which are potential candidates for profound new technologies in quantum optics.

Moreover we have implemented a six-photon interferometer – the first of its kind – and demonstrated its experimental versatility in several applications in QIP:

- (ii) We have experimentally demonstrated quantum teleportation of a two-qubit composite system. We have been able to teleport a polarization entangled photon pair, which on the one hand denotes an important step towards the teleportation of complex systems but on the other hand and even more importantly constitutes the basis for various QIP schemes and protocols, such as the demonstration of a multiple swapping operation of an entangled state – in combination with quantum memory an indispensable prerequisite for large scale quantum communication networks – or to demonstrate a teleportation-based controlled-NOT operation for fault tolerant quantum computation. Besides

these two applications, whose experimental implementation was demonstrated within this thesis, the six photon interferometer can also be used to construct five- and six-photon clusters.

- (iii) We have further demonstrated entanglement swapping over multiple stages. By this we have generated entanglement between particles that have never interacted in the past with the help of ancillary particles that also do not share any common history. The swapping procedure constitutes one of the key elements for a quantum relay, and a full quantum repeater if combined with quantum purification and quantum memory. As a result, quantum communication becomes feasible despite of realistic noise and imperfections and at the same time, the overhead for the used resources and communication time only increase polynomially with the distance.

- (iv)

  For large-scale quantum computation the inevitable coupling of physical qubits to the noisy environment and residual imperfections in physical systems impose a major challenge to a practical implementation. Quantum error correction codes and fault-tolerant quantum gates are therefore critical components in QIP. We have reported the first successful realization of the novel protocol to implement any quantum gate needed for quantum computation in a fault-tolerant manner proposed by Gottesman and Chuang. The in-principle demonstration shows the feasibility of the scheme and opens doors for possible future large scale implementations of quantum networks as well as it is an important step towards the feasibility of realistic quantum computers.

Although significant theoretical and experimental progress in the field of linear optic QIP has been demonstrated over the last few years, it is still a long way towards efficient, scalable and large-scale multi-photon implementations:

One obvious drawback of the current realization of linear optic QIP is the process of generating entangled photons by the process of SPDC. Although it yields high quality entanglement of photons and – by employing a pulsed laser setup – can be used to generate multi-photon entanglement, its probabilistic nature makes scalable and thus large-scale implementations impossible. With our six-photon interferometer we were approaching the maximum number of entangled photons that can be generated via SPDC. A problem we tried to fight by implementing the heralded photon source proposed by Śliwa and Banaszek.

There exist various promising alternatives to generate photonic entanglement: Quantum dots can be used to generate single photons on demand [65]but still suffer from poor quality and the lack of ability to develop a large number of identical sources. Another promising approach is the application of atomic ensembles as quantum memories and single photon sources [76].

The second huge problem of the current technology is the poor overall coupling efficiency of the widely available photon detectors. Mainly due to insufficient mode matching and additional loses at the filters only $\sim 15\%$ of the generated photons are actually detected. Thus, even with a deterministic single photon source, large scale quantum operations are severely limited by this drawback. A miniaturization of bulk optics setups as approached by [82] is a promising solution to this problem and would allow to enhance performance and reduce resource requirements.

Even though presented techniques and demonstrated experiments need to be combined with other physical systems and technical developments to show their different strengths and advantages, in this thesis we have proven several important QIP protocols and their applications in quantum communication, quantum teleportation and quantum computation.

As a final remark, we would like to note that a number of text paragraphs in Chapters 3 to 6 were taken from our publications listed in the Appendix. The formulations found there are difficult to improve.

APPENDIX

Associated publications:

Within the framework of this thesis the following publications have been achieved:

- Qiang Zhang, Alexander Goebel, Claudia Wagenknecht, Yu-Ao Chen, Bo Zhao, Tao Yang, Alois Mair, Joerg Schmiedmayer and Jian-Wei Pan. Experimental Quantum Teleportation of a Two-Qubit Composite System. Nature Physics 2, 678 - 682 (2006) (Chapter 4)

- Alexander M. Goebel, Claudia Wagenknecht, Qiang Zhang, Yu-Ao Chen, Kai Chen, Joerg Schmiedmayer and Jian-Wei Pan. Multistage Entanglement Swapping. Phys. Rev. Lett. 101, 080403 (2008) (Chapter 5)

- Alexander M. Goebel, Claudia Wagenknecht, Qiang Zhang, Yu-Ao Chen and Jian-Wei Pan. Teleportation-Based Controlled-NOT Gate for Fault-Tolerant Quantum Computation. submitted to PRL, preprint: www.arXiv.org:0809.3583 (Chapter 6)

- Claudia Wagenknecht, Che-Ming Li, Andreas Reingruber, Xiao-Hui Bao, Alexander Goebel, Yu-Ao Chen, Qiang Zhang, Kai Chen and Jian-Wei Pan. Experimental Demonstration of an Event-Ready Entanglement Source. in preparation (Chapter 3)

Acknowledgment

Many people have contributed to the work presented in this thesis and supported me during my Ph.D. studies. I would like to take this opportunity to express my gratitude to all of them.

I would like to thank my advisor Prof. Jian-Wei Pan for giving me the opportunity to conduct research in this highly interesting field of physics. I am very thankful for his guidance and support and his generous availability in discussing experimental problems. Moreover, I'm indebted to him for always respecting my situation as a single mum, giving me all possible support and never pushing me over the limit.

I would like to thank my second advisor Prof. Mete Atatüre for critically reviewing this thesis.

I would like to thank Dr. Agnes Speck from the office for gender equality and Prof. Johanna Stachel for generously supporting my application for the Schlieben-Lange-Programme of the European Social Funds and the Universities in Baden-Wuerttemberg, which helped me to finish this work without concerns.

The most special thanks go to Dr. Alexander Goebel for working together in the last four years, for continuing the experiment in the afternoons when I had to run to kindergarten, for all the discussions about physics and his patient support in handling computer problems. Special thanks also go to Dr. Qiang Zhang and Dr. Yu-Ao Chen, from whom I have learned all about photonics experiments, as well as Dr. Che-Ming Li, Xiao-Hui Bao and Dr. Kai Chen for support on the theoretical side. Thanks a lot to my two lab mates Che-Ming and Andreas Reingruber: it was a pleasure to work with you. I deeply enjoyed the discussions with my office mates Alex, Andreas and Che-Ming, and also Dr. Thorsten Strassel about physics, politics and the general meaning of life. I further would like to thank all members of the QUO group for their general support: Dr. Zhen-Sheng Yuan, Dr. Bo Zhao, Dr. Shuai Chen, Dr. Yang Fan, Yong Zhao, Alexander Dueck, Xiaofan Xi, Christian Lutz and Peter Dietrich.

Moreover, I would especially like to thank Dr. Che-Ming Li for his kind help to revise this thesis.

My thanks also go to all the people in the institute, who supported me throughout my PhD time, to the secretaries and the staff in the electronic and mechanic workshops,

whose support and technical developments helped to realize our experiments. I would particularly like to thank Mr. Stahl, who always found a way to realize our most weird ideas in no time.

In the last two years my work was funded by the Schlieben-Lange-Programm of the European Social Funds, which is meant to support women in Science. I'm very grateful for being accepted to this fellowship, since it allowed me to finish my PhD studies without financial concerns.

I was fortunate to meet many good friends during my studies in Heidelberg. I would like to thank all of you for standing at my side, for your company and your various support. Just some of them I can mention here: Juergen-Matthias Seeler, Matthias Kleinmann, Michael Wormit, Emanuela Rota & Leonardo della Pietra, Ana & Igor Kitanovic, Alban Hessler, Jessica Agarwal, Barbara Boehm, Stephan Schneider and Debora Stern. Special thanks got to Debora for the many times babysitting Johannes.

Last but not least, I would like to thank my family: my son Johannes for being a lovely, healthy baby and now, being a small boy, for not stressing my nerves too much. And of course my mum, who always supported me through all the years of my studies, mostly without any complaints. Thank you for that!

Bibliography

[1] L. Marton, J.A. Simpson, and J.A. Suddeth. Electron beam interferometer. *Phys. Rev.*, 90:490, 1954.

[2] H. Rauch, W. Treimar, and U. Bonse. Test of a single crystal neutron interferometer. *Phys. Lett. A*, 57:369, 1974.

[3] O. Carnal and J. Mlynek. Young s double-slit experiment with atoms: A simple atom interferometer. *Phys. Rev. Lett.*, 66:2689–2692, 1991.

[4] D.W. Keith, C.R. Ekstrom, Q.A. Turchette, and D.E. Pritchard. An interferometer for atoms. *Phys. Rev. Lett.*, 66:2693–2696, 1991.

[5] A. Einstein, B. Podolsky, and N. Rosen. Can quantum mechanical description of physical reality be considered complete? *Phys. Rev.*, 47:777, 1935.

[6] J. S. Bell. On the Einstein Poldolsky Rosen paradox. *Physics (Long Island City, N.Y.)*, 1:195, 1964.

[7] A. Aspect, P. Grangier, and G. Roger. Experimental tests of realistic local theories via Bell's theorem. *Phys. Rev. Lett.*, 47:460–463, 1981.

[8] A. Aspect, P. Grangier, and G. Roger. Experimental realization of Einstein-Podolsky-Rosen-Bohm gedankenexperiment: A new violation of Bell's inequalities. *Phys. Rev. Lett.*, 49:91–94, 1982.

[9] A. Aspect, J. Dalibard, and G. Roger. Experimental test of Bell's inequalities using time- varying analyzers. *Phys. Rev. Lett.*, 49:1804–1807, 1982.

[10] P. Walther, M. Aspelmeyer, K. J. Resch, and Anton Zeilinger. Experimental violation of a cluster state Bell inequality. *Phys. Rev. Lett.*, 95:020403, 2005.

[11] C. Simon and W. T. M. Irvine. Robust long-distance entanglement and a loophole-free Bell test with ions and photons. *Phys. Rev. Lett.*, 91:110405, 2003.

[12] R. Feynman. Simulating physics with computers. *International Journal of Theoretical Physics*, 21:467Ű488, 1982.

[13] J.-W. Pan, Z.-B. Chen, M. Żukowski, H. Weinfurter, and Anton Zeilinger. Multi-photon entanglement and interferometry. Rev. Mod. Phys., in press (2007).

[14] C. H. Bennett. "Quantum and classical information: Transmission and computation". *Physics Today*, 48(10):24–30, 1995.

[15] D. Bouwmeester, A. Ekert, and A. Zeilinger. *The Physics of quantum information*. Springer-Verlag Berlin: Heidelberg, 2000.

[16] C. H. Bennett and G. Brassard. Quantum cryptography: Public key distribution and coin-tossing. *in Proc. IEEE Int. Conf. on Computers, systems, and signal processing*, Bangalore, India:(IEEE, New York, 1984), 175.

[17] A. K. Ekert. Quantum cryptography based on Bell's theorem. *Phys. Rev. Lett.*, 67:661–663, 1991.

[18] C. H. Bennett and S. J. Wiesner. Communication via one- and two-particle operators on Einstein-Podolsky-Rosen states. *Phys. Rev. Lett.*, 69:2881–2884, 1992.

[19] M. Aspelmeyer, H. R. Böhm, T. Gyatso, T. Jennewein, R. Kaltenbaek, M. Lindenthal, G. Molina-Terriza, A. Poppe, K. Resch, M. Taraba, R. Ursin, P. Walther, and A. Zeilinger. Long-distance free-space distribution of quantum entanglement. *Science*, 301:621–623, 2003.

[20] R. Ursin, F. Tiefenbacher, T. Schmitt-Manderbach, H. Weier, T. Scheidl, M. Lindenthal, B. Blauensteiner, T. Jennewein, J. Perdigues, P. Trojek, B. Ömer, M. Fürst, M. Meyenburg, J. Rarity, Z. Sodnik, C. Barbieri, H. Weinfurter, and A. Zeilinger. Entanglement-based quantum communication over 144 km. *Nature Physics*, 3:481, 2007.

[21] H. J. Briegel, W. Dur, J. I. Cirac, and P. Zoller. Quantum repeaters: the role of imperfect local operations in quantum communication. *Phys. Rev. Lett.*, 81:5932–5935, 1998.

[22] W. Dür, H.-J. Briegel, J. I. Cirac, and P. Zoller. Quantum repeaters based on entanglement purification. *Phys. Rev. A*, 59:169–181, 1999.

[23] P. W. Shor. Polynomial-time algorithms for prime factorization and discrete logarithms on a quantum computer. In *Proceedings of the 35th Annual Symposium on Foundations of Computer Science*, 1994.

[24] H. Häffner, W. Hänsel, C. F. Roos, J. Benhelm, D. Chek al kar1, M. Chwalla, T. Körber, U. D. Rapol, M. Riebe, P. O. Schmidt, C. Becher, O. Gühne, W. Dür, and R. Blatt. Scalable multiparticle entanglement of trapped ions. *Nature*, 438:643–646, 2005.

[25] L. M. K. Vandersypen, M. Steffen, G. Breyta, C. S. Yannoni, M. H. Sherwood, and I. L. Chuang. Experimental realization of shor's quantum factoring algorithm using nuclear magnetic resonance. *Nature*, 414:883–887, 2001.

[26] A. Imamoğlu A. Kiraz, M. Atature. Quantum dot single photon sources: Prospects for applications in linear optics quantum information processing. *Phys. Rev. A*, 69:032305, 2004.

[27] D. Loss and D. P. DiVincenzo. Quantum computation with quantum dots. *Phys. Rev. A*, 57:120, 1998.

[28] Y. Nakamura, Y. A. Pashkin, and J. S. Tsai. Coherent control of macroscopic quantum states in a single-cooper-pair box. *Nature*, 398:786, 1999.

[29] E. Knill, R. Laflamme, and G. J. Milburn. A scheme for efficient quantum computation with linear optics. *Nature*, 409:46–52, 2001.

[30] P. G. Kwiat, K. Mattle, H. Weinfurter, A. Zeilinger, A. V. Sergienko, and Y. Shih. New high-intensity source of polarization-entangled photon pairs. *Phys. Rev. Lett.*, 75:4337–4341, 1995.

[31] E. Schrödinger. Die gegenwärtige Situation in der Quantenmechanik. 23:807–812; 823–828; 844–849, 1935.

[32] C. H. Bennett, G. Brassard, C. Crepeau, R. Jozsa, A. Peres, and W. K. Wootters. Teleporting an unknown quantum state via dual classic and Einstein-Podolsky-Rosen channels. *Phys. Rev. Lett.*, 70:1895–1899, 1993.

[33] D. Bouwmeester, J.-W. Pan, K. Mattle, M. Eibl, H. Weinfurter, and A. Zeilinger. Experimental quantum teleportation. *Nature*, 390:575–579, 1997.

[34] K. Mattle, H. Weinfurter, P. G. Kwiat, and A. Zeilinger. Dense coding in experimental quantum communication. *Phys. Rev. Lett.*, 76:4656–4659, 1996.

[35] B. E. A. Saleh and M. C. Teich. *Fundamentals of Photonics*. Wiley, New York, 1991.

[36] A. Zeilinger. General properties of lossless beam splitters in interferometry. *Am. J. Phys.*, 49:882, 1981.

[37] P. Kok, W. J. Munro, K. Nemoto, T. C. Ralph, J. P. Dowling, and G. J. Milburn. Linear optical quantum computing with photonic qubits. *Rev. Mod. Phys.*, 79:135–174, 2007.

[38] E. Santos. *Phys. Rev. A*, 46:3646, 1992.

[39] L. De Caro and A. Garuccio. Reliability of bell inequality measurements using polarization correlations in parametricdown-conversion photons sources. *Phys. Rev. A*, 50:R2803–R2805, 1994.

[40] P. Kok and S. Braunstein. Post-selected versus non-post-selected quantum teleportation using parametric down-conversion. *Phys. Rev. A*.

[41] D. Bouwmeester A. Lamas-Linares, J. Howell. Stimulated emission of polarization-entangled photons. *Phys. Rev. Lett.*, 412:887, 2001.

[42] M. H. Rubin, D. N. Klyshko, Y. H. Shih, and A. V. Sergienko. Theory of two-photon entanglement in type-II optical parametric down-conversion. *Phys. Rev. A*, 50:5122–5133, 1994.

[43] D. M. Greenberger, M. A. Horne, A. Shimony, and A. Zeilinger. Bell's theorem without inequalities. *Am. J. Phys.*, 58:1131–1143, 1990.

[44] D.M. Greenberger, M.A. Horne, and A. Zeilinger. *Bell's Theorem, Quantum Theory, and Conceptions of the Universe*, page 69. Kluwer, Dordrecht, 1989.

[45] J.-W. Pan, D. Bouwmeester, M. Daniell, H. Weinfurter, and A. Zeilinger. Experimental test of quantum nonlocality in three-photon Greenberger-Horne-Zeilinger entanglement. *Nature*, 403:515–519, 2000.

[46] L. K. Grover. Quantum mechanics helps in searching for a needle in a haystack. *Phys. Rev. Lett.*, 79:325, 1997.

[47] D. Deutsch and R. Jozsa. Rapid solutions of problems by quantum computation. *Proceedings of the Royal Society of London A*, 439:553, 1992.

[48] A. Zeilinger, M. A. Horne, H. Weinfurter, and M. Zukowksi. Three-particle entanglements from two entangled pairs. *Phys. Rev. Lett.*, 78:3031–3034, 1997.

[49] J.-W. Pan and A. Zeilinger. Greenberger-Horne-Zeilinger-state analyzer. *Phys. Rev. A*, 57:2208–2211, 1998.

[50] W. Dür, G. Vidal, and J. I. Cirac. Three qubits can be entangled in two inequivalent ways. *Phys. Rev. A*, 62:062314, 2000.

[51] N.D. Mermin. Extreme quantum entanglement in a superposition of macroscopically distinct states. *Phys. Rev. Lett.*, 65:1838–1840, 1990.

[52] V. Scarani, A. Acín, E. Schenck, and M. Aspelmeyer. Nonlocality of cluster states of qubits. *Phys. Rev. A*, 71:042325, 2005.

[53] M. Hillery, V. Bužek, and A. Berthiaume. Quantum secret sharing. *Phys. Rev. A*, 59:1829–1834, 1999.

[54] Z. Zhao, Y.-A. Chen, A.-N. Zhang, T. Yang, H. Briegel, and J.-W. Pan. Experimental demonstration of five-photon entanglement and open-destination teleportation. *Nature*, 430:54–57, 2004.

[55] D. Gottesman and I. L. Chuang. Demonstrating the viability of universal quantum computation using teleportation and single-qubit operations. *Nature*, 402:390–393, 1999.

[56] N. Gisin. Nonlocality criteria for quantum teleportation. *Phys. Lett. A*, 210:157–159, 1996.

[57] M. Hein, J. Eisert, and H. J. Briegel. Multiparty entanglement in graph states. *Phys. Rev. A*, 69:062311, 2004.

[58] H. Häffner W. Hänsel J. Benhelm G. P. T. Lancaster C. Becher F. Schmidt-Kaler C. F. Roos, M. Riebe and R. Blatt. Control and measurement of three-qubit entangled states. *Science*, 304:1478–1480, 2004.

[59] J.-W. Pan, D. Bouwmeester, H. Weinfurter, and A. Zeilinger. Experimental entanglement swapping: entangling photons that never interacted. *Phys. Rev. Lett.*, 80:3891–3894, 1998.

[60] O. Gühne and G. Tóth. Entanglement detection. *Physics Reports*, 474:1–75, 2009.

[61] O. Gühne, P. Hyllus, D. Bruß, A. Ekert, M. Lewenstein, C. Macchiavello, and A. Sanpera. Detection of entanglement with few local measurements. *Phys. Rev. A*, 66:062305, 2002.

[62] M A. Nielsen and Isaac L. Chuang. *Quantum Computation and Quantum Information*. 2001.

[63] C. Santori *et al.* Polarization-correlated photon pairs from a single quantum dot. *Phys. Rev. B*, 66:045308, 2002.

[64] G. J. Milburn T.M. Stace and year = 2003 volume = 67 pages = 085317 owner = claudia timestamp = 2009.09.18 C.H.W. Barnes title = An entangled two photon source using biexciton emission of an asymmetric quantum dot in a cavity., journal = Phys. Rev. B.

[65] R. M. Stevenson, R. J. Young, P. Atkinson, K. Cooper, D. A. Ritchie, and A. J. Shields. A semiconductor source of triggered entangled photon pairs. *Nature*, 439:179–182, 2006.

[66] B. Zhao, Z.-B. Chen, Y.-A. Chen, J. Schmiedmayer, and J.-W. Pan. Robust creation of entanglement between remote memory qubits. *Phys. Rev. Lett.*, 98:240502, 2007.

[67] D. E. Browne and T. Rudolph. Resource-efficient linear optical quantum computation. *Phys. Rev. Lett.*, 95:010501, 2005.

[68] P. Kok. *State Preparation in Quantum Optics.* PhD thesis, University of Wales, Bangor, 2000.

[69] P. Kok and S. Braunstein. Limitations on the creation of maximal entanglement. *Phys. Rev. A*, 62:064301, 2000.

[70] C. Sliwa and K. Banaszek. Conditional preparation of maximal polarization entanglement. *Phys. Rev. A*, 67:030101(R), 2003.

[71] T.B. Pittman *et al.* Heralded two-photon entanglement from probabilistic quantum logic operations on multiple parametric down-conversion sources. *IEEE J. Sel. Top. Quantum Electron.*, 9:1478, 2003.

[72] A.A. Hnilo. Three-photon frequency down-conversion as an event-ready source of entangled states. *Phys. Rev. A*, 71:033820, 2005.

[73] J.F. Hodelin H.S. Eisenberg.

[74] P. Walther, K. J. Resch, T. Rudolph, E. Schenck, H. Weinfurter, V. Vedral, M. Aspelmeyer, and A. Zeilinger. Experimental one-way quantum computing. *Nature*, 434:169–176, 2005.

[75] Q. Zhang, X.-H. Bao, C.-Y. Lu, X.-Q. Zhou, T. Yang, T. Rudolph, and J.-W. Pan. Demonstration of efficient scheme for generation of "event ready" entangled photon pairs from single photon source. *Phys. Rev. A*, 77:062316, 2008.

[76] Y.-A. Chen, S. Chen, Z.-S. Yuan, B. Zhao, C.-S. Chuu, J. Schmiedmayer, and J.-W. Pan. Memory-built-in quantum teleportation with photonic and atomic qubits. *Nature Phys.*, 4:103, 2008.

[77] A. Stefanov J.C.F. Matthews, A. Politi and J. L. O'Brien. Manipulation of multiphoton entanglement in waveguide quantum circuits. *Nature photonics*, 3:364–350, 2009.

[78] C. K. Hong, Z. Y. Ou, and L. Mandel. Measurement of subpicosecond time intervals between two photons by interference. *Phys. Rev. Lett.*, 59:2044–2046, 1987.

[79] M. Żukowski, A. Zelinger, and H. Weinfurter. Entangling photons radiated by independent pulsed source. *Ann. N.Y. Acad. Sci.*, 755:91, 1995.

[80] M. Żukowski, A. Zeilinger, M. A. Horne, and A. K. Ekert. "event-ready-detectors" Bell experiment via entanglement swapping. *Phys. Rev. Lett.*, 71:4287–4290, 1993.

[81] J. F. Clauser, M. A. Home, A. Shimony, and R. A. Holt. Proposed experiment to test local hidden-variable theories. *Phys. Rev. Lett.*, 23:880–884, 1969.

[82] J. G. Rarity S. Yu A. Politi, M. J. Cryan and J. L. O'Brien. Silica-on-silicon waveguide quantum circuits. *Science*, 320:646, 2008.

[83] J. G. Rarity W. J. Wadsworth A. S. Clark, J. Fulconis and J. L. O'Brien. An all optical fibre quantum controlled-not gate. *Phys. Rev. A*, 79:030303(R), 2009.

[84] L. K. Grover. Quantum telecomputation. arXiv:quant-ph/9704012.

[85] W. K. Wootters and W. H. Zurek. A single quantum cannot be cloned. *Nature*, 299:802–803, 1982.

[86] S. Bose, V. Vedral, and P.L. Knight. Multiparticle generalization of entanglement swapping. *Phys. Rev. A*, 57:822–829, 1998.

[87] D. Boschi, S. Branca, F. De Martini, L. Hardy, and S. Popescu. Experimental realization of teleporting an unknown pure quantum state via dual classical and Einstein-Podolsky-Rosen channels. *Phys. Rev. Lett.*, 80:1121–1125, 1998.

[88] M. D. Barrett, J. Chiaverini, T. Schaetz, J. Britton, W. M. Itano, J. D. Jost, E. Knill, C. Langer, D. Leibfried, R. Ozeri, and D. J. Wineland. Deterministic quantum teleportation of atomic qubits. *Nature*, 429:737–739, 2004.

[89] M. Riebe, H. Häffner, C. F. Roos, W. Hänsel, J. Benhelm, G. P. T. Lancaster, T. W. Körber, C. Becher, F. Schmidt-Kaler, D. F. V. James, and R. Blatt. Deterministic quantum teleportation with atoms. *Nature*, 429:734–737, 2004.

[90] I. Marcikic, H. de Riedmatten, W. Tittel, H. Zbinden, and N. Gisin. Long-distance teleportation of qubits at telecommunication wavelengths. *Nature*, 421:509–513, 2003.

[91] R. Ursin, T. Jennewein, M. Aspelmeyer, R. Kaltenbaek, M. Lindenthal, P. Walther, and A. Zeilinger. Communications quantum teleportation across the danube. *Nature*, 430:849, 2004.

[92] B. C. Jacobs, T. B. Ptitman, and J. D. Franson. Quantum relays and noise suppression using linear optics. *Phys. Rev. A*, 66:052307, 2002.

[93] A. R. Calderbank and P. W. Shor. Good quantum error-correcting codes exist. *Phys. Rev. A*, 54:1098–1105, 1996.

[94] R. Raussendorf and H. J. Briegel. A one-way quantum computer. *Phys. Rev. Lett.*, 86:5188–5191, 2001.

[95] J. Lee and M. S. Kim. Entanglement teleportation via Werner states. *Phys. Rev. Lett.*, 84:4236–4239, 2000.

[96] Y. Yeo and W. K. Chua. Teleportation and dense coding with genuine multipartite entanglement. *Phys. Rev. Lett.*, 96:060502, 2006.

[97] G. Rigolin. Quantum teleportation of an arbitrary two-qubit state and its relation to multipartite entanglement. *Phys. Rev. A*, 71:032303, 2005.

[98] R. Cleve, D. Gottesman, and H.-K. Lo. How to share a quantum secret. *Phys. Rev. Lett.*, 83:648–651, 1999.

[99] Y.H. Shih and C.O. Alley. New type of einstein-podolsky-rosen-bohm experiment using pairs of light quanta produced by optical parametric down conversion. *Phys. Rev. Lett.*, 61:2921, 1988.

[100] J.-W. Pan, M. Daniell, S. Gasparoni, G. Weihs, and A. Zeilinger. Experimental demonstration of four-photon entanglement and high-fidelity teleportation. *Phys. Rev. Lett.*, 86:4435, 2001.

[101] A. Hayashi, T. Hashimoto, and M. Horibe. Reexamination of optimal quantum state estimation of pure states. *Phys. Rev. A*, 72:032325, 2005.

[102] D. Collins, N. Gisin, and H.D. Riedmatten. Quantum relays for long distance quantum cryptography. *J. Mod. Opt.*, 52:735, 2005.

[103] J.I. Cirac, L.M. Duan, and P. Zoller. Experimental quantum computation and information. In *Proceedings of the International School of Physics "Enrico Fermi", Course CXLVIII, edited by F. Di Martini and C. Monroe (IOS Press, Amsterdam)*, 2002.

[104] C. H. Bennett, D. P. DiVincenzo, J. A. Smolin, and W. K. Wootters. Mixed-state entanglement and quantum error correction. *Phys. Rev. A*, 54:3824–3851, 1996.

[105] P.G. Kwiat, S. Barraza-Lopez, A. Stefanov, and N. Gisin. Experimental entanglement distillation and 'hidden' non-locality. *Nature*, 409:1014, 2001.

[106] J.-W. Pan, C. Simon, C. Brukner, and A. Zeilinger. Entanglement purification for quantum communication. *Nature*, 410:1067–1070, 2001.

[107] J.-W. Pan, S. Gasparoni, U. Rupert, G. Weihs, and A. Zeilinger. Experimental entanglement purification of arbitrary unknown states. *Nature*, 423:417–422, 2003.

[108] T. Chanelière, D. N. Matsukevich, S. D. Jenkins, S.-Y. Lan, T. A. B. Kennedy, and A. Kuzmich. Storage and retrieval of single photons transmitted between remote quantum memories. *Nature*, 438:833–836, 2005.

[109] D. Felinto, C. W. Chou, J. Laurat, E. W. Schomburg, H. de Riedmatten, and H. J. Kimble. Conditional control of the quantum states of remote atomic memories for quantum networking. *Nature Physics*, 2:844, 2006.

[110] T. Jennewein, G. Weihs, J.-W. Pan, and A. Zeilinger. Experimental nonlocality proof of quantum teleportation and entanglement swapping. *Phys. Rev. Lett.*, 88:017903, 2002.

[111] H. de Riedmatten, I. Marcikic, J. A. W. van Houwelingen, W. Tittel, H. Zbinden, and N. Gisin. Long-distance entanglement swapping with photons from separated sources. *Phys. Rev. A*, 71:050302, 2005.

[112] R. E. S. Polkinghorne and T. C. Ralph. Continuous variable entanglement swapping. *Phys. Rev. Lett.*, 83:2095–2099, 1999.

[113] X. Jia, X. Su, Q. Pan, J. Gao, C. Xie, and K. Peng. Experimental demonstration of unconditional entanglement swapping for continuous variables. *Phys. Rev. Lett.*, 93:250503, 2004.

[114] N. Takei, H. Yonezawa, T. Aoki, and A. Furusawa. High-fidelity teleportation beyond the no-cloning limit and entanglement swapping for continuous variables. *Phys. Rev. Lett.*, 94:220502, 2005.

[115] M. Barbieri, F. De Martini, G. Di Nepi, P. Mataloni, G. M. D'Ariano, and C. Macchiavello. Detection of entanglement with polarized photons: Experimental realization of an entanglement witness. *Phys. Rev. Lett.*, 91:227901, 2003.

[116] V. Scarania, H. de Riedmatten, I. Marcikic, H. Zbinden, and N. Gisin. Four-photon correction in two-photon bell experiments. *Eur. Phys. J. D*, 32:129, 2005.

[117] M. Barbieri. Effects of frequency correlation in linear optical entangling gates operated with independent photons. *Phys. Rev. A*, 76:043825, 2007.

[118] W. K. Wootters. Entanglement of formation of an arbitrary state of two qubits. *Phys. Rev. Lett.*, 80:2245–2248, 1998.

[119] J. Preskill. Reliable quantum computers. *Proc. R. Soc. Lond. A*, 454:385–410, 1998.

[120] A. M. Steane. Efficient fault tolerant quantum computing. *Nature*, 399:124–126, 1999.

[121] D. Gottesman. Theory of fault-tolerant quantum computation. *Phys. Rev. A*, 57:127–137, 1998.

[122] P. W. Shor. Scheme for reducing decoherence in quantum computer memory. *Phys. Rev. A*, 52:R2493–R2496, 1995.

[123] A. M. Steane. Error correcting codes in quantum theory. *Phys. Rev. Lett.*, 77:793–797, 1996.

[124] D. Gottesman. Stabilizer codes and quantum error correction. *arXiv:quant-ph/9705052*, 1997.

[125] R. Laflamme, C. Miquel, J. P. Paz, and W. H. Zurek. Perfect quantum error correcting code. *Phys. Rev. Lett.*, 77:198–201, 1996.

[126] Q. Zhang, A. Goebel, C. Wagenknecht, Y.-A. Chen, B. Zhao, T. Yang, A. Mair, J. Schmiedmayer, and J.-W. Pan. Experimental quantum teleportation of a two-qubit composite system. *Nature Physics*, 2:678–682, 2006.

[127] N. Kiesel, C. Schmid, U. Weber, G. Tóth, O. Gühne, R. Ursin, and H. Weinfurter. Experimental analysis of a four-qubit photon cluster state. *Phys. Rev. Lett.*, 95:210502, 2005.

[128] A. Barenco, C.H. Bennett, D.P. DiVincenzo, N. Margolus, P. Shor, T. Sleator, J. Smolin, and H. Weinfurter. Elementary gates for quantum computation. *Phys. Rev. A*, 52:3457–3467, 1995.

[129] M. A. Nielsen. Optical quantum computation using cluster states. *Phys. Rev. Lett.*, 93:040503, 2004.

[130] R. Raussendorf, D. E. Browne, and H. J. Briegel. Measurement-based quantum computation on cluster states. *Phys. Rev. A*, 68:022312, 2003.

[131] C.-Y. Lu, X.-Q. Zhou, O. Gühne, W.-B. Gao, J. Zhang, Z.-S. Yuan, A. Goebel, Tao Yang, and Jian-Wei Pan. Experimental entanglement of six photons in graph states. *Nature Physics*, 3:91–95, 2007.

[132] Qiang Zhang Yu-Ao Chen Kai Chen Joerg Schmiedmayer Jian-Wei Pan Alexander M. Goebel, Claudia Wagenknecht. Multistage entanglement swapping. *Phys. Rev. Lett.*, 101:080403, 2008.